

SIMULATING THE EFFECT OF RAINFALL
ON MICROWAVE ATTENUATION

BY

ESSIEN, EYO EFFIONG ESSIEN

RegNo: MTH/Ph.D/11/002

A PhD THESIS CARRIED OUT

in

COMPUTER SCIENCE

SUBMITTED TO

GRADUATE SCHOOL

of

UNIVERSITY OF CALABAR

CALABAR, NIGERIA

IN PARTIAL FULFILLMENT OF THE REQUIREMENTS
FOR THE AWARD OF DOCTOR OF PHILOSOPHY (Ph.D)
DEGREE IN COMPUTER SCIENCE

FEBRUARY, 2016

CERTIFICATION

I, Essien, Eyo Effiong Essien with registration number MTH/PHD/11/002, hereby certify that this thesis "SIMULATING THE EFFECT OF RAINFALL ON MICROWAVE ATTENUATION" is original, and has been written by me. It is a record of my research work and has not been presented before in any previous publication.

Name: Essien, Eyo E. Essien

(Student/Candidate)


Date: 1-8-2016

Signature: 


DECLARATION

We declare that this thesis entitled "SIMULATING THE EFFECT OF RAIN-FALL ON MICROVAVE ATTENUATION" by Essien, Eyo Effiong Essien (with registration number MTH/PHD/11/002) carried out under our supervision, has been found to have met the regulations of the University of Calabar. We therefore, recommend the work for the award of the Doctor of Philosophy degree in Computer Science.


1. Name: Prof. Zsolt Lipcsey
(Chief Supervisor)
Qualification: B.Sc, MSc, Ph.D.
Status: Professor

Signature: 
Date: 28/10/2016


2. Name: Prof. Joseph O. Esin
(Supervisor)
Qualification: B.Sc, M.A. ED.D
Status: Professor of Research

Signature: 
Date: 28/7/2016

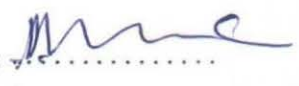
3. Name: Dr. Azom E. Edim
(Head of Department)
Qualification: B.Sc, MSc, Ph.D.
Status: Senior Lecturer

Signature: 
Date: 28/7/2016

4. Name: Dr. Rufus Okoro
(Graduate School Representative)
Qualification: B.Sc, MSc, Ph.D.
Status: Reader

Signature: 
Date: 28/7/16

5. Name: Enoch O. Nwachukwu
(External Examiner)
Qualification: B.Sc, MSc, Ph.D., FNCS, FCPN
Status: Professor of Computer Science

Signature: 
Date: 28/07/16

ACKNOWLEDGEMENT

I wish to express my warm thanks to Prof. Zsolt Lipcsey for his untiring guidance and support. Also to Prof. Joseph Esin in the United States for all his contributions and support through my study. I would also like to express gratitude to everyone who supported me throughout the course of this research and all my external guide especially Dr. Ranjan Bose in the department of Electrical Engineering, Indian Institute of Technology and all the people who provided me with the facilities being required and conducive conditions for my Doctoral research.

ABSTRACT

Current frequency allocations below Ku-band are becoming increasingly congested. The problem continues to grow as the use of telecommunications and wireless data communication becomes more popular. In order to compensate for increase in demand for bandwidth, telecommunication operating frequencies have to be raised, yielding larger channel capacity. This research studies the effect of raising the operating frequency to transmit signals in rain. A scenario of transmit and reception of microwave under falling rain drops is assumed and the volume extracted from the transmitter power emission was used as a basis of deriving the Rain Attenuation Model (RAM). MATLAB was used to simulate the RAM with inputs of rain-drop size measurement and a 14-year variations of one-minute rainfall rates from 37 sites covering 36 states capitals and Abuja in Nigeria; sourced at Tropical Rainfall Measurement Mission (TRMM) satellite database and validated with precipitation prediction estimates from Nigerian Meteorological Agency (NIMET). The Okumura-Hata Free Space Propagation Model (FSPM) was simulated in the same manner and used to validate the results of the RAM. The overall result show full agreement with the trend of the FSPM. This means that the RAM can be used to predict coverage of wireless radio signal in areas dominated by rain.

Contents

CERTIFICATION	i
DECLARATION	ii
ACKNOWLEDGEMENT	iii
ABSTRACT	iv
TABLE OF CONTENTS	v
LIST OF FIGURES	ix
LIST OF TABLES	xvii
ACRONYMS	xxi
LIST OF SYMBOLS	xxiii
CHAPTER ONE	1
1 GENERAL INTRODUCTION	1
1.1 Background of Study	2
1.1.1 EHF and SHF satellite systems	3
1.1.2 Frequency allocations for Earth-space links	5
1.1.3 Operating bandwidth	5
1.2 Statement of Problem	6
1.3 Aim and Objectives	7
1.4 Scope of Study	7
1.5 Significance of Study	8
1.6 Definition of terms	8
CHAPTER TWO	12
2 LITERATURE REVIEW	12
2.1 Introduction	12
2.2 Satellite systems	14
2.3 The Troposphere	15
2.3.1 Rain	15

2.3.2	Formation in warm clouds	16
2.3.3	Formation in cold clouds	16
2.3.4	Strati-form and Convective rain	17
2.3.5	Convective rainfall	17
2.3.6	Rain cells	18
2.3.7	Fall velocity and shape of raindrops	19
2.4	The Concept of Wave Propagation	24
2.4.1	Diffraction	27
2.5	Reflection	27
2.5.1	Dielectrics Reflection	28
2.5.2	Ground Reflection Model (Two Rays)	33
2.6	Scattering of radio waves	40
2.7	Radio Propagation Models	41
2.7.1	COST-Hata-Model	42
2.7.2	Egli Model	43
2.7.3	Young Model	43
2.7.4	Okumura Model	44
2.7.5	Hata Model for Urban Areas	44
2.7.6	Point To Point Lee Model	45
2.7.7	ITU Terrain Model	46
2.7.8	Weissberger's Model	47
2.7.9	Early ITU Model	48
2.7.10	One Woodland Terminal Model	48
2.7.11	The ITU Single Vegetative Obstruction Model	49
2.8	Work Specific	49

CHAPTER THREE 54

3 METHODOLOGY 54

3.1	Introduction	54
-----	------------------------	----

3.2	Attenuation by Rain	54
3.3	Consideration for the Shape of Rain Drop	57
3.4	Raindrop Size Distribution	57
3.5	The Proposed Model	58
3.5.1	Radiation pattern	64
3.6	Data Collection	68
 CHAPTER FOUR		71
4	RESULTS AND DISCUSSION	71
4.1	Simulation of the Formulated Model	71
4.2	The Formulated Model for Simulation	71
4.3	Flow Chart for Simulation	71
4.4	Choice of Implementation Platform	74
4.5	Simulation of the Model using MATLAB	74
4.6	Simulating Free Space Propagation Model	76
4.7	Results Presentation and Discussion	77
4.7.1	Results Presentation	77
4.7.2	Discussion of the Results	78
4.7.3	Comparison of the Received Power, P_r , as a function of the separation between the two antennas $d(\text{km})$ for the RAM and FSPM at three different frequencies (4GHz, 10GHz and 20GHz)	157
4.7.4	Chances of satisfactory performance of wireless communica- tion system in a region dominated by rain.	158
 CHAPTER FIVE		159
5	SUMMARY, CONCLUSION AND RECOMMENDATIONS	159
5.1	Summary	159
5.2	Conclusion	160

5.3 Recommendation	160
REFERENCES	162
APPENDIX A	168
APPENDIX B	169
APPENDIX C	209

List of Figures

1	Radio frequency band allocations as defined in ITU-R V.431-7.	4
2	Equilibrium raindrop shapes at radius: 1mm, 2mm, 3mm and 4m.	22
3	Raindrop with diameter greater than 5 mm forming a parachute (a), a large inverted bag (b) and breaking up (c).	23
4	Illustration of the canting angle of a raindrop and the forces involved.	25
5	Reflection of wave from plane surface.	26
6	An E-field in parallel with respect to the surface of plane of incidence.	30
7	An E-field perpendicular to the surface of plane of incidence.	31
8	A ground reflection model (Two Ways)	36
9	Scattering of radio signals by rain drops	56
10	Volume extracted from the transmitter-power emission.	59
11	Survey areas comprising of state capitals in Nigeria-sourced from https://www.pinterest.com	70
12	Flowchart of the Simulation of the RAM and FSPM .	73

13. Path loss against separation between two antennas in free space	79
14. Path loss against separation between two antennas in Abeokuta	80
15. Path loss against separation between two antennas in Ado Ekiti	81
16. Path loss against separation between two antennas in Akure	82
17. Path loss against separation between two antennas in Ibadan	83
18. Path loss against separation between two antennas in Ikeja	84
19. Path loss against separation between two antennas in Osogbo	85
20. Path loss against separation between two antennas in Abakaliki	86
21. Path loss against separation between two antennas in Awka	87
22. Path loss against separation between two antennas in Enugu	88
23. Path loss against separation between two antennas in Owerri	89
24. Path loss against separation between two antennas in Umuahia	90

25. Path loss against separation between two antennas in Asaba	91
26. Path loss against separation between two antennas in Benin	92
27. Path loss against separation between two antennas in Calabar	93
28. Path loss against separation between two antennas in Port Harcourt	94
29. Path loss against separation between two antennas in Uyo	95
30. Path loss against separation between two antennas in Yenogoa	96
31. Path loss against separation between two antennas in Abuja	97
32. Path loss against separation between two antennas in Illorin	98
33. Path loss against separation between two antennas in lafia	99
34. Path loss against separation between two antennas in Lokoja	100
35. Path loss against separation between two antennas in Makurdi	101
36. Path loss against separation between two antennas in Mina	102

37. Path loss against separation between two antennas in Jos	103
38. Path loss against separation between two antennas in Birini Kebbi	104
39. Path loss against separation between two antennas in Gasau	105
40. Path loss against separation between two antennas in Kaduna	106
41. Path loss against separation between two antennas in Kano	107
42. Path loss against separation between two antennas in Katsina	108
43. Path loss against separation between two antennas in Sokoto	109
44. Path loss against separation between two antennas in Yola	110
45. Path loss against separation between two antennas in Bauchi	111
46. Path loss against separation between two antennas in Damaturu	112
47. Path loss against separation between two antennas in Dutse	113
48. Path loss against separation between two antennas in Gombe	114

49. Path loss against separation between two antennas in Jalingo	115
50. Path loss against separation between two antennas in Maiduguri	116
51. Received power against the separation between two antennas in Abeokuta	117
52. Received power against the separation between two antennas in Ado Ekiti	118
53. Received power against the separation between two antennas in Akure	119
54. Received power against the separation between two antennas in Ibadan	120
55. Received power against the separation between two antennas in Ikeja	121
56. Received power against the separation between two antennas in Osogbo	122
57. Received power against the separation between two antennas in Abakaliki	123
58. Received power against the separation between two antennas in Awka	124
59. Received power against the separation between two antennas in Enugu	125
60. Received power against the separation between two antennas in Owerri	126

61.	Received power against the separation between two antennas in Umuahia	127
62.	Received power against the separation between two antennas in Asaba	128
63.	Received power against the separation between two antennas in Benin	129
64.	Received power against the separation between two antennas in Calabar	130
65.	Received power against the separation between two antennas in Port Harcourt	131
66.	Received power against the separation between two antennas in Uyo	132
67.	Received power against the separation between two antennas in Yenogoa	133
68.	Received power against the separation between two antennas in Abuja	134
69.	Received power against the separation between two antennas in Illorin	135
70.	Received power against the separation between two antennas in Lafia	136
71.	Received power against the separation between two antennas in Lokoja	137
72.	Received power against the separation between two antennas in Makurdi	138

73.	Received power against the separation between two antennas in Mina	139
74.	Received power against the separation between two antennas in Jos	140
75.	Received power against the separation between two antennas in Birini Kebbi	141
76.	Received power against the separation between two antennas in Gasau	142
77.	Received power against the separation between two antennas in Kaduna	143
78.	Received power against the separation between two antennas in Kano	144
79.	Received power against the separation between two antennas in Katsina	145
80.	Received power against the separation between two antennas in Sokoto	146
81.	Received power against the separation between two antennas in Bauchi	147
82.	Received power against the separation between two antennas in Damaturu	148
83.	Received power against the separation between two antennas in Dutse	149
84.	Received power against the separation between two antennas in Gombe	150

85. Received power against the separation between two antennas in Jalingo	151
86. Received power against the separation between two antennas in Maiduguri	152
87. Received power against the separation between two antennas in Yola	153
88. Received power against the separation between two antennas in Free Space	154

Table 11. Simulated result showing path loss and power received for ENUGU.	180
Table 12. Simulated result showing path loss and power received for OWERRI	181
Table 13. Simulated result showing path loss and power received for UMUAHIA	182
Table 14. Simulated result showing path loss and power received for ASABA	183
Table 15. Simulated result showing path loss and power received for BENIN	184
Table 16. Simulated result showing path loss and power received for CALABAR	185
Table 17. Simulated result showing path loss and power received for PORT HARCOURT	186
Table 18. Simulated result showing path loss and power received for UYO	187
Table 19. Simulated result showing path loss and power received for YENOGOA	188
Table 20. Simulated result showing path loss and power received for ABUJA	189
Table 21. Simulated result showing path loss and power received for ILLORIN	190
Table 22. Simulated result showing path loss and power received for LAFIA	191

Table 23. Simulated result showing path loss and power received for LOKOJA	192
Table 24. Simulated result showing path loss and power received for MAKURDI	193
Table 25. Simulated result showing path loss and power received for MINA	194
Table 26. Simulated result showing path loss and power received for JOS	195
Table 27. Simulated result showing path loss and power received for BIRINI KEBBI	196
Table 28. Simulated result showing path loss and power received for GASAU	197
Table 29. Simulated result showing path loss and power received for KADUNA	198
Table 30. Simulated results showing path and power re- ceived for KANO	199
Table 31. Simulated results showing path and power re- ceived for KATSINA	200
Table 32. Simulated results showing path and power re- ceived for SOKOTO	201
Table 33. Simulated results showing path and power re- ceived for BAUCHI	202
Table 34. Simulated results showing path and power re- ceived for DAMATURU	203

Table 35. Simulated results showing path and power received for DUTSE	204
Table 36. Simulated results showing path and power received for GOMBE	205
Table 37. Simulated results showing path and power received for JALINGO	206
Table 38. Simulated results showing path and power received for MAIDUGURI	207
Table 39. Simulated results showing path and power received for YOLA	208

Acronyms

AEHF	Advanced Extremely High Frequency
AH	Absolute Humidity
BADC	British Atmospheric Data Centre
BER	Bit error rate
BTS	Base Transceiver Station
CAPE	Convective Available Potential Energy
CDF	Cumulative Density Function
COMSAT	Communication Satellite Corporation
DSD	Raindrop Size Distribution
DVB	Digital Video Broadcasting
EHF	Extra High Frequency
EIRP	Effective Isotropic Radiated Power
ESA	European Space Agency
FMT	Fade Mitigation Technique
FSPM	Free Space Propagation Model
INTELSAT	International Telecommunication Satellite Organisation
IP	Internet Protocol
ITU	International Telecommunications Union
LoS	Line of Sight
LWC	Liquid Water Content
MSG	Meteosat Second Generation
MRO	Mars Reconnaissance Orbiter
NASA	National Aeronautics and Space Administration
PCA	Principal Component Analysis

PVAF	Percentage Variance Accounted For
QoS	Quality of Service
RH	Relative Humidity
RMS	Root Mean Square
SHF	Super High Frequency
SMOS	Soil Moisture and Ocean Salinity
TRMM	Tropical Rainfall Measurement Mission
TTC	Tracking Telemetry and Command stations
UHF	Ultra High Frequency
NIMET	Nigerian Meteorological Agency
RAF	Royal Air Force
RCA	Radio Corporation of America
COST	Coperation europeenne dans le domaine de la recherché Scientifique et Technique

List of Symbols

ΔD	Bin width of drop size class
Γ	Fresnel reflection coefficient
μ	Distribution shape
A	Specific attenuation
\bar{A}	Mean attenuation
c_i	Speed of light
D	Drop diameter
\bar{D}	Drop size arithmetic mean
f	frequency
G	Antenna gain
λ	wavelength
$N(D)$	Raindrop size distribution
N_T	Mean drop concentration
N_t	Total number of drops in a given volume
$v(D)$	Raindrop fall velocity of drop diameter D
ϵ_1	Permittivity
μ_1	Permeability
σ_1	Conductivity
h_t	Transmitter antenna height
h_r	Receiver antenna height
d	distance
Δ	Path difference
G_t	Transmitter antenna gain
G_r	Receive antenna gain
P_r	Received Power
P_t	Transmit Power
ρ_s	Scattering loss factor
δ_h	Standard deviation of the surface height
dB	decibel
L	Median path loss
H_B	base station antenna effective height

A_{MU}	Median attenuation
H_{MG}	Mobile station antenna height gain factor
H_{BG}	Base station antenna height gain factor
$K_{correction}$	Correction factor gain
L_U	Path loss in urban areas
C_H	Antenna height correction factor
H_{ET}	Effective height of terrain
C_N	Normalized terrain clearance
F_1	radius of first Fresnel zone
A_v	Attenuation due to vegetation
γ	Specific attenuation for short
P_{sc}	Scattered Power
P_{ab}	Absorbed Power
σ_{total}	Extinction cross section
σ_{sc}	Scattering cross section
σ_{ab}	Absorption cross section
a	raindrop radius
$w(a)$	Average power density
A_e	Effective area

Chapter 1

GENERAL INTRODUCTION

The development of complex radio access networks had resulted in the increase of spectrum occupancy necessitated from the demand for higher bandwidths. Hence, it is imperative to employ the advantages of higher frequencies, which are capable of supporting these demands (Bossa and Villermaux, 2009). The obvious candidates are microwave and millimetre bands. The advantages offered by microwave and millimetre waves have attracted immense interest from academia and the communications industry. The main characteristics of both waves include short wavelength, large bandwidth, and frequency re-use. An electromagnetic wave propagating through a region containing raindrops tend to encounter two attenuating effects such as absorption through which part of its energy is absorbed by the raindrops and transformed into heat; and the other is scattering where part of energy is scattered in all directions (Ajewole and Oguchi, 2001). The calculation of these two attenuating mechanisms is based on the understanding of the characteristics of raindrops. Rain attenuation is caused by the scattering and absorption of electromagnetic waves by drops of water. When radio waves encounter drops of rain, there is scattering and absorption of signals. Scattering diffuses the signal while the absorption involves the resonance of the waves with individual molecules of water. Further more, absorption increases the molecular energy corresponding to the slight increase in temperature and results in equivalent loss of signal energy. The study of radio waves scattering and absorption by rain drops is therefore very important since rain attenuation data due to radio waves scattering and absorption are needed in many important applications, including microwave propagating systems, remote sensing systems, radar systems (Murat, 2001). From the view point of radio communication engineering, communication medium can be viewed as imperfect bit pipes; since the bit pipes can delay, lose or modify the information carried by it (Longley-Rice, 1999). Rain attenuation is affected by various factors such as rain rates, operating frequency, the physical size of rain drops and polar-

ization (Murat, 2001) (Theodore and Rappaport, 2000). In the design of radio communication systems, it is important to consider factors which may be useful for the determination of the characteristics of the electromagnetic signals. Baltas and Mimikou (2002) noted that one of such characteristics is the power level of the signal to be transmitted which plays an important role in knowing the amount of signal at the receive antenna within the service area. This helps to determine the number of base stations and their spacing for improved communication within the area in question. The medium between the transmitter and the receiver has a big role to play on the quality and performance of signals that are transmitted, consequently the attenuation due to the medium the signal traverses.

Rain affects the design of any communication system that relies on the propagation of electromagnetic waves. Casternet (2001) asserted that above a certain threshold, the attenuation due to rain becomes one of the most important limits to the performance of microwave links. Rain attenuation, which is the dominant fading mechanism at these frequencies, is based on nature, that can vary from location to location and from year to year. Daily rainfall accumulations, universally recorded on hourly basis, are also fairly widely available by national weather bureaus (Goldhirsh, 2000).

1.1 Background of Study

Telecommunications and broadcasting services are in a rapid phase of expansion. Users are demanding more multimedia services such as high-speed internet, on demand digital Television services, video conferencing, tele-medicine and tele-education to name a few. Such services require high-speed data rates to cope with demand and hence guaranteeing customers a high quality of service (QoS).

The current microwave frequency spectrum allocated for telecommunication and broadcast services has become congested and proposed broadband systems will require higher bandwidths. SHF (Super High Frequency) and EHF (Extremely High Frequency) services are relatively free of congestion and can cope with higher data rates than popular microwave systems. However, above Ka-band, attenuation due

to atmospheric gases, clouds and rain increases significantly. Whilst attenuation is caused more frequently by clouds and gases, it is rain that causes the largest attenuation.

The use of numerical weather data combined with propagation models can be used to forecast telecommunication link attenuation, (Hodges, 2006). The forecast of link attenuation can be used to improve the effectiveness of fade mitigation techniques. For a given rainfall rate, the raindrop size distribution (DSD) can vary considerably, resulting in significant variation in attenuation. This thesis investigates attenuation caused by rain and the effect of the DSD in order to better understand the impact of using SHF/EHF, and ultimately help improve the effectiveness of propagation models.

1.1.1 EHF and SHF satellite systems

Typical satellite systems operate in the UHF, EHF and SHF frequency bands. Figure 1 shows the frequency allocation of the radio spectrum. EUTELSAT HOT BIRD 10 is an example of a Ku-band satellite broadcasting almost 1100 channels to 120 million homes in Europe, North Africa and the Middle East. KA-SAT is an example of a Ka-band satellite launched in December 2010 (Townsend and Watson, 2011). The satellite is an advanced, multi-spot satellite that utilises over 80 spot beams, which will be the beginning of a new satellite infrastructure that will expand the capacity of broadband services across Europe and the Mediterranean Basin. KA-SAT will join the HOT BIRD broadcasting satellites with the aim of providing new media services through Ka-band frequencies.

300Hz	ULF	Military Use	
3KHz	VLF	Maritime Navigation	
30KHz	LF	Navigation Aids	
300KHz	MF	AM Radio	
3MHz	HF	Shortwave Radio	
30MHz	VHF	FM Radio	
300MHz	UHF	Mobile Phones, GPS] L- Band (1.5 GHz) S- Band (2.5 GHz) C- Band (4/6 GHz) Ku- Band (11/12/14 GHz) K- Band (20 GHz) Ka- Band (30 GHz) V- Band (40 GHz)
3GHz	SHF	Satellite Communications	
30GHz	EHF	Radar Landing Systems	
300GHz			

Figure 1: Radio frequency band allocations as defined in ITU-R V.431-7.

The growing demand on satellite communication systems has resulted in the current frequency bands becoming increasingly congested (Panagopoulos, Arapoglou, and Cottis, 2004). In order to compensate for the increase in demand, satellite operating frequencies have to be raised to deliver larger channel capacity, for example EUTELSAT HOT BIRD 6 and the United States Air Force's Advanced Extremely High Frequency (AEHF) satellites are operating at Ku- and Ka-band frequencies. However, raising the operating frequency has both advantages and disadvantages on the design and implementation of satellite communications.

1.1.2 Frequency allocations for Earth-space links

As shown in figure 1, the current frequency allocations at L-, S-, C- and Ku-bands are becoming increasingly congested. This problem continues to escalate as the use of satellite communications becomes more popular and larger throughputs are required. Further allocation of frequency space requires increasingly complex methods for frequency reuse and allocation. As a result of this, higher frequencies, such as V-band, are of great interest, because they are currently congestion free and have theoretically a larger capacity.

The number of geostationary satellites in orbit is another significant issue. Physical space in geostationary orbits above heavily populated areas, where communication is in great demand, is becoming limited. The increase of operating frequencies would reduce the number of satellites required, because the increased capacity of higher frequency systems would reduce the number of payloads for a given service. High frequency systems, Ka-bands and above would also improve directivity of satellite beams, which could be exploited to increase satellite density.

1.1.3 Operating bandwidth

Increasing the operating frequency of satellites provides the option for larger bandwidths (Baltas and Mimikou, 2002). This has the potential of providing services with bit-rates in the order of Gbs^{-1} , which is required for future high-definition services. Large bandwidths will lead to the use of return-channel links and broadband connections via satellite. Internet protocol (IP) over satellite is de-

signed to provide broadband services to remote areas of the world, disaster areas and locations without sufficient infrastructure to provide broadband over terrestrial networks.

1.2 Statement of Problem

(Berne and Uijlenhoet, 2007) asserted that the use of propagation channel modelling will help to determine the attenuation on a radio link and improve the effectiveness of fade mitigation techniques. However, there is still uncertainty in the estimation of attenuation from propagation models, that can result in under estimation or overestimation of attenuation. Over estimation can constitute wasted power resources and underestimation can likewise result in loss of signal and reduction in quality of service. In certain circumstances, such as financial transactions and safety critical systems, loss of signal will lead to disastrous consequence.

Traditionally, a fixed fade margin is typically to compensate for attenuation by assuming the worst case scenario. A fade margin of 40dB for a 48GHz link is predicted to maintain a system availability of 99.99%, (Hodges, 2006). Propagation models are used to determine a dynamic fade margin to increase the power efficiency of a system.

The Communication industry is faced with the problem of determining whether the signal projected by the transmitter, the intended signal of communication system, actually covers the targeted area and also meet the design specifications. It is the task of engineers to ensure that the intensity of the signal is adequate to cover the targeted area called the service area; considering the fact that some of the signals are attenuated by climatic and environmental conditions at the receiving end. (Castanet, 2001) noted that the quality of service (QoS) and the performance of any communication system are determined by the communication medium relative to other associated factors. Thus, it is important to vividly generate the analysis of a particular medium before planning and designing a base transceiver station (BTS) within that geographical area. One can convincingly say that, since performance and the quality of service (QoS) of radio waves is determined by the climatic

and environmental conditions, the limited or poor service experienced at the receiving end is probably be due to one of the factors or conditions especially in areas with dominant rainfall, thick vegetation, high rise buildings, and tall mountains, etc. The aim of this research is investigating into how rainfall adversely affects the performance of radio signals traversing from transmitter to the receiver. This would be achieved by determining how much of the radio wave signals are being attenuated and possibly providing the solution on the various ways of reducing the attenuation and possibly improving the quality of service (QoS) of radio signals in affected area.

1.3 Aim and Objectives

The primary aim of this research is to investigate the effect of rainfall on microwave attenuation. In addition, the study will examine the possible impact of rainfall on the performance of radio wave as it traverse from transmitter to receiver.

The objectives of this research are:

1. To investigate how rainfall adversely affects the performance of radio signals traversing from transmitter to the receiver by determining how much of the radio wave signals are being attenuated.
2. To determine the chances of satisfactory performance of a wireless communication system that depends on radio wave propagation in an environment dominated by rain.

1.4 Scope of Study

There are quite a number of ways through which signals from an antenna get impaired as they traverse through different medium. There are also many climatic and environmental factors associated with attenuation of radio signals such as mountains, tall building and structures and vegetation.

The research formulates and simulates a model that determines the path loss or deviation of a radio signal that is propagated in rain with respect to the transmitter and the receiver.

1.5 Significance of Study

The study of radio waves scattering and absorption by rain drops is very important and beneficial for any environment. Rain attenuation data due to radio waves scattering and absorption are needed in many important applications, including microwave propagating systems, remote sensing systems, radar systems, global positioning systems. Notably, every application that depends on satellite communication also rely on attenuation prediction data for improved design and functionality (Castanet, 2001).

The study will provide the radio engineer ability to understand how to plan and implement radio frequency systems, for the purpose of its coverage analysis; which uses the propagation model and rainfall data to predict the radio frequency coverage area for a transmitter, the received signal strength at the end of a wireless link, the path loss from the transmitter to a distance receiver, the minimum antenna height to establish Line of Sight (LoS) communication path and channel impairment as delay spread due to multi-path fading.

1.6 Definition of terms

Attenuation

Attenuation is the loss of transmitted radio signal due to scattering, absorption and refraction of microwave. It is the fading of radio signal as it travels towards the receive antenna.

Propagation model:

A radio propagation model, also known as the Radio Wave Propagation Model is an empirical mathematical formulation for the characterization of radio wave propagation as a function of frequency, distance and other conditions.

Troposphere:

the lowest layer of the atmosphere, 6 miles (10 km) high in some areas and as much as 12 miles (20 km) high in others, within which there is a steady drop in

temperature with increasing altitude and within which nearly all cloud formations occur and weather conditions manifest themselves.

Wave:

A wave is a cycle of repetitive to and fro motion that passes through a medium, at a speed determined by the properties of the medium.

Transmitter:

A transmitter is a set of equipment used to generate and transmit electromagnetic waves carrying messages or signals, especially those of radio or television.

Receiver:

A receiver is a device, as in a radio, that converts incoming radio, microwave, or electrical signals to a form, such as data, sound and light, that can be understood.

Antenna:

An antenna is a specialized transducer that converts radio-frequency (RF) fields into alternating current (AC) or vice-versa. There are two basic types: the receiving antenna, which intercepts RF energy and delivers AC to electronic equipment, and the transmitting antenna, which is fed with AC from electronic equipment and generates an RF field.

Transducer:

A transducer is an electronic device that converts energy from one form to another.

Rain:

Water condensed from atmospheric vapor and falling in drops.

Satellite:

Satellite is an artificial body placed in orbit round the earth or another planet in order to collect information or for communication.

Frequency:

Frequency is the rate per second of a vibration constituting a wave, either in a material, as in sound waves, or in an electromagnetic field, as in radio waves and light.

Reflection:

Reflection is the return of light, sound or electromagnetic waves from a surface.

Refraction:

Refraction is the deflection of a wave, such as a light, sound or electromagnetic wave, when it passes obliquely from one medium into another having a different index of refraction.

Diffraction:

the process by which a beam of light or other system of waves is spread out as a result of passing through a narrow aperture or across an edge, typically accompanied by interference between the wave forms produced.

Polarization:

Polarization is the process or phenomenon in which the waves of light or other electromagnetic radiation are restricted to certain directions of vibration, usually specified in terms of the electric field vector

Dielectric:

A dielectric material is a substance that is a poor conductor of electricity, but an efficient supporter of electrostatic fields.

Signal:

A signal is an electrical impulse or radio wave transmitted or received.

Free space:

Free space is space unoccupied by matter, more particularly, containing no electromagnetic or gravitational field and used as a reference.

Chapter 2

LITERATURE REVIEW

2.1 Introduction

Chapter two introduces the satellite system, the troposphere and outlines factors which cause attenuation of propagating radio waves at frequencies above 20 GHz. (Arbesser-Rastburg and Paraboni, 1997) noted that rainfall can lead to the largest values of radio wave attenuation at Ka-band frequencies. The emphasis is on rain formation, shape, velocity, measurement and the micro-physics of precipitation. Different types of models for radio propagation discussed in this study include: Egli Model, Longley-Rice Model, Young Model, Okumura Model, COST Hata Model, Hata Model, Lee Model, Weissberger's model, Environmental Directivity Antenna Model, One Woodland Model, ITU terrain Model. This would lead to the review of contributions from other researchers. The primary focus of this research is to formulate a mathematical model based on the shortcoming of Okumura model which does not include the effect of rainfall on radio signals. The projected mathematical model will be utilized to determine the percentage of coverage area from the attenuated microwave signal due to rainfall.

During World War II, the rapid advancement of missile and microwave technology led to the development of satellite communications (Gloaguen and Lawergnat, 1996). The initial satellite concept originated with Royal Air Force (RAF), officer Arthur C. Clarke. In his proposal, 'Wireless World', he described how manned satellites orbiting the Earth can distribute television broadcasts. Though famous today for both science fiction stories and his inventions, Clarke's satellite concept had little impact, even after being repeated in 1951. In 1954 the potential of satellite communications became evident, after John R. Pierce, of AT&T's Bell Telephone Laboratories, conducted a detailed evaluation of the technical and financial potential of satellites. Pierce decided to compare the first transatlantic telephone cable, carrying only 35 simultaneous calls at an installation cost of 30-50

million dollars in 1954, to a satellite that could implement 1000 simultaneous calls, worth one billion dollars.

The satellite era began in 1957 with the emergence of the first satellite, Sputnik I, was launched by Russia prompting America to respond by developing and producing its own satellites (Panagopoulos et al., 2004). Therefore, NASA decided to develop passive communication satellites, such as the passive repeater ECHO 1, while the Department of Defence concentrated on active satellites. In 1961, the formal start of medium-earth-orbit satellites such as TELSTAR, by AT&T, and RELAY, by the company Radio Cooperation of America (RCA), began. A further contract was awarded to Hughes Aircraft Company to design a 24 hour orbiting satellite, known as SYNCOM. The TELSTAR and RELAY satellites were first launched in 1962 and successfully broadcasting parts of the 1964 Olympics from Tokyo. At this time, Communication Satellite Corporation (COMSAT) began developing its first satellite, which led to the launch of the EARLY BIRD, in 1965; initiating global communications. Early Bird or INTELSAT 1 was the first geostationary satellite. 1965 also saw the start of the first Soviet communication satellites launched with the MOLNYA series (Zinevich et al., 2008).

In 1964 an agreement was signed by thirteen countries with existing satellite technology such as the United States, United Kingdom, France, Germany, Italy, Brazil, and Japan; to create the International Telecommunications Satellite Organisation, INTELSAT. The organisation had the ultimate aim to assume ownership of all satellites and take responsibility for the management of global systems. INTELSAT has grown to have more members than the United Nations and is able to provide hundreds of thousands of telephone circuits. The use of satellite communications has rapidly increased, facilitated by the development of new technology and reduced production costs that make the various services both affordable and useful to the consumer.

The process of increasing expertise, advancing technology and the reduction of costs in the satellite industry have led to reliable launchers and more complex

satellites with increasingly advanced technology for multiple uses. Satellite objectives range from measuring the Earth's water cycle, for example the Soil Moisture and Ocean Salinity (SMOS) satellite programme launched by ESA in 2009, to global navigation satellite systems such as the European Union project Galileo. New advancements include contoured multi-beam antennas where beams adapt to the shape of the continents and frequency reuse from one beam to another. These advances have led to increased efficiency and capacity, which has in turn reduced costs further (Zinevich et al., 2008).

2.2 Satellite systems

The design of a satellite system is based on the service required such as video, voice or data transmission and is constrained by variables such as cost and available technology. It may also be required to form part of a larger network operating within the complete system, often requiring complex design to achieve an optimum configuration.

A typical satellite system consists of space, control and ground components. The space segment is comprised of several active and spare satellites. The control aspects, tracking telemetry and command stations (TTC), include facilities for monitoring and controlling satellite traffic and resources. Finally, the ground segment incorporates earth traffic stations, such as mobile stations or handsets.

Satellites orbit the Earth in a variety of different ways, including low earth orbits (≈ 780 km), for real-time communication, medium earth orbits ($\approx 10,000$ km with an orbit around 6 hours) and geostationary orbits (35,786 km) with period equal to the rotation of the earth (Murat, 2001).

Satellite communication links consist of uplinks, downlinks or inter-satellite links. Uplinks and downlinks are radio-frequency modulated carriers whereas inter-satellite links are classified as radio or optical signals. When designing a satellite system it is important to consider the transmit performance, measured by the effective isotropic radiated power (EIRP). The transmitted power must be resilient enough to overcome propagation losses in order to ensure a signal is successfully

received. Link performance is measured by the ratio of received carrier power, and the noise power spectral density, and is used to determine quality of service, in terms of signal to noise ratio or bit error rate (BER).

Additional considerations include the amount and type of data being transmitted. A larger amount of data will require higher frequencies and larger bandwidths.

(Baltas and Mimikou, 2002) noted that bandwidth depends on base band signal and type of modulation. There is a trade-off between the required carrier power and occupied bandwidth particularly users of satellites are charged for power or bandwidth resources used. Frequency not only affects the amount of data that can be transmitted but also the signal fade along the propagation path. To maintain efficient and economical use of the radio frequency spectrum, regulations are necessary. The International Telecommunication Union (ITU), a United Nations organisation, creates radio regulations and standards.

2.3 The Troposphere

The troposphere is the lowest region of the Earth's atmosphere, and responsible for approximately 75% of the atmosphere's mass. The height of the troposphere, according to (Tokay et al., 2001) is relative to sea level ranges from 7 km near the poles to 20 km in tropical regions, with an approximate average of 17 km. Furthermore, the troposphere contains almost 99% of the atmosphere's water vapour and aerosols and tend to be the densest atmospheric layer, contains 78% nitrogen, 21% oxygen and small concentrations of other trace gases. The temperature of the troposphere decreases with altitude until it reaches the tropopause, a layer between the troposphere and stratosphere known as the region of temperature inversion.

2.3.1 Rain

Rain is the liquid precipitation of atmospheric water vapour. The formation of rain occurs in several different ways. The formation process is dependent on the type of cloud, i.e. warm or cold. In the case of warm clouds, there are two main processes through which rain drops are created. The first is condensation and the second is collision and coalescence. Condensation begins with the generation

of small raindrops up to radii approximately $10\ \mu\text{m}$. Collision and coalescence generate larger rain drops (Austin, 1987) and (Tokay et al., 2001).

2.3.2 Formation in warm clouds

Condensation

The process of condensation begins with the ascent of warm air parcels. This results in air expanding and adiabatically cooling until eventually reaching saturation. If the air continues to rise, the parcel will become supersaturated. A cloud of small water droplets forms as water vapour condenses onto the aerosol and cloud condensation nuclei in the air. The droplets could also form due to spontaneous nucleation where the aid of aerosol is not required. Spontaneous nucleation is described as a process of chance collisions of water droplets in vapour phase coming together to form small embryonic water droplets, (Wallace and Hobbs, 2006) (Holton, Curry, and Pyle, 2003).

Collision and coalescence

Condensation forms small droplets, whereas the collision and coalescence process creates larger droplets (Wallace and Hobbs, 2006). The fall velocity of larger droplets is greater than smaller drops. Faster droplets are likely to collide with slower droplets in their path. However, not all droplets necessarily collide, since many of the smaller drops tend to follow the stream lines around the larger ones. It is not guaranteed that colliding droplets will coalesce with one another as the droplets may bounce off a layer of air trapped amongst each other. Alternatively, the resulting drop could become unstable and breakup. If the cushion of air is squeezed out between the drops before rebound can occur, the two surfaces make physical contact and coalescence will occur (Doswell-III and Rasmussen, 1994) and (Wallace and Hobbs, 2006).

2.3.3 Formation in cold clouds

A cloud that exists above the zero-degree isotherm level is known as "cold cloud". It contain both ice crystals and super-cooled water droplets. Super-cooled

droplets are water droplets that exist in clouds even though the temperature is below 0° C. A mixed cloud contains both ice crystals and super cooled water droplets, a glaciated cloud contains only ice crystals. Rain can form in cold clouds by vapour, riming and aggregation. Growth by vapour cannot produce significantly large ice crystals. Ice crystal growth can occur by riming, where super-cooled droplets that collide with ice crystals increasing the mass of the ice crystal. An ice crystal can also grow by aggregation where ice crystals collide and adhere to one another. Growth by riming and aggregation can produce a wide range of particle sizes, which melt to create larger raindrops.

2.3.4 Strati-form and Convective rain

There are two main types of rain, strati-form and convective. Convective rain usually falls from cumulus and cumulonimbus clouds while strati-form rain precipitates from nimbostratus clouds, (Houze, 1993) and (Castanet, 2001).

Strati-form rainfall

Strati-form rain is caused by frontal weather systems converging into areas of low pressure, the situation when warm air meets cool air. A warm front arises from warm air overriding cool air, as the warm air rises it cools leading to precipitation. Cold fronts dislodge masses of warm air, which leads to more intense but shorter rainfall (Castanet, 2001). Generally, strati-form is more widespread rainfall that usually occurs for rainfall rates below 5mmhr^{-1} . Strati-form rain occurs in clouds with extensive horizontal development, such as nimbo-stratus clouds, rather than vertical development (Feral, Mesnard, Sauvageot, Castanet, and Lemorton, 2000).

2.3.5 Convective rainfall

Convective rainfall occurs when a moist atmosphere is heated above the temperature of its surroundings leading to significant upward movement, which eventually results in convective clouds. Convective rainfall also occur from cold fronts. A cold front undercutting warm air dislodges masses of air at a rate higher than the steady rise of air at a warm front. The air is usually more unstable leading

to the formation of cumulonimbus clouds. (Townsend and Watson, 2011) points out that, orographic uplift, is a process when air is forced from a low elevation to a high elevation over rising terrain such as mountains, can lead to significant upward movement and convective rain. Convective rainfall usually consists of larger, heavier raindrops, which usually occurs at rainfall rates above 10mmhr^{-1} over a relatively short time period, and when the atmosphere is more unstable.

2.3.6 Rain cells

There have been many studies into the size and shape of rain cells using radars, such as those by (Konrad, 1978), (Crane, 1990) and (Goldhirsh, 2000). There have also been studies using long-term time series measurements made from rain gauges (with a time resolution such as 1 minute), which are used to estimate rain cell sizes using the synthetic storm technique, (Yau and Rogers, 1984).

The shape of a rain cell is generally irregular at the ground, however investigators have compared the perimeter of a rain cell to an ellipse. (F'eral, Mesnard, Sauvageot, Castanet, and Lemorton, 2000) showed the statistics of rain cell geometry were independent of their location and threshold with an average ellipticity factor of 0.5. The ellipticity infers that, on average, rain cells were twice as long as they were wide.

A model could be used to represent a measured rain cell. There are several models that have been derived to estimate rain cells. Some profile models are based on a cylindrical or Gaussian shape, (Mass, 1987), (Bryant, Adimula, and Riva, 2001). Two well-known rain cell models include the EXCELL model, (Capsoni, Fedi, Magistrone, Paraboni, and Pawlina, 1987), and the HYCELL model, (F'eral, Sauvageot, and Castanet, 2003). The EXCELL model describes the variation in rainfall rate within a cell as exponential, with circular and elliptical profile. The HYCELL model is a hybrid cell that combines exponential and Gaussian shapes. The Gaussian component models the high-intensity, convective rainfall rate and the exponential component represents the surrounding widespread rainfall. Both models are defined only by a few parameters, which have significant advantages

including reduced storage space and computational time when processing the cells in comparison to complete rainfall data.

Rain cells are used to improve the effectiveness of propagation models, especially for systems with multiple paths, when predicting attenuation due to rain. The prediction of signal fade can greatly improve the effectiveness of fade mitigation techniques, and help maintain high-quality communication services (Tokay, Kruger, and Krajewski, 2001) and (Panagopoulos et al., 2004).

2.3.7 Fall velocity and shape of raindrops

Velocity

The velocity and shape of raindrops are vital factors for calculating the rainfall rate and resulting radio wave attenuation. Gunn and Kinzer (1949) determined a method to measure the terminal velocity of raindrops. The experiment involved a dropper capable of producing water drops of any size from 0.1 to 100,000 μg . Below is an insulated ring-shaped electrode. When droplets detached from nozzle, they would fall through and a free charge would be placed on the droplet. To calculate the fall velocity, a drop was passed through two inducing rings approximately one metre apart. A free electrical charge, deposited on each droplet, generated a pulse on each inductive ring as it descended. The time difference and spacing of the rings were used to measure the average velocity. The drop masses were determined using a highly-sensitive chemical balance (Crane, 1990).

Using these results (Gunn and Kinzer, 1949), and similar work by other authors, for example, Atlas and Sekhon (Atlas and Ulbrich, 1977) and (Baltas and Mimikou, 2002) an expression for the terminal velocity was calculated and is shown in equation (1) The results followed the pattern that the larger the raindrop the faster it would fall. However, as the diameter of the drop increases above 2 mm the increase in velocity begins to decrease. Once the diameter is close to 4 mm, the drops terminal velocity reaches a maximum.

$$v(D) = 9.65 - 10.3\exp(-0.6D) \quad (1)$$

D is the drop diameter given in mm and $v(D)$ is the raindrop velocity of drop diameter D in ms^{-1} .

Raindrop shape

Raindrops vary in both shape and size, (Spilhaus, 1947). A water drop with no noticeable motion relative to the surrounding air will assume a spherical shape due to the surface tension of water. The surface tension of water results in the inside spherical pressure of the drop greater than atmospheric. When the drop falls, unequal pressure forms over the surface. As pressure increases at the bottom of the drop, and decreases at the top and sides, the pressure change deforms the water drop by flattening the bottom surface and spreading the shape sideways (Aydin and Lure, 1991) and (Baltas and Mimikou, 2002).

Experimental results which investigate photographs of raindrops falling were obtained by (Pruppacher and Beard, 1970). Measurements showed that raindrops above 2.0 mm in diameter were affected by the change in pressure on the outside of the drop and became oblate spheroidal in shape. As shown in figure 2, different types of raindrop shapes for given sizes. Generally, raindrops larger than 8mm in diameter are hydrodynamically unstable and tend to break up, as observed in (Pruppacher and Pitter, 1971) and (Baltas and Mimikou, 2002).

The size of the raindrop effects the way in which the raindrop is deformed (Beard and Chuang, 1986).

Breakup of raindrops

Raindrops above 2 mm in diameter become flattened on their underside in free fall and gradually change from a spherical to an almost parachute shape. In any event that the diameter of the drop is greater than 5 mm, the parachute becomes a large inverted bag, with a toroidal ring of water around its rim. Studies have shown that the drop bag bursts to produce a fine spray of droplets, the toroidal ring breaks up into a number of large drops, which forms an exponential raindrop size distribution, (Bossa and Villermaux, 2009). A representation of this process is shown in Figure 3. There is some controversy over whether collisions between

drops that are the largest and cause of breakup. It has been suggested that the number of collisions is not large enough for a stable distribution to emerge, and coalescence is thought to be the main ingredient (Wallace and Hobbs, 2006). The bursting time is also much smaller than the falling time (Illingworth, 2004) and (Testud, Oury, Black, Amayenc, and Dou, 2001).

Raindrop canting angle

Raindrops can fall with different canting angles, which will change the resultant fading levels for linear polarisation on non-spherical raindrops and reduce polarisation discrimination.

Horizontal wind speed varies with height, therefore relative airflow to a drop is not even along the length of the drop as it is accelerated or retarded in the horizontal direction and canting the drop. Vertical wind gradients also result in a horizontal force on raindrops, (Brussaard, 1974). If the wind speed is constant and independent of height, the drops will assume the same horizontal speed as the surrounding air, therefore, the relative airflow to the drop will be vertical. The canting angle is a function of the differential of the vertical wind profile, not the absolute value of the wind speed (Best, 1950) and (Testud et al., 2001).

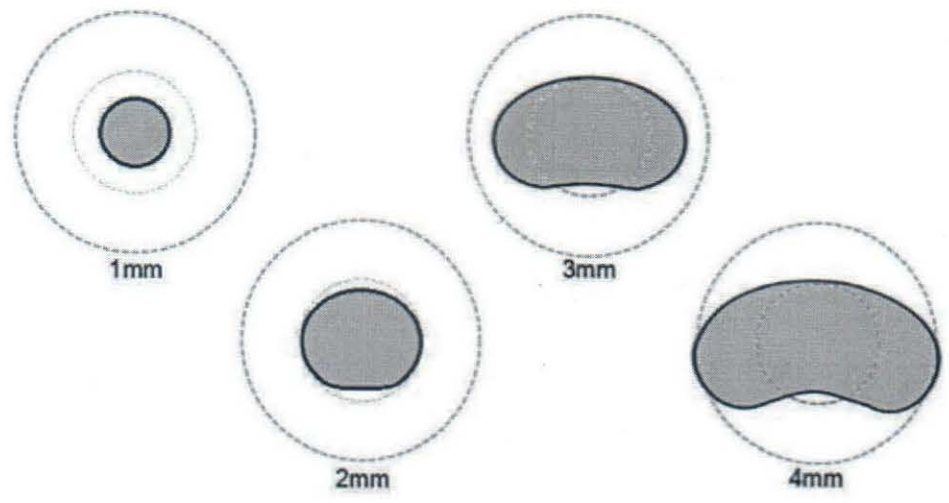


Figure 2: Equilibrium raindrop shapes at radius: 1mm, 2mm, 3mm and 4m.

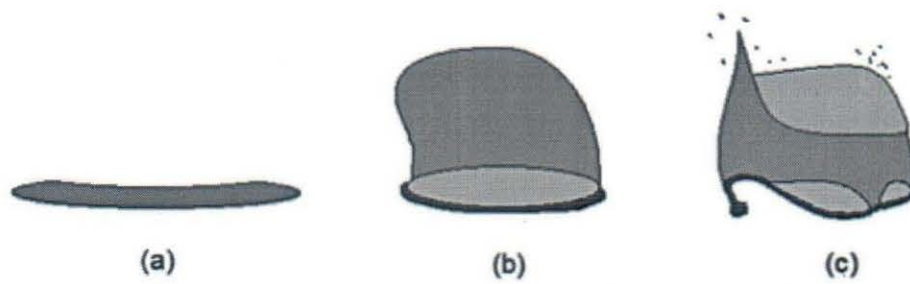


Figure 3: Raindrop with diameter greater than 5 mm forming a parachute (a), a large inverted bag (b) and breaking up (c).

2.4 The Concept of Wave Propagation

The principle of propagation of electromagnetic wave as it waves traverse from one medium to another with different refractive indices has diverse interpretation (Testud et al., 2001). The major contributing factors are attributed to the effect of reflection, diffraction, and scattering of signals as waves traverse through different propagating medium. Radio systems have different regions of operation; some operate in regions where there is thick vegetative cover. Majority of radio system operate in urban areas where there are high-rise buildings that cause severe diffraction loss and decrease line-of-sight (LoS) path between the transmitter and the receiver. There are multiple reflections from various obstacles that exist between these media. The electromagnetic wave traversing along different paths of varying lengths and medium suffers attenuation of their signals. The interaction between these waves causes multipath fading at a specific location, and strengths of the waves decrease as the distance between the transmitter and receiver increases. Reflection generally occurs when a propagating electromagnetic wave come in contact with an obstacle in its path of propagation having very large dimension compared to the wavelength of the propagating wave. Reflection also occurs from the surface of the earth and from buildings/walls. Figure 5 shows how signals can be reflected from a plane surface.

Refraction is also possible for radio waves that are traversing in different medium. It is found that the direction of electromagnetic wave changes as it moves from an area of refractive index to another. The angle of incidence and the angle of refraction are linked by Snell's Law such that:

$$\eta_1 \times \sin(\theta_1) = \eta_2 \times \sin(\theta_2) \quad (2)$$

Where η is the intrinsic impedance of the i^{th} medium. This is given as the ratio of electric field to magnetic field for a uniform plane wave in a particular medium. Thus, $\eta = \sqrt{\frac{\mu}{\epsilon}}$.

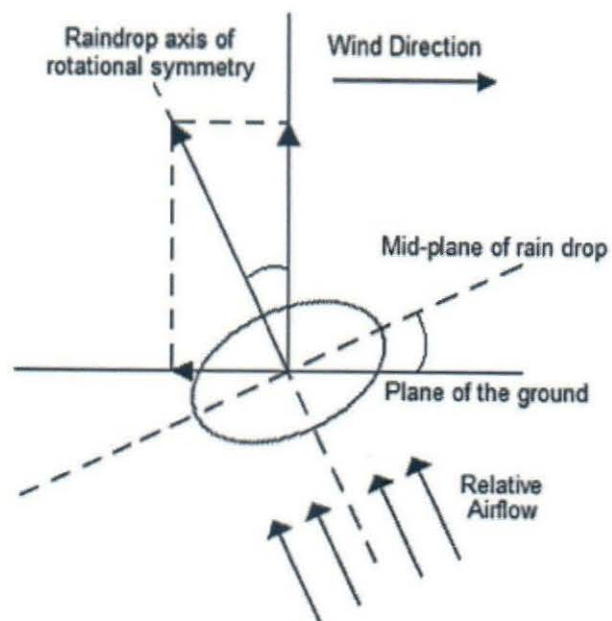


Figure 4: Illustration of the canting angle of a raindrop and the forces involved.

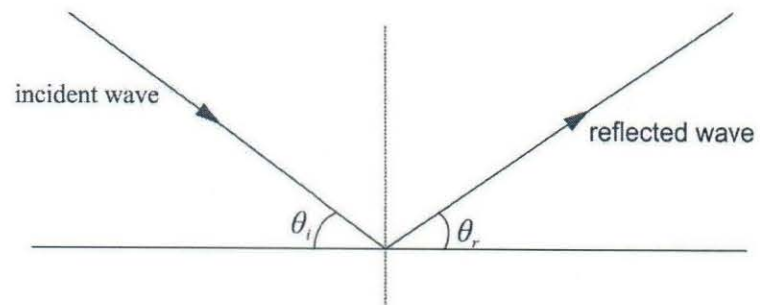


Figure 5: Reflection of wave from plane surface.

For radio signals there are comparatively few instances where the signals move abruptly from a region with one refractive index, to a region with another. It is far more common for these to be comparatively gradually change. This causes the direction of the signal to bend rather than undergo an immediate change in direction.

2.4.1 Diffraction

A radio wave that meets an obstacle has a natural tendency to bend around it. The bending of waves is known as diffraction; which results in a change of direction of part of the wave energy from the normal line-of-sight path. This change makes it possible to receive energy around the edges of an obstacle at some distances below the highest point of an obstruction. Although diffracted radio frequency (RF) energy is usually weak, and some signals can still be detected by a suitable receiver.

The principal effect of diffraction extends the radio range beyond the visible horizon. In certain cases, the use of high power and very low frequencies transmitters, radio waves can be made to encircle the Earth by diffraction. At high frequencies, diffraction, like reflection, depends on the geometry of the object as well as the amplitude, phase and polarization of the incident wave at the point of diffraction. Scattering occurs when the medium through which the wave traverses consist of objects with dimensions that are small compared to their wave length, and where the number of obstacles per unit volume is large. Scattered waves are produced by rough surface, small objects, and other irregularities in the channel. In practice, climatic conditions such as rainfall, mist, and fog can result in scattering of the signals transmitted in a radio communications system (Lin and Chen, 2009).

2.5 Reflection

Reflection of radio waves is a very common phenomenon that adversely distorts effective communication. When a radio wave propagated in one medium impinges upon another medium that have different electrical properties, the wave is reflected

and partially transmitted through the medium. If the plane wave is incident on a perfect dielectric, then part of the energy is transmitted into the second medium and part of the energy is reflected into the first medium and there is no loss of energy in absorption. In the case of a perfect conductor, all the incident energy is reflected into the first medium without loss of energy. The electric field intensity of the reflected and transmitted waves may be related to the incident wave in the medium of origin through Fresnel reflection coefficient denoted as (Γ). The reflection coefficient generally depends on factors such as the frequency of the propagating wave, the angle of incidence, and the wave polarization (Liebe, 1989) and (Crook, 1996).

The polarization of electromagnetic wave is very important in the analysis of the propagation of waves. Polarization is one of the properties of electromagnetic waves; the polarization of electromagnetic waves implies that the wave has instantaneous electric field components are orthogonal. A polarized wave are represented as the sum of two spatially orthogonal components. These components are in the vertical and horizontal direction and also classified as the left-hand and right-hand circularly polarized components.

2.5.1 Dielectrics Reflection

When the plane wave is incident on a perfect dielectric, then part of the energy is transmitted into the second medium and other portion of the energy is reflected back into the first medium and there is no loss of energy in absorption. Hence when an electromagnetic wave is incident on a plane existing between two dielectrics materials at an angle say θ_i part of the waves is reflected at a certain angle θ_r , while part of the signal is refracted at an angle θ_T into the next medium of different dielectric. It is clear to see that the plane of incidence now contains those signals incidence to the plane, those signals that are reflected from the plane and those that are refracted into the plane (Castanet, 2001) and (Chuang and Beard, 1990). The reflection of the signals varies with the direction of polarization of the Electric field or in short form the E-field. This reflection occurs in such a way that the

E-field is polarized either in parallel with the incidence plane or is perpendicular to the plane of incidence. When the E-field is polarized in parallel with plane of incidence, it implies that the E-field has its normal component with respect to the reflecting surface; on the other hand, when the polarization of the E-field is perpendicular to the incidence plane, it implies that the E-field is in such a direction to obey the thumb rule (Castanet, Deloues, and Lemorton, 2003).

Figure 6 shows an E-field in parallel with respect to the surface of plane of incidence while figure 7 shows an E-field perpendicular to the surface of the plane of incidence. The parameters $\varepsilon_1, \mu_1, \sigma_1$ represent permittivity, permeability and conductivity respectively of the first medium and $\varepsilon_2, \mu_2, \sigma_2$ respectively represent the permittivity, permeability, conductivity of the second medium. According to (Lin and Chen, 2009), the relative permittivity of medium ε_r is related to the permittivity of free space ε_0 and the dielectric constant for lossless material by the equation as shown below:

$$\varepsilon = \varepsilon_0 \varepsilon_r \quad (3)$$

where ε_0 , has a constant value of $8.85 \times 10^{-12} \text{F/m}$.

For a lossy dielectric material where there is absorption of power in the medium through which the material is propagated, the dielectric constant is given by the equation (4).

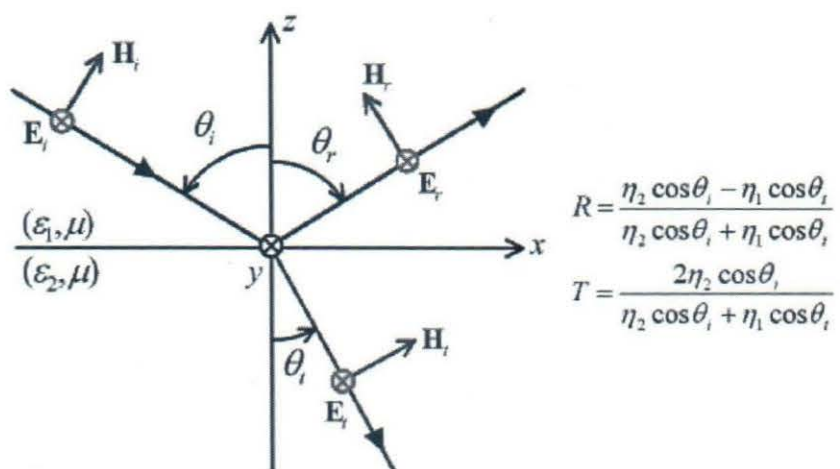


Figure 6: An E-field in parallel with respect to the surface of plane of incidence.

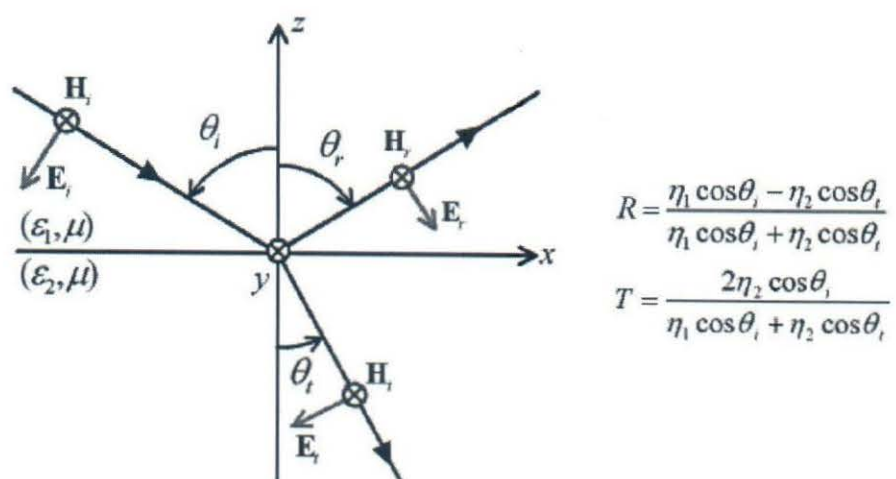


Figure 7: An E-field perpendicular to the surface of plane of incidence.

$$\varepsilon = \varepsilon_0 \varepsilon_r - j\varepsilon^y \quad (4)$$

$$\varepsilon^y = \frac{\sigma}{2\pi f} \quad (5)$$

The electric field intensity of the reflected and transmitted waves is related to the incident wave in the medium of origin through Fresnel coefficient given by (Γ) as mentioned earlier (Giuli, Toccafondi, Biffi Gentili, and Freni, 1991).

Fresnel reflection coefficient occurs in such a way that the E-field is polarized either horizontal with the incidence plane or is vertical to the surface of plane of incidence. In (Lin and Chen, 2009), the reflection coefficient for the horizontal e-field polarization at the boundary of two dielectric materials is given as:

$$\Gamma_{ue1} = \frac{E_r}{E_I} = \frac{\eta_2 \sin \theta_t - \eta_1 \sin \theta_i}{\eta_2 \sin \theta_t + \eta_1 \sin \theta_i} \quad (6)$$

that is

$$\theta_i = \theta_r \quad (9)$$

$$\Gamma E_i = E_r \quad (10)$$

Similarly,

$$E_t = (1 + \Gamma) \quad (11)$$

Γ can be either parallel or perpendicular depending on how E-field is polarized on the plane of incidence, whether in the horizontal or in the vertical direction as mentioned above. That is, whether the E-field is vertical or horizontal to the surface of the plane of incidence.

The reflection coefficient for the parallel and perpendicular polarization can be further simplified to equations (12) and (13) respectively based on the assumption that the first medium the wave is propagated is a free space and that $\mu_1 = \mu_2$.

$$\Gamma_{\text{vertical}} = \frac{\varepsilon_r \sin \theta_i - \sqrt{\varepsilon_r - \cos^2 \theta_i}}{\varepsilon_r \sin \theta_i + \sqrt{\varepsilon_r - \cos^2 \theta_i}} \quad (12)$$

$$\Gamma_{\text{horizontal}} = \frac{\varepsilon_r \sin \theta_i - \sqrt{\varepsilon_r - \cos^2 \theta_i}}{\varepsilon_r \sin \theta_i + \sqrt{\varepsilon_r - \cos^2 \theta_i}} \quad (13)$$

2.5.2 Ground Reflection Model (Two Rays)

The two rays ground reflection model is a useful propagation model that has its basis on geometric optics. This model considers the direct line of sight path as well as the ground reflection path between transmit and the receive antennas. Hence,

in treating a radio communication medium between a transmitter and receiver, a simple direct line of sight alone cannot form the only physical way through which radio signals are propagated. Thus free space is not adequate in carrying out this analysis. In analysis of long distance transmission of signals of relatively higher strength, the ground reflection model provides an accurate prediction for radio systems that use tall towers and direct line of sight channels in urban and sub-urban regions (Calla and Purohit, 1971), (Gremont, Filip, Gallois, and Bate, 1999). A flats earth approximation is assumed in cases where the distance from the transmitter and the receiver is only some few kilometres. The diagram for the two ray ground reflection is illustrated in figure 8 below. The transmitting antenna has a height of h_t and the height of the receiver denoted as h_r . If d_0 is some distance from the transmitter such that $d_0 < d$, then the E-field propagating through free space is as shown in equation (14)'

$$E(d, t) = E_0 \frac{d_0}{d} \cos \left(\omega_c \left(t - \frac{d}{c} \right) \right) \quad (14)$$

When this model is considered in the analysis of radio propagation as shown above, two paths through which the radio signals traverse to receive antenna will be considered. First, the direct waves travel a distance $d_i = i$ to the receiver and the reflected wave through a distance $d_r = x + x'$. Thus, for the direct wave, the E-field at the receiving end is given by:

$$E(d_i, t) = E_0 \frac{d_0}{d} \cos \left(\omega_c \left(t - \frac{d_i}{c} \right) \right) \quad (15)$$

Similarly, the E-field due to the ground reflected wave is given by the equation;

$$E(d_r, t) = \Gamma E_0 \frac{d_0}{d} \cos \left(\omega_c \left(t - \frac{d_r}{c} \right) \right) \quad (16)$$

Applying the boundary conditions and Maxwell's equations of (9), (10) and (11) to figure 8 then equation (17), (18) and (19) can be deduced as shown below:

$$\theta_i = \theta_g \quad (17)$$

$$E_g = \Gamma E_i \quad (18)$$

Similarly,

$$E_t = (1 + \Gamma) E_i \quad (19)$$

where, Γ is the ground reflection coefficient. The resultant E-field polarization and ground reflection ($\Gamma_{lar} = -1$ and $E_t = 0$) is the sum vector E_{los} and E_g hence the total E-field is given by equation (20) below:

$$|E_T| = |E_{los} + E_g| \quad (20)$$

where E_T is the total or resultant E-field. Putting equations (15) and (16) into equation (20), the total E-field becomes as shown in (21);

$$E_T(d, t) = E_0 \frac{d_0}{d} \cos \left(\omega_c \left(t - \frac{d_i}{c} \right) \right) + (-1) E_0 \frac{d_0}{d} \cos \left(\omega_c \left(t - \frac{d_r}{c} \right) \right) \quad (21)$$

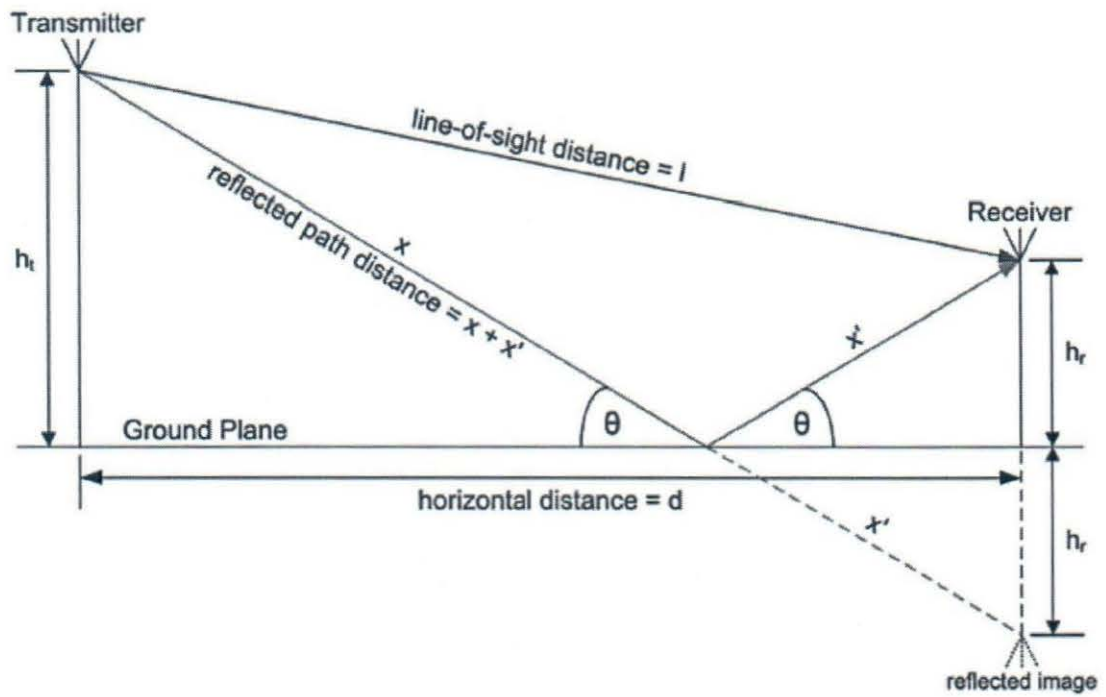


Figure 8: A ground reflection model (Two Ways)

From figure 8, it can easily be seen that the two rays are out of phase due to difference in path length and due to phase shifts at the reflection area. If Δ is the path difference between the liner sight and the ground reflected paths, then it can be represented by equation as shown below:

$$\Delta = d_r - d_i \quad (22)$$

From geometry of figure 8, the path along the line of sight d_r is obtained as

$$d_r = \sqrt{(h_t + h_r)^2 + d^2} \quad (23)$$

Similarly,

$$d_i = \sqrt{(h_t - h_r)^2 + d^2} \quad (24)$$

Thus, putting equations (23) and (24) into equation (22), the result is as shown below;

$$\Delta = \sqrt{(h_t + h_r)^2 + d^2} - \sqrt{(h_t - h_r)^2 + d^2} \quad (25)$$

The path difference is further simplified by Taylor's series approximation when the distance of the separation between the transmitter and the receiver is large compared to the sum of the height of transmitter and the receiver. Hence equation (25) becomes

$$\Delta = \frac{2h_t h_r}{d} \quad (26)$$

The phase difference between the direct and the ground-reflected wave is found from the two-ray approximation considering only a line-of-sight and a ground reflection. Denoting the transmit and receive antenna heights as h_t and h_r respec-

tively, the phase difference can be expressed as

$$\Delta_{ph} = \frac{2\pi\Delta}{\lambda} = \frac{\Delta\omega_c}{C} \quad (27)$$

where

$$\frac{2\pi C}{\lambda} = 2\pi f_c = \omega_c \quad (28)$$

The time delay, denoted as τ_d between the arrival of the two E-field components can also be calculated once the path difference and the phase difference are known. Hence the time delay is as shown in equation (29).

$$\tau_d = \frac{\Delta}{C} = \frac{\Delta_{ph}}{2\pi f_c} \quad (29)$$

The difference between the distances d_r and d_i are severely affected when the distance between transmit and the receive antennas become very large; this causes the differences between the distances d_r and d_i to become very small and thus the magnitudes of the E_{los} and E_g become almost identical and differ only in the phase shift.

$$\left| \frac{E_0 d_0}{d} \right| = \left| \frac{E_0 d_0}{d_r} \right| = \left| \frac{E_0 d_0}{d_i} \right| \quad (30)$$

Evaluating the E-field at a certain delay time say $\tau = \frac{d_r}{c}$ the resultant E-field will be as shown below

$$\begin{aligned} E_T \left(d, \frac{d_r}{c} \right) &= E_0 \frac{d_0}{d} \cos \left(\omega_c \left(\frac{d_r}{c} - \frac{d_i}{c} \right) \right) + \\ &+ (-1) E_0 \frac{d_0}{d} \cos \left(\omega_c \left(\frac{d_r}{c} - \frac{d_i}{c} \right) \right) \end{aligned} \quad (31)$$

$$E_T \left(d, \frac{d_r}{c} \right) = E_0 \frac{d_0}{d} \cos \left(\omega_c \left(\frac{d_r - d_i}{C} \right) \right) - E_0 \frac{d_0}{d} \cos 0 \quad (32)$$

Hence, equation (32) can be further reduced when the direct and the ground reflected rays combine; the total E-field at the receive antenna is given by

$$|E_T| = \frac{E_0 d_0}{d} \sqrt{2 - 2 \cos \Delta_{ph}} \quad (33)$$

Hence, applying trigonometric identities

$$|E_T| = 2 \frac{E_0 d_0}{d} \sin \left(\frac{\Delta_{ph}}{2} \right) \quad (34)$$

Equation (26) can be further reduced as shown below; this depends on the distance of separation between the transmit and the receive antenna. Thus if

$$d > \frac{20\pi h_t h_r}{3\lambda} = \frac{20 \times 3.142 h_t h_r}{3\lambda} = \frac{20 h_t h_r}{\lambda} \quad (35)$$

then the E-field can be further simplified if the value of the separation between the two antennas, d (m), satisfies equation (36) and thus can be approximated by

$$E_T 2 \frac{E_0 d_0}{d} \cdot \frac{2\pi h_t h_r}{d\lambda} = \frac{K}{d^2} \quad (36)$$

K is a constant related to transmit and receive antenna heights, the wavelength and the E-field due to the ground reflection.

Manipulation of some equation relating to the free space power received at a distance d , the received power for the two-ray ground model can be obtained as

$$P_r = P_t G_t G_r \frac{h_t^2 h_r^2}{d^2} P_r \quad (37)$$

P_r is the received power at a distance d from the transmitter, P_t is the power transmitted, G_t and G_r are the gains of the transmit and the receive antennas respectively.

2.6 Scattering of radio waves

Scattering of radio waves within the troposphere is caused when a radio wave impinges an irregular surface and the energy reflected is spread out in all directions. Thus, the actual received signal in a mobile radio environment is often stronger than what is predicted by just reflected. Natural phenomenon such as rainfall, humidity, trees can scatter radio waves and throw them in all directions, this paves way for additional energy at the receiver, (Lin and Chen, 2009), (Dru-fuca, 1974). Scattering of radio waves depends primarily on the surface at which the waves come in contact with. For flat and smooth surfaces, the dimension is much larger compared to the wavelength, thus can be modelled as reflective surfaces. For rough surfaces, there exist induced propagation effects different from ordinary reflection discussed above and it is measured using Rayleigh scattering criterion. The Rayleigh criterion defines a critical height denoted by h_c of the surface protuberances for any given angle of incidence θ_i and is given by

$$h_c = \frac{\lambda}{8 \sin \theta_i} \quad (38)$$

If a surface has its maximum to minimum protuberances h such that h is less than h_c then the surface is considered to be smooth; on the other hand, if the protuberance is greater than h_c , the surface is considered to be rough. Also, to take care of the diminishing reflection field, the flat surface reflection coefficient has to be multiplied by a scattering loss factor denoted as ρ_s and is obtained according to (Lin and Chen, 2009) as shown below

$$\rho_s = \exp \left[-8 \left(\frac{\pi \delta_h \sin \theta_i}{\lambda} \right)^2 \right] \quad (39)$$

where δ_h is the standard deviation of the surface height. This equation can be further modified as shown according to (Lin and Chen, 2009).

$$\rho_s = \exp \left[-8 \left(\frac{\pi \delta_h \sin \theta_i}{\lambda} \right)^2 \right] l_0 \left[8 \left(\frac{\pi \delta_h \sin \theta_i}{\lambda} \right)^2 \right] \quad (40)$$

where l_0 is the Bessel function of the first kind and zero order.

Reflected E-fields for $h > h_c$ can be solved for rough surfaces using modified reflection coefficient as given below:

$$Rough = \rho_s r \quad (41)$$

2.7 Radio Propagation Models

Radio propagation models are empirical in nature because they are developed based on large collections of data for the specific scenario. For any model, the collection of data has to be sufficiently large to provide enough likeliness or scope to all kind of situations that can happen in that specific scenario. Similar to all empirical models, radio propagation models do not point out the exact performance of a link, rather, they predict the most likely behaviour the link may exhibit under the specified conditions. A single model is usually developed to predict the behaviour of propagation for all similar links under similar constraints (Dossi, 1990) and (Van de Kamp, 1999). These models are created with the goal of formalizing the way radio waves are propagated from one place to another. The models typically predict the path loss along a link or the effective coverage area of a transmitter. The radio propagation models also typically focus on realization of the path loss with the auxiliary task or predicting the area of coverage for a transmitter or modelling the distribution of signals over different regions. There are several various models that are used to estimate and predict the transmission path loss of a free space and thus improve propagation of radio transmission. These models have been developed to meet the needs of realizing the propagation behaviour under different conditions (Illingworth, 2004). The following subsections highlights various models for radio

propagation included in this thesis work.

2.7.1 COST-Hata-Model

The COST-Hata-Model also known as Hata Model PCS Extension is based on Okumura Model and the most often cited of the COST 231 models. It extends the Hata Model to cover a more elaborated range of frequencies. Coperation europeenne dans le domaine de la recherché Scientifique et Technique (COST) is a European Union Forum for cooperative scientific research which has developed this model accordingly to various experiments and researches (Lin and Chen, 2009). This model is applicable to urban areas. To further evaluate Path Loss in Suburban and Rural Quasi-open/open Areas, this path loss has to be substituted into Urban to Rural and Urban to Suburban Conversions. The COST-Hata-Model is formulated as,

$$L = 46.3 + 33.9 \log f - 13.82 \log h_B - a(h_R) + [44.9 - 66.5 \log h_B] \log d + C \quad (42)$$

$$a(h_R) = (1.1 \log f - 0.7) h_R - (1.56 \log f - 0.8) \quad (43)$$

$$C = \begin{cases} 0\text{dB} & \text{for medium cities and suburban areas} \\ 3\text{db} & \text{for metropolitan areas} \end{cases} \quad (44)$$

where, L is Median path loss, Unit: Decibel (dB), f is Frequency of Transmission. H_B is Base Station Antenna effective height. d is Link distance. h_R is Mobile Station Antenna effective height. ah_R is Mobile station Antenna height correction factor as described in the Hata Model for Urban Areas. This mode has a limitation that, the base station antenna is higher than all adjacent rooftops.

2.7.2 Egli Model

The Egli Model is a terrain model for radio frequency propagation. This model was first introduced by John Egli in 1957, was derived from real-world data on UHF and VHF television transmission in several large cities. It predicts the total path loss for a point-to-point link and used for outdoor line-of-sight transmission, this model provides the path loss as a single quantity. The Egli model is normally suitable for cellular communication scenarios where one antenna is fixed and another is mobile. The model is applicable to scenarios where the transmission has to go over an irregular terrain. However, the model does not take into account travel through some vegetative obstruction, such as trees and shrubbery. The model is usually applied to VHF and UHF spectrum transmissions and the Egli model is formally expressed as:

$$L = G_B G_M \left[\frac{h_b h_M}{d^2} \right]^2 \left[\frac{40}{f} \right]^2 \quad (45)$$

where, G_B is Gain of the base station antenna, G_M is Gain of the mobile station antenna, h_B is height of the base station antenna (m), h_M is Height of the mobile station antenna (m), d is Distance from base station antenna (m), f is Frequency of transmission (MHz). This model predicts the path loss as a whole and does not subdivide the loss into free space loss and other losses.

2.7.3 Young Model

Young model is classified as radio propagation model that was built on the data collected on New York City. It typically models the behaviour of cellular communication systems in large cities. It covers a frequency ranging from 150 MHz to 3700 MHz and the model was built on the data of 1952 in New York City (Lin and Chen, 2009). It is as shown below:

$$L = G_B G_M \left[\frac{h_B h_M}{d^2} \right]^2 \beta \quad (46)$$

Here, L is the median path loss (dB), L_0 is the reference path loss along 1 km (dB), γ is the slope of the path loss curve (decibels per decade), d is the distance on which the path loss is to be calculated (km), F_A is Adjustment factor, H_{ET} is the Effective height of terrain (m)

2.7.7 ITU Terrain Model

The ITU Terrain Loss Model is a radio propagation model that provides a method to predict the median path loss of a telecommunication link. Developed on the basis of diffraction theory, the model predicts the path loss as a function of the height of path blockage and the First Fresnel zone or the transmission link (ITU, 2006). The model is applicable on any terrain and accounts for obstructions in the middle of the telecommunication link, and therefore, is suitable to be used inside cities as well as in open fields. It is ideal for modelling a line-of-sight link in any terrain. The model is mathematically formulated as

$$A = 10 - 20C_N \quad (49)$$

$$C_N = \frac{h}{F_1} \quad (50)$$

$$H = h_L - h_0 \quad (51)$$

$$F_1 = 17.3 \sqrt{\frac{d_1 d_2}{fd}} \quad (52)$$

where,

- A = Additional loss (in excess of free-space loss) due to diffraction (dB);

- C_N = Normalized terrain clearance;
- H = The height difference (negative in the case that the LOS path is; completely obscured) (m);
- h_L = Height of the line-of-sight link (m);
- h_0 = Height of the obstruction (m);
- F_1 = Radius of the first Fresnel zone (m);
- d_2 = Distance of obstruction from the other terminal (km);
- f = Frequency of transmission (GHz);
- d = Distance from transmitter to receiver (km);

2.7.8 Weissberger's Model

Weissberger's modified exponential decay model code-named Weissberger's model, is a radio wave propagation model that estimates the path loss due to the presence of one or more trees in a point-to-point telecommunication link. This model belongs to the category: Foliage or Vegetation models, and is applicable to the cases of line of sight propagation. Example is microwave transmission. The model is only applicable when there is an obstruction made by some foliage in the link; that is in between the transmitter and receiver (Lin and Chen, 2009). The model is ideal for application in station where the line of sight (LoS) path is blocked by dense, dry and leafy trees. The Weissberger's model is significant for frequency ranging from 230MHz to 95GHz only and useful up to a foliage depth of 400m. Weissberger's model was formulated in 1982, and it is development of the ITU Model for Exponential Decay (MED). Weissberger's model is formally expressed as by the equation:

$$L = \begin{cases} 1.33f^{0.284}d^{0.588}, & \text{if } 14 < d \leq 400 \\ 0.45f^{0.284}d, & \text{if } 0 < d \leq 14 \end{cases} \quad (53)$$

horizontal attenuation. The link consists of a transmitter operating at a frequency of 35GHz and a receiver operating at the same frequency. In their experiment, they placed a rain gauge, and dust particle near the receiver to avoid shadowing effect due to nearby objects. The specification of the LoS link can also be used for the horizontal path attenuation (Berne and Uijlenhoet, 2007). The vertical path attenuation was then estimated by subtracting clear sky attenuation (free space) from excess attenuation (rainy medium) due to rain. They calculated the slant path using rain height (H_G) and is given as shown below

$$H_G = \frac{A_H}{\alpha} \quad (57)$$

where A_H is the total zenith attenuation, α is specific attenuation.

The horizontal path attenuation according to this group resulted in calculating the effective path length l_{eff} which is a function of the rain rate, link distance and is given as

$$l_{eff} = La_t R^{bt} = \frac{A}{a}. \quad (58)$$

The combination of vertical and horizontal path attenuations give the slant path attenuation as shown below

$$A_s = \int_0^L a(s)ds, \quad (59)$$

A_s is the slant path attenuation, S is the distance along the path, and $a(s)$ is the specific attenuation

(Henry et al., 2007) researched on rain induced bi-static scattering at 60GHz. The group used first order multiple scattering which assumes that the wave interacts only with one particle and suffers attenuation on its way from the transmitter to the receiver. In their work, they operated at 94GHz as proposed by (Gloaguen

and Lawergnat, 1996) and (Liebe, 1989). The first order multiple scattering approximation is applicable to the scattering at 60 GHz. Hence they used the bi-static radar equation (BRE) for the particle scattering by rain which is shown bellow

$$\frac{P_r}{P_t} = \iiint \frac{\lambda G_t G_r A_1 A_2}{V_c (4\pi)^2 R_1^2 R_2^2} \rho \sigma_{bi} \exp(-y_1 - y_2) dv, \quad (60)$$

P_r is the received power, P_t is the transmitted power, V_c is the common volume, G_t is the transmit antenna gain, G_r is the receiver antenna gain, A_2 is the attenuation of the path from the common volume to the receiver and A_1 is the attenuation of the path from the transmitter to the common volume. During the development of the model, results were regularly checked with the program Mie-plot. A good agreement between the model and the results of Mie-plot was found (Henry et al., 2007).

Ojo, Adewole, and Sarkar (2008) researched on rain rate and rain attenuation prediction for satellite communication in Ku and Ka bands over Nigeria. They used a model that was developed by Moupfouma and Martins to predict rain rate and concluded that the model is good for tropical and temperate climate (Moupfouma and Martin, 1995). The map for the rain attenuation over Nigeria was developed using ITU rain attenuation (Crane, 1990). The results obtained from their research confirm that 0.1% of time of rain attenuation is needed for Very Small Aperture Terminal (VSAT) network service availability. The group therefore concluded that the information from the map will be useful in the preliminary design of both terrestrial and earth satellite links, and to provide a broad idea of rain attenuation to microwave engineers for a proposed launching of satellites in Nigeria.

(Capsoni et al., 1987) researched on the multiple excel model for the prediction of the radio interference due to hydrometer scattering. They used physically-based method for the prediction of the radio interference due to hydrometer scattering. The coupling-by-scattering mechanism allows for evaluation of interference levels when the electrical and geometrical characteristics as well as the distribution of scatterers in the common volume are known. Hence, the solution to population of

isolated exponential rain cells (EXCELL) model which generates complex synthetic rain fields reflecting the total first and second order features of the rainfall process (Capsoni, Luni, Paraboni, and Riva, 2006).

The accuracy of the model for estimating the path loss was tested by comparing the results of the model with the DBSEB database provided by ITU-R. The comparison pointed out the benefits of introducing a new model called multi-cell. The results indicated that synthetic rain fields can be correctly used to estimate the amount of attenuation experienced by the propagating wave along the transmitter-scatter and scatter-receiver path.

Saikia, Devi, Barbara, and Sarmar (2009) worked on rain attenuation of centimetre radio waves in which they used the laser disdrometer for calibrating and profiling of rain drop size distribution. The rain drop signature is extracted by allowing the drops to pass through a controlled field of view of a sensor. The laser beam was used as the signal source, the photo-transistor was used as detector-cum-amplifier and optical fibre as trans-receiving ports. Rain drop size and rain rate at different weather condition were measured. The specific attenuation of the line of sight radio signals at 10-30 GHz of various drop diameters were then calculated using standard attenuation equations and model values of scattering function. The attenuation values were then compared with those given by the model shown in equation below

$$A = .3434x10^3 \int_0^{\infty} \lambda f(D) N(D) dD \quad (61)$$

where A is the specific rain attenuation, f is a *complex scattering function* and λ is the signal wavelength. The result of the research showed that rain attenuation calculated by using imaginary part of scattering function matches with values of the existing model for rain rate below $100mmhr^{-1}$. Thus, both approaches is used for calculating rain attenuation in the frequency ranging from 10 to 30 GHz. It was found that the contribution to specific attenuation is mainly limited to rain drops of diameter not exceeding 2mm within the frequency range of consideration.



Okumura model noted in (John and Seybold, 2005) studies for urban area is a radio propagating model that was built using data collected in the city of Tokyo, Japan. The model is ideal for use in cities with many urban structures but not many tall blocking structures. The model served as a base for the Hata model. The Okumura model was built into three models, the models for urban, suburban and open areas. The model for urban areas was built first and used as the base for others. The Okumura model is formally expressed as in equation (47).

Chapter 3

METHODOLOGY

3.1 Introduction

Chapter three deals with the methodological approach and strategies to be used to achieve the objectives of this study. Research methodology is a tool that provides scaffolding structures for the validation, proper analysis and interpretation of data towards guiding a researcher for the realization of the set goal and objectives. It is simply the various processes, procedures, methods and instrumentalities, by which data are secured, specified, collated, processed and analysed.

This chapter focus on the process of deriving the mathematical model for rain attenuation in Nigeria. The scenario of attenuation of radio signals in rain would be examined in section 3.2 and the total cross session would be obtained from the scattered and absorbed radio signals as they traverse in rain. Consideration would be given for the rain drop size and shape; then the model formulation would start with an illustration of the volume extracted from the transmitter power emission. The total power, absorbed power and scattered power would then be estimated from the power density of the emitted radiation in a spherical wave generated from a spherical beam cone formed by the emitted power. Considering the radiation pattern, the rain attenuation model would finally be derived.

3.2 Attenuation by Rain

Communication in frequencies above 10 GHz in centimetre and millimetre wave length region suffers severe impairment due to rain attenuation, and in some situations the signals may be completely lost (Walsch and Bertoni, 1998), (Barksdale, 1987) and (Tzler, 1994). Although studies of rain attenuation of microwave signals have been conducted in Europe and the United States dating back to the 1940s, it is now common knowledge that the rain-attenuation models and raindrop size distribution models are highly region-dependent (Laboratory, 1990), (Committee, 1996). Therefore, there is a serious need that rain-attenuation models and raindrop

size distribution models be developed for different climatic environments. Careful design and adequate rain margins are essential for successful system performance. The attenuation of radio signals by rain is mainly the interaction of the radio signals with rain. In reality, attenuation by raindrops is greater than attenuation due to any other form of precipitation. Attenuation of radio signals is caused mainly by absorption of the radio signals, in which the raindrop acting as a poor dielectric, absorbs power from the radio wave and dissipates the power by heat loss and by scattering (Zinevich, Alpert, and Messer, 2008) and (Watson et al., 1999).

Attenuation by raindrop is due to scattering and absorption, greater percentage of the attenuation is caused by scattering than by absorption at frequencies above 100 megahertz. The diagram in figure 9 illustrates the scattering of radio waves by raindrops. In the process, a drop of rain is shown by a spherical shape which assumes the shape of tears.

As seen in figure 9, some of the signals (wave front) from the transmit antenna are being scattered in diverse directions, some are being absorbed by the rain drop; which acts as a poor dielectric, absorbing power from the radio wave and dissipating the power by heat loss (Townsend and Watson, 2011).

In analysing the attenuation caused by rainfall, it is imperative to take into cognizance the scattering cross section, σ_{sc} , and the absorption cross section σ_{ab} , for a drop size at different frequencies. The bracket denotes the estimated value of the scattering cross section and the cross section due to absorption respectively. The extinction, total, cross section is the sum of the scattering and absorbing cross sections for a drop of rain fall which can be denoted as σ_{total} and can be as shown in equation (62) .

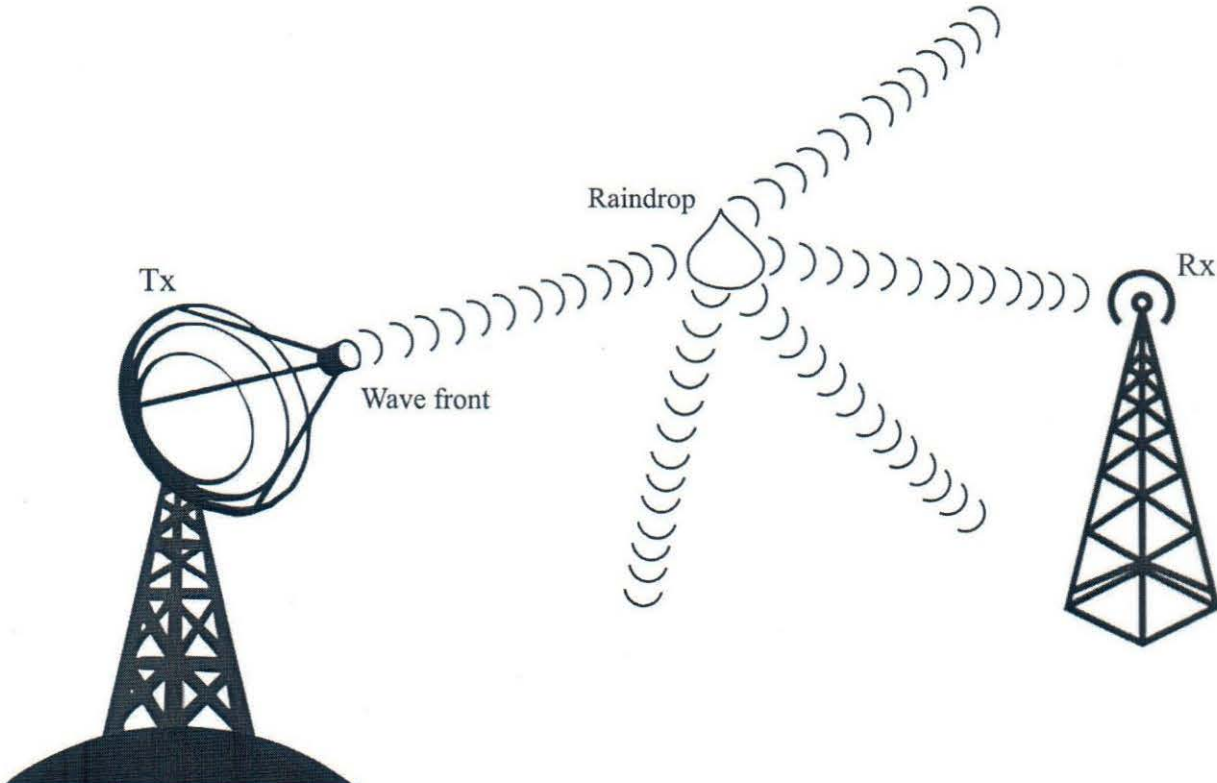


Figure 9: Scattering of radio signals by rain drops

$$\sigma_{total} = \sigma_{sc} + \sigma_{ab} \quad (62)$$

The extinction cross section for the rain drop is important in estimating the attenuation due to rainfall for any given raindrop size distribution, (Savic, 1953). As mentioned above, the power loss from the signals is mainly due to scattering of the electromagnetic waves incident on the rain drop and also due to absorption from poor dielectric of the rain drop; thus, the total power loss due to scattering of signals and absorption by drops of rain can be assumed to be as shown in equation (63) below,

$$P_{total} = P_{sc} + P_{ab} \quad (63)$$

3.3 Consideration for the Shape of Rain Drop

The tear drop shape of the raindrop applies as the drop falls from a surface and would then take a spherical form, and distort to a shape like an oblate spheroid referred to as a hamburger shape. This is mainly because of the drag force on the falling drop using it to be flattened (figure 2 and 3 and other factors that give a raindrop its shape. Five key factors commonly agreed to affect the raindrop shape are surface tension, hydrostatic pressure, aerodynamic pressure, internal circulation and electric stress (Joss and Gori, 1978) (Kubesh and Beard, 1993).

To carry out the analysis in this work, and derive an expression for the attenuation of the electric field that propagates through drops of rainfall, one assumes an oblate spheroid shape for a drop of rain, (Waterman, 1969).

3.4 Raindrop Size Distribution

Raindrop size distribution function have a great difference in various regions. There are many raindrop size distributions used in the calculation of possible specific attenuation values. The Laws and Parsons (LP) distribution (Laws and Par-

sons, 1943) is a reasonable choice for a mean drop-size spectrum in continental temperate rainfall at a rain rate below about 35 mm/h. The Marshall-Palmer (MP) distribution is most applicable to widespread rain, in the lower rain-rate range, in continental temperate climates at a rain rate from 1 to 50 mm/h. The "Thunderstorm" (J-T) distribution was fitted to the average drop-size spectrum measured in convective rain (in the higher rain-rate range) (Laws and Parsons, 1943). Singapore's tropical distribution was fitted by (Lin and Chen, 2009) (Joss, Thams, and Waldvogel, 1968) for rain rate in the range from 1 to 50 mm/h (Kliche, Smith, and Johnson, 2007), (Townsend, Watson, and Hodges, 2009). The raindrop size distribution in most rain is approximately described by a theoretical distribution having the negative exponential form which will be used in this work and is given by

$$N(d) = N_0 e^{-(\Lambda a)}, \quad \Lambda = \alpha R^{-\beta} \quad (64)$$

Where N_0 , α , β are constants and R is the rain rate in millimetres per hour, a is the rain drop radius (Kliche, Smith, and Johnson, 2006) and (Kubesh and Beard, 1993).

3.5 The Proposed Model

In deriving the attenuation of electromagnetic waves traversing through rain, consideration is given to a volume, which is bounded by the volume of a cone of the power flux lines and two spherical surfaces; that is the volume extracted from the power emitted from the transmitter, (Barber and Yeh, 1975) as shown in figure 10. P_i corresponds to the component of power emitted from the transmitter (that is the source power). Some of the powers are absorbed in the volume while some are scattered by the different components in the volume (Tzler, 1994). Those components of power that are not neither scattered nor absorbed in the volume is refracted and then reaches the transmitter (Tzler, 1994).

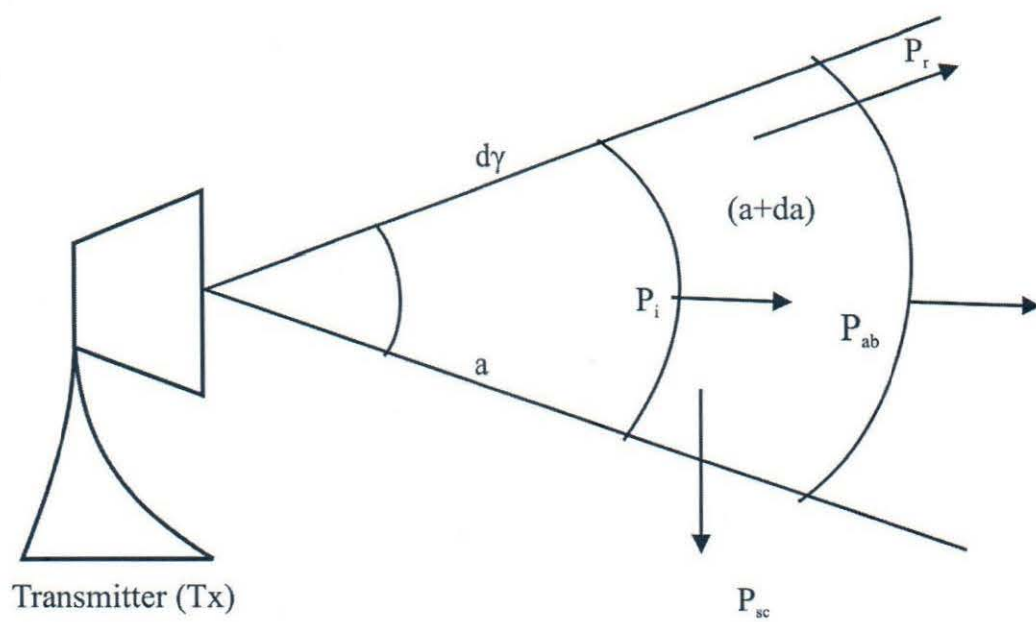


Figure 10: Volume extracted from the transmitter-power emission.

If P_{sc} represents the power that is scattered by the component of rain drops in the volume, P_{ab} represents the component of power that is absorbed by rain drops in the volume, and P_r represents that component of power that is refracted or transmitted (one that reaches that receiver). Then, the power balance in the beam is given by Walsch and Bertoni [1998]

$$P_i - P_r = P_{sc} + P_{ab}. \quad (65)$$

This equation can be rewritten as $P_i = P_{sc} + P_{ab} + P_r$ therefore

$$P_i = P_r + P_{total} \quad (66)$$

The equation is feasible because, the incident power P_i radiated from the source is split into various components of power as the waves come in contact with a drop of rain (Tzler, 1994). Each of the power components can therefore be expressed in terms of the time average poynting vector. Hence, the flux of electromagnetic energy radiated from a current source at far distances is given by the time-average poynting vector, calculated in terms of the radiation fields W (Barksdale, 1987) (Appendix A)

$$W_{av}(a) = \{W(a, t)\} = \frac{1}{2R_e} \{E(a, w) \times H^*(a, w)\}. \quad (67)$$

The equation of the time average poynting vector gives the value of the power density ($\frac{w}{m^2}$). Hence each component of the power can be easily evaluated in terms of the time average poynting vector

$$P_i = W_{av}(a) \cdot n a^2 d\Omega. \quad (68)$$

In this case, n is the normal of the first surface and $a^2 d\Omega$ is the spherical surface area where $d\Omega$ is the differential solid angle and is equal to $d\Omega = \sin\theta d\theta d\phi$. The symmetry is spherical, thus the projection of the average power density is the same

as the average power density (Tzler, 1994) and (James, 1993).

$$W_{av}(a) = W_{av}(a) \cdot n \quad (69)$$

Each component of power can therefore be expressed in terms of the time average poynting vector (Ulaby and El-Rayes, 1987). To obtain the various components of power discussed earlier on, consideration is given to the drop size distribution denoted as $N(d)$, the scattering and absorption cross sessions in the volume in which the signal is scattered or absorbed. The scattering cross section is the region within which the signal is scattered in the volume and is denoted as σ_{sc} while the region or area within which the signal is absorbed by the rain drop in the volume is denoted as σ_{ab} (Oguchi, 1991). Hence the total cross section of scattering and absorption of the signal in the volume is the sum of the scattering and absorbing cross sections as earlier mentioned in equation (62) and is given by

$$\sigma_{total} = \sigma_{sc} + \sigma_{ab} \quad (70)$$

This leads to the assumption that the total power loss due to scattering and absorption is as mentioned earlier (Barnett, 1972). The power loss due to scattering can be obtained by multiplying the average power density, $w(a)$, the volume in which the signal is scattered, v , the drop size distribution, $N(d)$, and the scattering cross section, σ_{sc} (Tzler, 1994). Hence

$$P_{sc} = W(a)VN(d)\sigma_{sc} \quad (71)$$

Similarly, the power absorbed by rain drops is obtained as

$$P_{ab} = W(a)VN(d)\sigma_{ab} \quad (72)$$

The volume, V can therefore be approximated by $a^2dad\Omega$; that is multiplying the surface area by the solid angle (Ulaby and El-Rayes, 1987). Hence equations (71)

and (72) respectively becomes

$$P_{sc} = W(a)a_2dad\gamma N(d)\sigma_{sc} \quad (73)$$

and

$$P_{ab} = W(a)a_2dad\gamma N(d)\sigma_{ab} \quad (74)$$

where $a_2d\gamma$ is the surface area of the spherical beam and $a_2dad\gamma$ equals V and is equivalent to the volume of spherical beam cone formed by the power source. Finally, the power received by the antenna is evaluated to be

$$P_r = W(a+da)(a+da)^2d\gamma \quad (75)$$

Combining equations (71) and (72), the total power loss due to scattering and absorption of radio signals can be obtained; thus, equation ((63) becomes

$$\begin{aligned} P_{total} &= W(a)VN(d)\sigma_{ab} + W(a)VN(d)\sigma_{sc} = \\ &= W(a)a_2dad\gamma N(d)\sigma_{ab} + W(a)a_2dad\gamma N(d)\sigma_{sc} = \\ &= W(a)a_2dad\gamma N(d)(\sigma_{ab} + \sigma_{sc}) \end{aligned} \quad (76)$$

Putting equations (73), (74) and (75) into equation (66) yields

$$W(a)a^2d\gamma = W(a+da)(a+da)^2d\gamma + W(a)a^2dad\gamma N(d)(\sigma_{ab} + \sigma_{sc}) \quad (77)$$

Equation (77) can be simplified to give (78) as shown below;

$$\begin{aligned} \frac{W(a)(a+da)(a+da)^2 + a^2W(a)}{da} + \\ + a^2W(a)N(d)(\sigma_{ab} + \sigma_{sc}) = 0 \end{aligned} \quad (78)$$

Considering equation (70), this equation can be rewritten as

$$\frac{W(a)(a+da)(a+da)^2 + a^2W(a)}{da} + a^2W(a)N(d)\sigma_{total} = 0 \quad (79)$$

We can expand $(a+da)^2$ in equation ((79) further by using Taylor's series expansion to yield;

$$(a+da)^2 = a^2 \left(1 + \frac{da}{a}\right)^2 = a^2 \left(1 + 2\frac{da}{a}\right) = a^2 + da, \text{ for } \frac{da}{a} \ll 1$$

This reduces equation (79) into

$$\begin{aligned} & \frac{W(a)(a+da)(a+da)^2 + a^2W(a)}{da} + 2W(a)(a+da) + \\ & + a^2WN(d)\sigma_{total} = 0, \quad da \rightarrow 0 \end{aligned} \quad (80)$$

For further simplification of the equation, we shall take limits as da tends towards zero; $da \rightarrow 0$. Thus, equation (80) condenses into equation (81) is a differential equation for the power received or transmitted by the antenna is considered; hence the equation is as shown below

$$\frac{dW(a)a^3}{da} + 2aW(a) + a^2W(a)N(d)\sigma_{total} = 0 \quad (81)$$

This equation is of the second order differential equation and can better be simplified and rewritten as shown in the second order differential equation. Hence

$$W(a) = \frac{ce^{-[N(d)\sigma_{total}]a}}{a^2} \quad (82)$$

where c is constant that is arbitrary and can be computed from power density of the emitted radiation in a spherical wave generated from a spherical beam cone formed by the emitted power.

Putting equation (87) into equation (82), we have;

$$W(a) = \frac{P_s e^{-(N(d)\sigma_{total})a}}{4\pi a^2} a \neq 0 \quad (88)$$

However, an isotopic antenna is realizable in practice and is useful only for comparison purposes. A more practical type is the directional antenna which radiates more power in some directions and less power in other directions (Kirdyashav, Chuckhlantsev, and Sutko, 1979). A special case of the directional antenna is the omni-directional antenna whose radiation pattern may be constant in one plane (E-plane) and varies in an orthogonal plane (H-plane). Hence a directional antenna radiates electromagnetic waves in a more desirable direction as well as less desirable directions. This radiation are grouped into main lobes and minor lobes; therefore, the radiation lobe containing the direction of maximum impact is known as the main lobe whereas all other lobes are called minor lobes. These other lobes represent the radiation in undesired directions. The level of the minor lobes is usually expressed as a ratio of the power density in the lobe in question to that of the major lobe. This ratio is known as the side lobe level. It is interesting to know that the main lobe always points in the direction where the antenna is designed to have its maximum radiation. The region of maximum radiation is specified by the half power beam width which specifies and describes the sharpness of the antenna. This gives the antenna the ability to radiate power in a more focus direction, thereby, giving rise to the ability of the antenna to direct radiated power in a specific direction. Thus, commonly used parameter to measure the overall ability of an antenna to direct radiated power in a given direction is dimensionless quantity known as the directive gain. The directive gain is defined in terms of the radiation intensity. The radiation intensity, $I(\theta, \phi)$ is the time average power per unit solid angle. Since there are a^2 square meters for each unit solid angle, radiation intensity $I(\theta, \phi)$ equals a^2 multiplied by the magnitude of the time-average

poyniting vector W_{av} (Kirdyashav et al., 1979). Therefore,

$$I(\theta, \phi) = a^2 W_{av}(a, \theta, \phi) \quad (89)$$

The total radiated time-average power P_s is related with the radiation intensity hence given by

$$P_s = \oint I(\theta, \varphi) d\Omega \quad (90)$$

where $d\Omega$ is the vector differential surface and W is the magnitude of the time-average power is related with the poyniting vector (watts/m²).

The Directive Gain (G) is defined as the ratio of radiation intensity due to the test antenna to isotropic antenna (hypothetical antenna that radiates uniformly in all direction) can be written as;

$$G = \frac{4\pi U}{P_{radiated}} = \frac{4\pi U(\theta, \varphi)}{\oint U(\theta, \varphi) d\gamma} = \frac{4\pi U(\theta, \varphi)}{P_s} \quad (91)$$

As seen in equation (90), the directive gain G is defined in terms of the radiation intensity. Since the antenna has the ability to direct radiated power in a given direction and the directive gain of the antenna also has a major role to play in the quality and quantity of the signals obtained by the receiver. Furthermore, the directive gain $G_d(\theta, \phi)$ of an antenna pattern is therefore the ratio of the radiation intensity in the direction (θ, ϕ) to the average radiation intensity

$$G_d = \frac{I(\theta, \varphi)}{P_s/4\pi} \quad (92)$$

Since the radiation from the antenna is not uniformly distributed, the expression of the attenuated time-average power density of equation (88), has to be improved on to consider this properly. Substituting equation (89) into equation (92) yields

$$W_{av}(a, \theta, \varphi) = \frac{P_s}{4\pi a^2} G_d(\theta, \varphi)$$

This equation for the transmitted time-average power density in free space, which can be used to restate equation (89) which yields

$$W_{av}(a) = \frac{P_s e^{-(N(d)\sigma_{total})a}}{4\pi a^2} G_d(\theta, \varphi), \quad a \neq 0 \quad (93)$$

If a receiving antenna is used to measure the transmitted power P_t at a distance “ a ” from the transmitter, that is the power is neither absorbed nor scattered in the volume; the properties of the receiving antenna have to be considered (Kirdyashav et al., 1979) (Abramowitz and Stegun, 1965). The incident waves are being received in an area that is small compared to the physical area of the receiving antenna. This is the effective area $A_e(\theta, \phi)$ of the antenna and is defined as the ratio of the average power delivered to a matched load to the time-average power density of the incident wave (Kirdyashav et al., 1979). Hence

$$P_L = W a_e(\theta, \phi) \quad (94)$$

Where P_L is the maximum average power transferred to the load with the receiving antenna oriented with the polarization of the incident wave (Kirdyashav et al., 1979). The ratio of the directive and the effective area of the antenna is a universal constant (Kirdyashav et al., 1979) and;

$$A_e(\theta, \phi) = \frac{\lambda^2}{4\pi} G_d(\theta, \phi) \quad (95)$$

An expression for the received power can therefore be obtained by multiplying the receiving antenna effective area $A_e(\theta, \phi)$ with the expression for the transmitted time-average power density (Ulaby and El-Rayes, 1987)

$$P_r = \frac{P_s e^{-(N(d)\sigma_{total})a}}{(4\pi a)^2} G_t(\theta, \varphi) A_e(\theta, \varphi) \quad (96)$$

Substituting equation (95) into equation (96), gives

$$P_r = \frac{P_s \lambda^2 G_t G_r}{(4\pi a)^2} e^{-(N(d)\sigma_{total})a} \quad (97)$$

Two antennas can be aligned in such a way that they have maximum value of the directive gain for effective radio communication. Hence, the maximum directive gain of an antenna can be represented by the directivity of the antenna (Tzler, 1994). Thus, if the directivity of the transmit antenna is represented by D_t and that of the receive antenna represented by D_r , equation (97) can be restated as

$$\frac{P_r}{P_s} = \frac{\lambda^2 D_t D_r}{(4\pi a)^2} e^{-[N(d)\sigma_{total}]a} \quad (98)$$

The path loss denoted by L can be evaluated by finding the reciprocal of equation (98), given as;

$$L = \frac{P_s}{P_r} = 10 \log \frac{(4\pi a)^2}{\lambda^2 D_t D_r} e^{[N(d)\sigma_{total}]a} \quad (99)$$

3.6 Data Collection

The targeted study sites cuts across the federal capital territory and all state capitals in Nigeria show in figure 11.

The cross-sectional survey method of research was adopted in this work because it has the advantage of generating sufficient data in a short time and at a reasonably low-cost. Also, it tend to produce relevant data which can be generalized to a wider population and make it possible for the researcher to reach an appropriate conclusion on issues concerning physical characteristics of a population. The general approach to this study is exploratory and descriptive based on both qualitative and quantitative research techniques. This is because the qualitative enquiries will help to explore the diversities in a situation or phenomenon while the extent or magnitude is determined through the quantitative means (Matricciani, 1996). Such a combined approach was thought to minimize limitations that could originate from

research techniques and contribute positively towards testing and increasing the validity and reliability of the data (Atlas and Ulbrich, 1977). The data needed from our derived rain-attenuation model is rainfall data that had been processed into one-minute rainfall rate measured in mm/h exceeded for 0.01 percent average for the year This was sourced from the tropical rainfall measurement mission satellite database and was validated by the Nigerian Meteorological Agency (NIMET) rainfall prediction from January 1998 to December 2012.

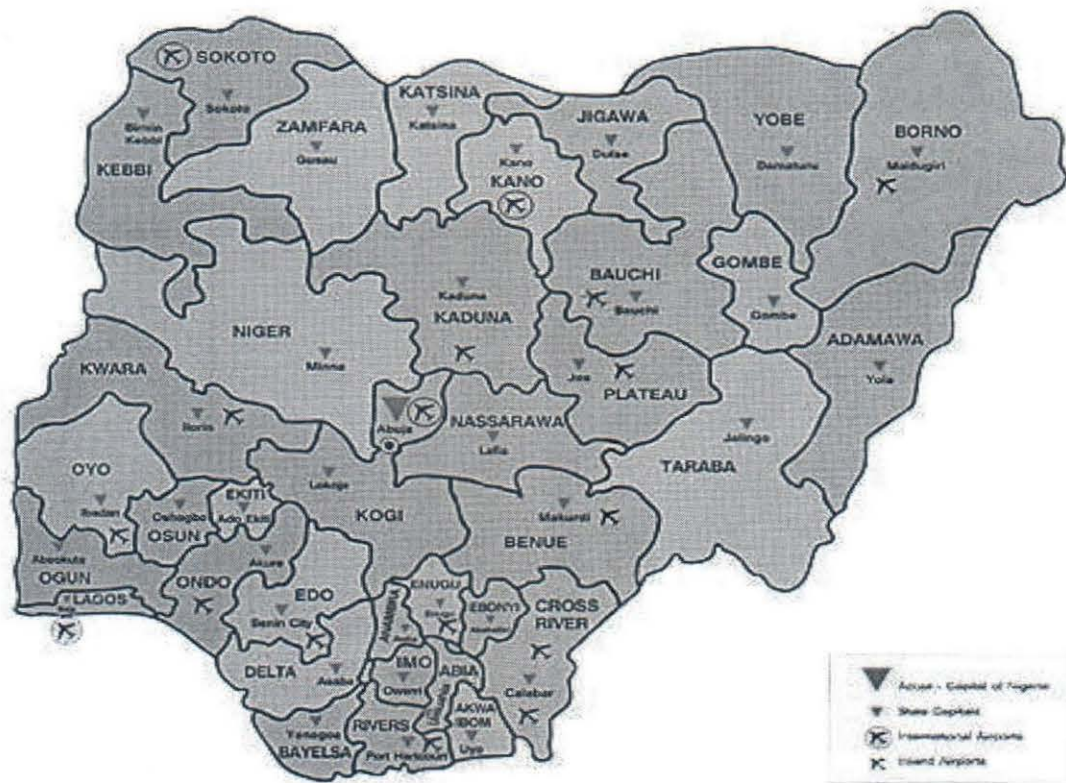


Figure 11: Survey areas comprising of state capitals in Nigeria- sourced from <https://www.pinterest.com>

Chapter 4

RESULTS AND DISCUSSION

4.1 Simulation of the Formulated Model

The previous chapter of this study deals intensively with the derivation of the rainfall attenuation model that takes into cognizance the effects of absorption and scattering of radio signals. This mathematical expression gives the path loss due to a drop of rain and show its relationship with the following parameters: density per unit volume of a drop of rain, the total cross section of a drop of rain, the frequency at which the signal traverse, the range of distance from transmit and the receive antennas and the maximum gains of the transmit and receive antennas.

4.2 The Formulated Model for Simulation

The model for simulation is a mathematical equation obtained in the previous chapter of this work. It was described according to the equation (99) and given as

$$L = \frac{P_s}{P_r} = 10 \log \frac{(4\pi a)^2}{\lambda^2 D_t D_r} e^{[N(d)\sigma_{total}]a} \quad (100)$$

where D_t and D_r are the maximum directive gains of the transmit and receive antennas respectively, $N(d)$ is the particle drop size distribution of drops per unit volume, σ_{total} is the total cross section of the scattering and absorption, λ is the wavelength of the radio signals and equals to $\frac{V}{f}$; where V is the velocity of the signal of the signal, f is the frequency of the signal, a is the distance apart of the transmit and the receive antennas, P_r is the total radiated power from the transmitter and P_s is the total received power.

4.3 Flow Chart for Simulation

The chart shows major stages of simulation of the RAM and FSPM. The program goes through the process of initializing all variables. The precipitation data collected against the locations are store in a file that would be read into the pro-

gram. The mean and standard deviation of these parameters are obtained before the values of frequencies are imputed as shown in the chart. The pathloss for the RAM is calculated and the graphs of the pathloss against the separation between the two antennas are plotted. Similarly, the simulation of the FSPM is carried out with imputed parameters peculiar to the model.

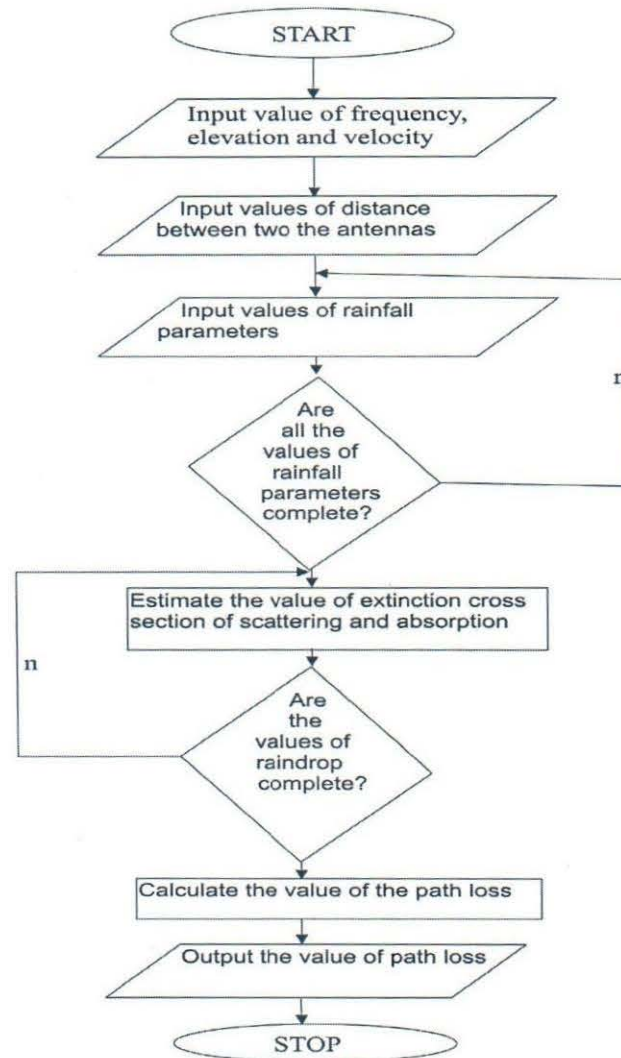


Figure 12: Flowchart of the Simulation of the RAM and FSPM

4.4 Choice of Implementation Platform

Matrix laboratory known as MATLAB is a multi-paradigm numerical computing environment and fourth-generation programming language. A proprietary programming language developed by MathWorks, MATLAB allows matrix manipulations, plotting of functions and data, implementation of algorithms, creation of user interfaces, and interfacing with programs written in other languages, including C, C++, Java, Fortran and Python. Although MATLAB is intended primarily for numerical computing, an optional toolbox uses the MuPAD symbolic engine, allowing access to symbolic computing capabilities. An additional package, Simulink, adds graphical multi-domain simulation and model-based design for dynamic and embedded systems. MATLAB is the high-level language and interactive environment used by engineers and scientists worldwide. It lets you explore and visualize ideas and collaborate across disciplines including signal and image processing, communications, control systems, and computational finance. MATLAB was used for simulation because of its ease of use in terms of flexibility, and the ability to handle mathematical expressions more conveniently

4.5 Simulation of the Model using MATLAB

This section presents a logical sequence leading to the simulation of the path loss or attenuation that a radio signal traversing through rain undergoes. Hence, this gives the order in which the simulation is carried out.

The rainfall attenuation model derived previously would be used to calculate the path loss, L (dB) of the radio signal as it traverses through rain from transmit to the receive antenna. As mentioned earlier, rainfall has considerable effect at very high frequencies at Ku and Ka bands; precisely from 3GHz and above. The simulation would be carried out at radio frequencies of 4GHz, 10GHz and 20GHz while the distance between the transmitter (source) and the receiver (destination) would vary from 1 to 30 km.

From the formulated model in equation (99), the logical sequence used for the simulation of this model is given below. First, the formula for the extinction

or total cross section of drops of rain was evaluated as given by the empirical formula in equation (101) (Tat-soon, 1998) and (Atlas, Ulbrich, Marks, Amitai, and Williams, 1999). Thus, if the total cross section is denoted as σ_{total} , then, the formula is expressed as a function of the rain drop radius is given as

$$\sigma_{total}(a_0) = C_0 + C_1 a_0 + c_2 a_0^2 + c_3 a_0^3, \quad 0.25 \leq a_0 \leq 0.45 \quad (101)$$

where $a_0(\text{cm})$ is the raindrop mean radius and C_0 to C_3 are coefficient for both parallel (E_x^i) and perpendicular (E_y^i) incident polarizations and are determined to be

$$\left. \begin{aligned} C_0 &= -0.277 + 2.22e^{-0.007f} \cos(13.446 + 0.484f) \\ C_1 &= 1.67 - 23.683e^{-0.017f} \cos(0.685 + 0.488f) \\ C_2 &= 3.66 + 69.546e^{-0.018f} \cos(13.02 + 0.495f) \\ C_3 &= -1.929 - 67.452e^{-0.02f} \cos(56.809 + 0.5f) \end{aligned} \right\} \quad (102)$$

where f is the operating frequency (GHz). After obtaining the total cross section σ_{total} for the drop with mean radius of a_0 , then we evaluate the particle drop size distribution of drops per unit volume $N(d)$. The particle drop size distribution is given by theoretical distribution having the negative exponential form, (Marshall and McK Palmer, 1948)

$$N(d) = N_0 e^{-(\Lambda a)}, \quad \Lambda = \alpha R^{-\beta} \quad (103)$$

where N_0, α, β are constants and R is the rain rate in millimetres per hour. $a = a_0$, is the rain drop mean radius. The constants have the following numerical values as shown below according to Marshall and Palmer (1948): $N_0 = 0.08(m^{-4}mm^{-1})$, $\alpha = 4.1$, $\beta = 0.21$. (Baltas and Mimikou, 2002)

If we denote the path loss by L , then

$$L = \frac{P_t}{P_r} = 20 \log_{10} (4\pi) + 20 \log_{10} (d) + 20 \log_{10} \lambda \quad (107)$$

Then substituting λ (km) = 0.3 and f (MHz) and rationalizing the equation produces the generic free space path loss formula, which is stated in equation (108) below

$$L = 32.45 + 20 \log_{10} (d) + 20 \log_{10} (f) \quad (108)$$

For d , f in meters and kilohertz, respectively, the constant becomes -87.55.

For d , f in meters and megahertz, respectively, the constant becomes -27.55.

For d , f in kilometres and gigahertz, respectively, the constant becomes 92.45.

The program code listing is presented in Appendix C

4.7 Results Presentation and Discussion

A mathematical model describing climatic factors affecting radio communication was formulated in chapter three of this research. The model was then simulated via m-script programming with MATLAB. The results obtained from the simulation will be presented in this section and analysis carried out based on the results obtained.

4.7.1 Results Presentation

In determining the extent to which rainfall affects the quality and quantity of radio signals received by an antenna as the radio waves traverse through rain, the power received by the antenna, P_r and the path loss by the radio signal, L , is determined using the proposed model. The model is then validated by comparing the results obtained due to the effect of rainfall and that due to free space computed from the free space model presented earlier. The simulation of the rainfall

attenuation model (RAM) and free space propagation model (FSPM) was successfully carried out and the results are tabulated in Appendix B: One minute rainfall rate measured in mm/h exceeded for 0.01 percent average for 37 sites from January 1998 to December 2012 sourced from TRMM Satellite and validated with NIMET rainfall prediction and Tabulated simulation result showing the path loss and power received in free space and various observation sites. The graphs are presented in the following figures:

4.7.2 Discussion of the Results

In this analysis, comparison of the path loss, L , for the two models as a function of the separation between the two antennas will be discussed. Table 2 (Appendix B) shows the simulated results of the path loss as a function of the separation between two antennas for the free space model while tables 3 through 39 shows the simulated results of the path loss as a function of the separation between two antennas for the rainfall attenuation model for the 37 sites consisting of 36 state capitals and Abuja in Nigeria.

Comparison the path loss, L , as a function of the separation, a , between two antennas for the two models at three different frequencies (4GHz, 10GHz and 20GHz)

Results from the simulation of the path loss, L , as a function of the separation between two antennas are tabulated as shown in the output tables presented in Appendix B. The graph describing the attenuation as a function of distance when radio signal is in contact with rain at different observation sites are illustrated in figures 14 through 50. The graph describing the behaviour of radio signals in free space is illustrated in figure 13. These results shall be analysed in three different frequencies as follows.

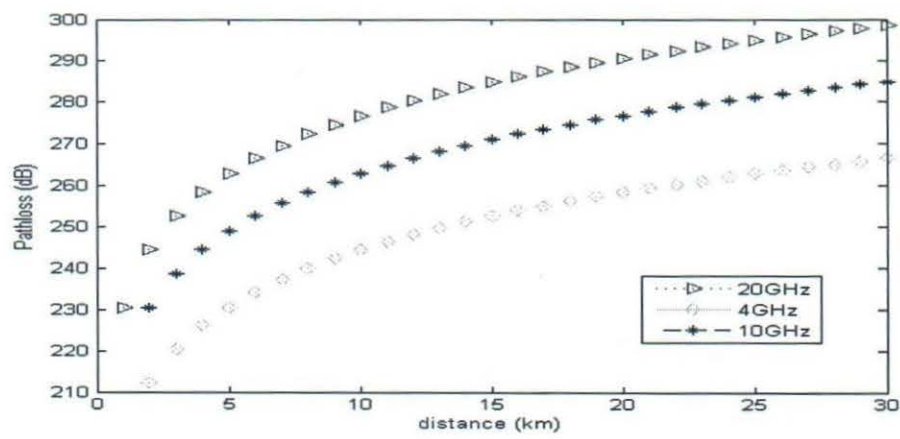


Figure 13. Path loss against separation between two antennas in free space

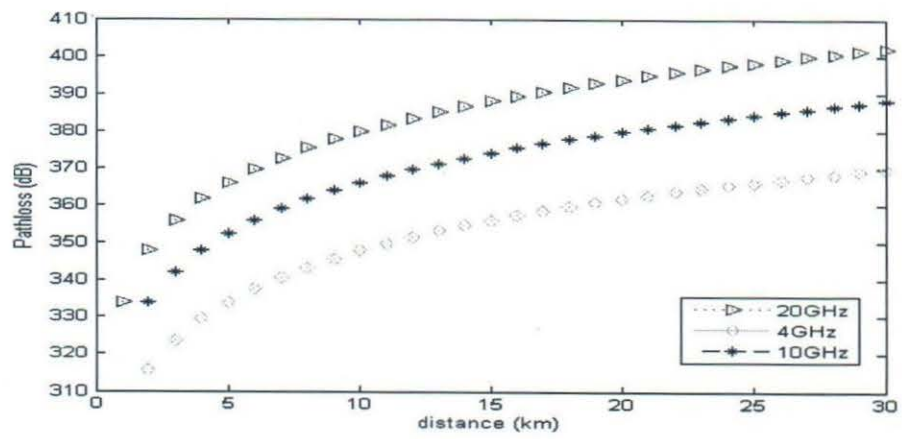


Figure 14. Path loss against separation between two antennas in Abeokuta

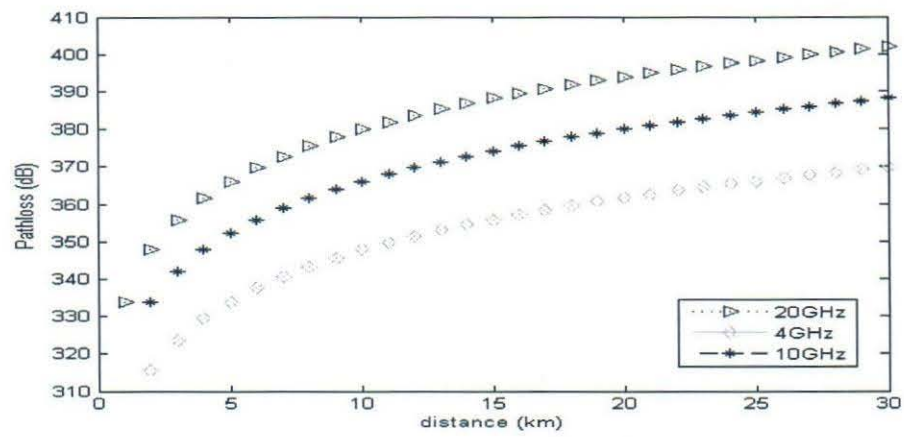


Figure 15. Path loss against separation between two antennas in Ado Ekiti

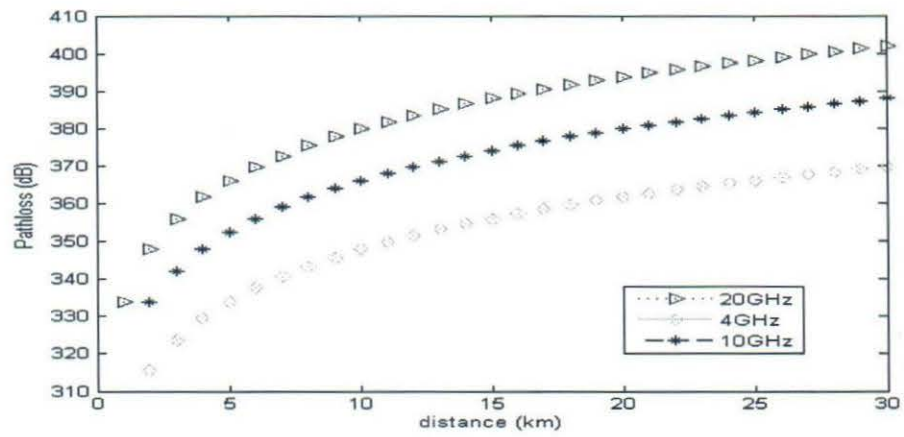


Figure 17. Path loss against separation between two antennas in Ibadan

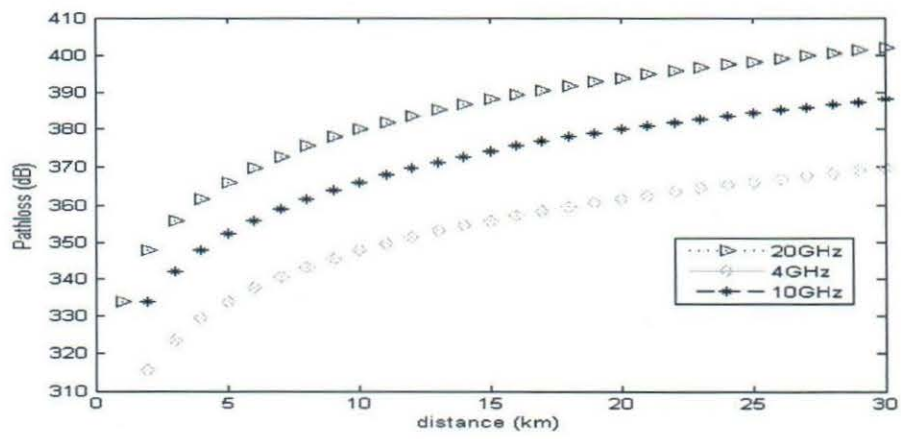


Figure 19. Path loss against separation between two antennas in Osogbo

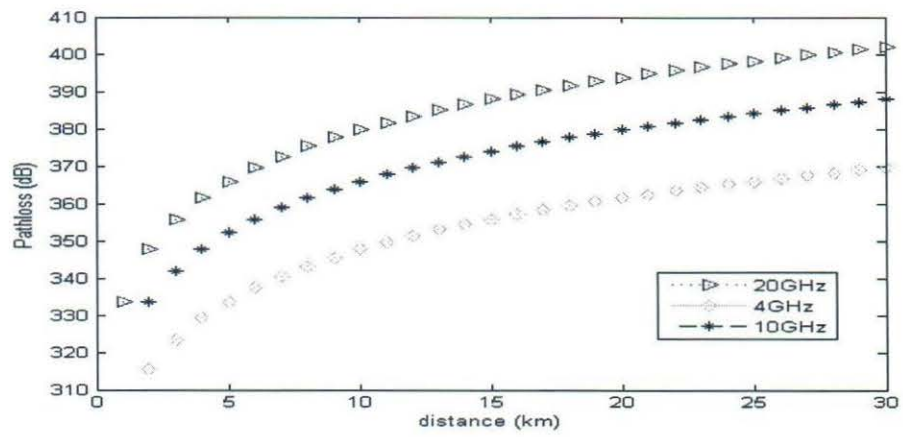


Figure 20. Path loss against separation between two antennas in Abakaliki

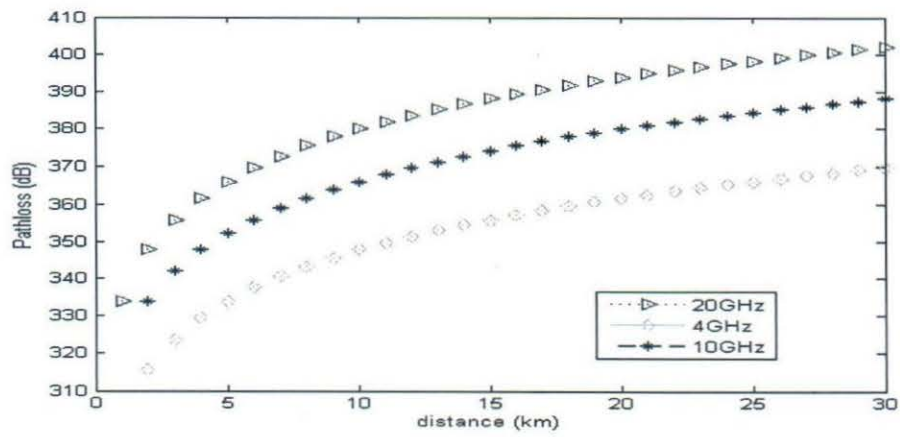


Figure 21. Path loss against separation between two antennas in Awka

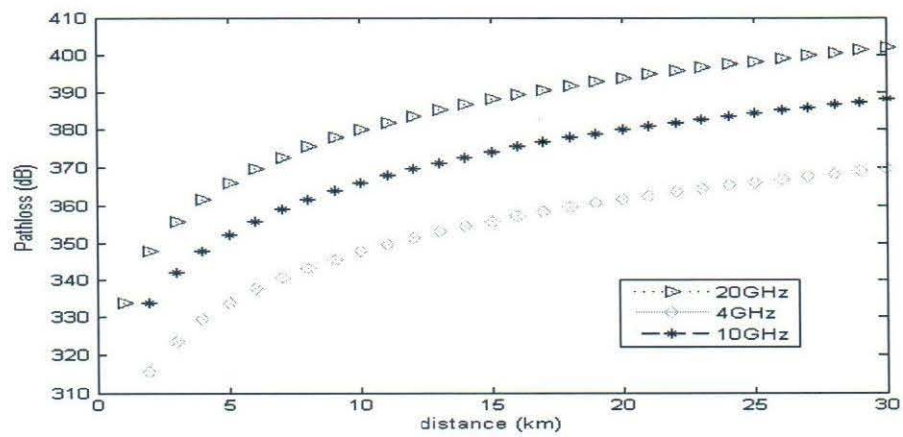


Figure 22. Path loss against separation between two antennas in Enugu

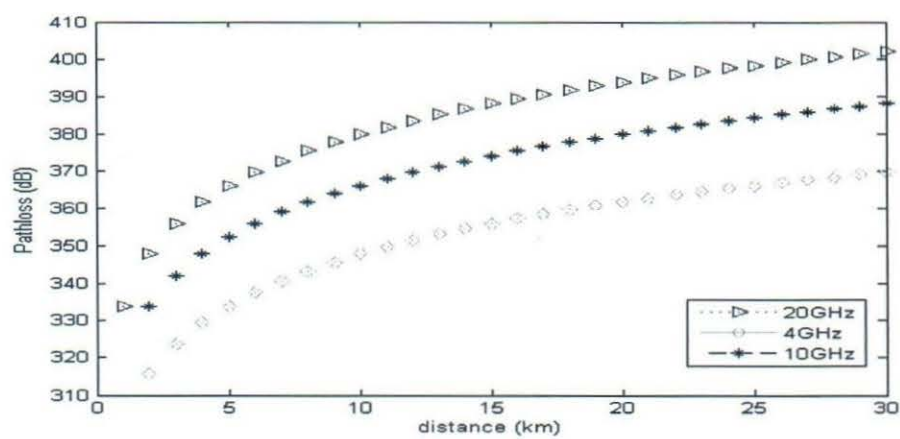


Figure 24. Path loss against separation between two antennas in Umuahia

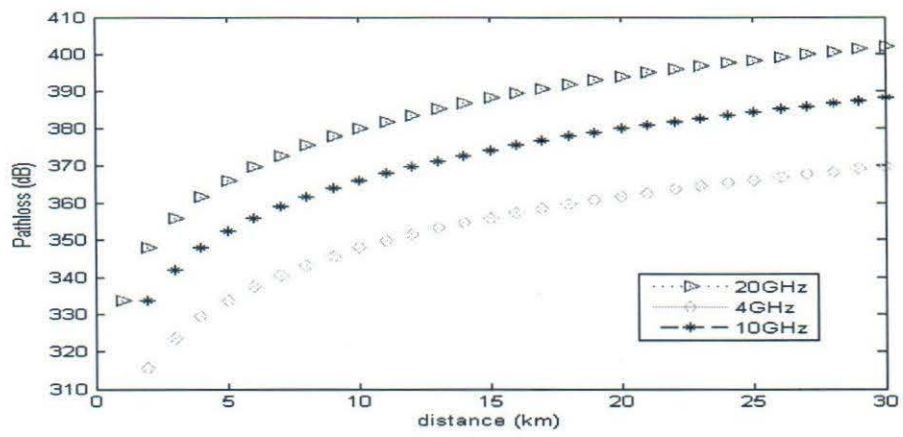


Figure 25. Path loss against separation between two antennas in Asaba

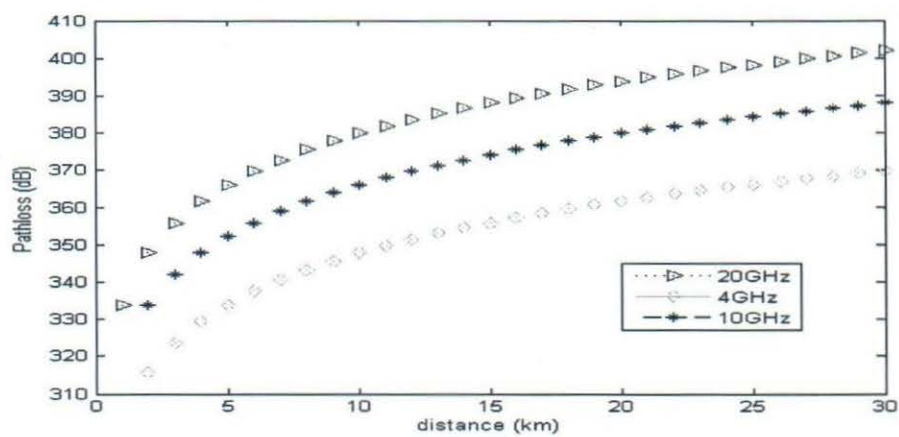


Figure 26. Path loss against separation between two antennas in Benin

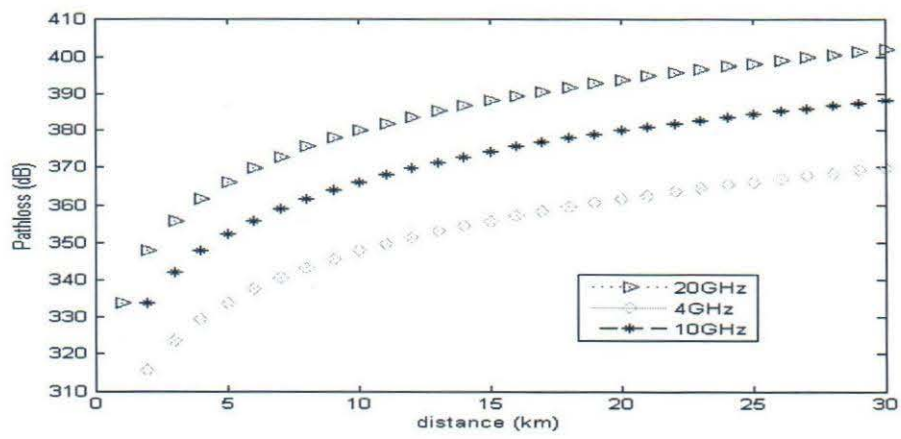


Figure 27. Path loss against separation between two antennas in Calabar

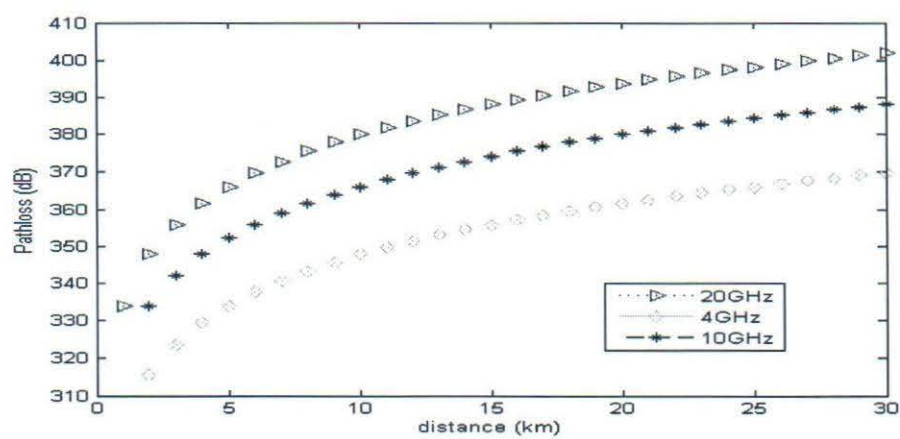


Figure 28. Path loss against separation between two antennas in Port Harcourt

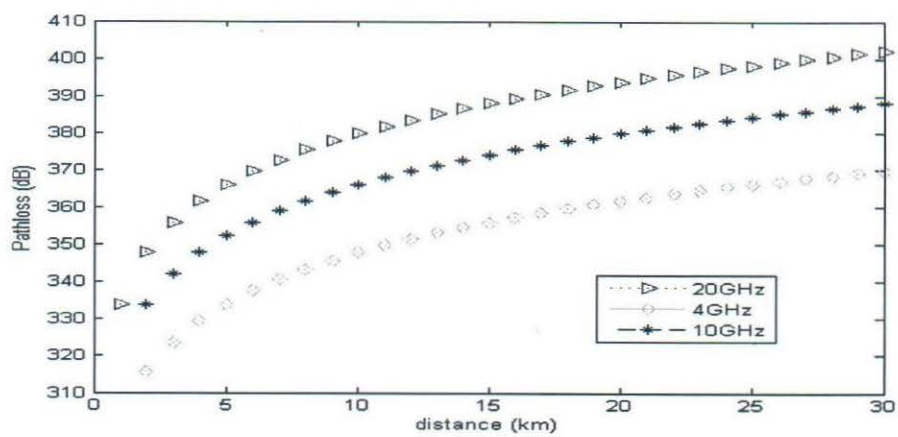


Figure 29. Path loss against separation between two antennas in Uyo

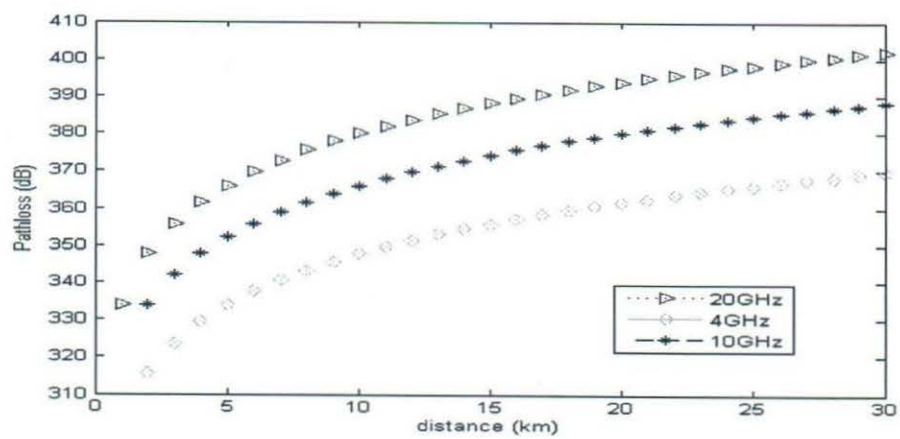


Figure 30. Path loss against separation between two antennas in Yenogoa

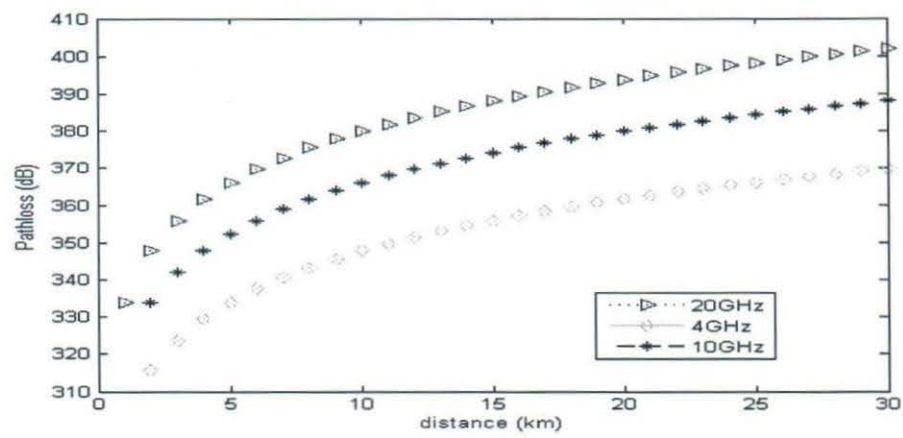


Figure 31. Path loss against separation between two antennas in Abuja

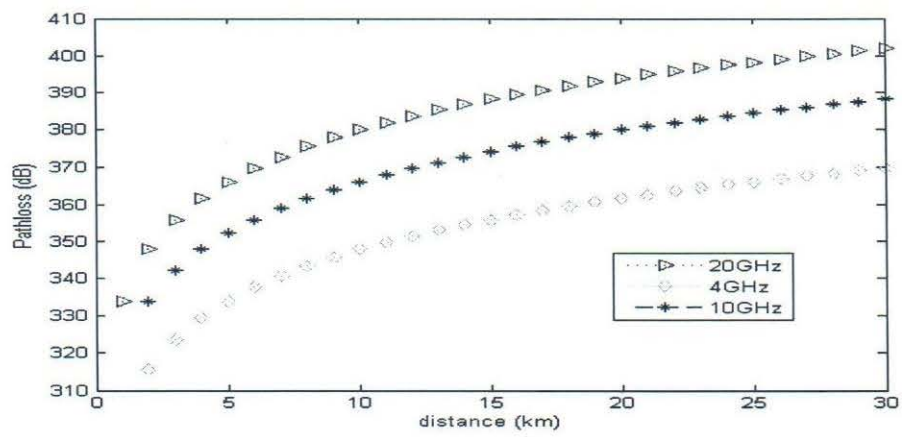


Figure 32. Path loss against separation between two antennas in Illorin

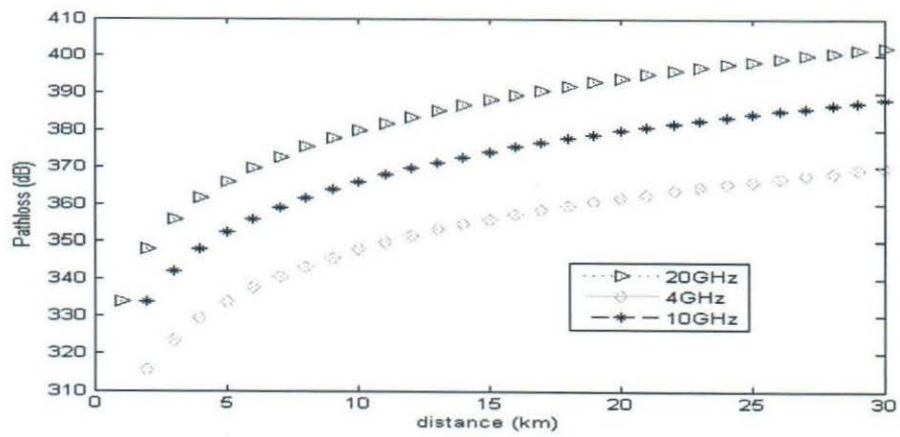


Figure 33. Path loss against separation between two antennas in lafia

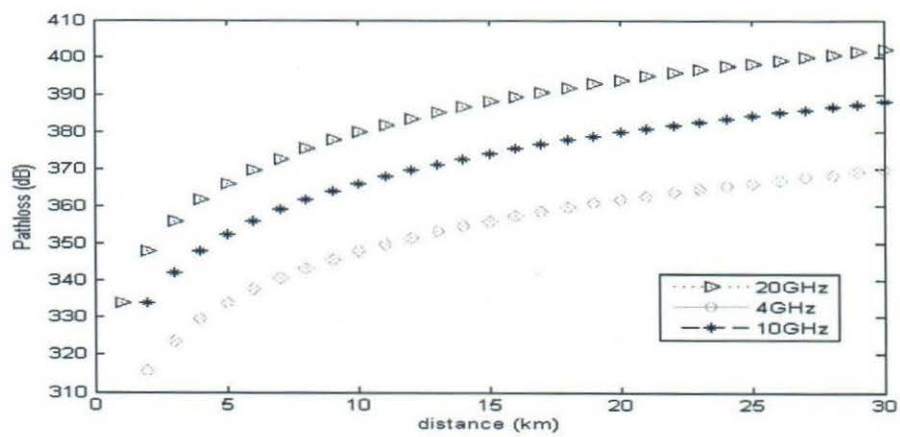


Figure 34. Path loss against separation between two antennas in Lokoja

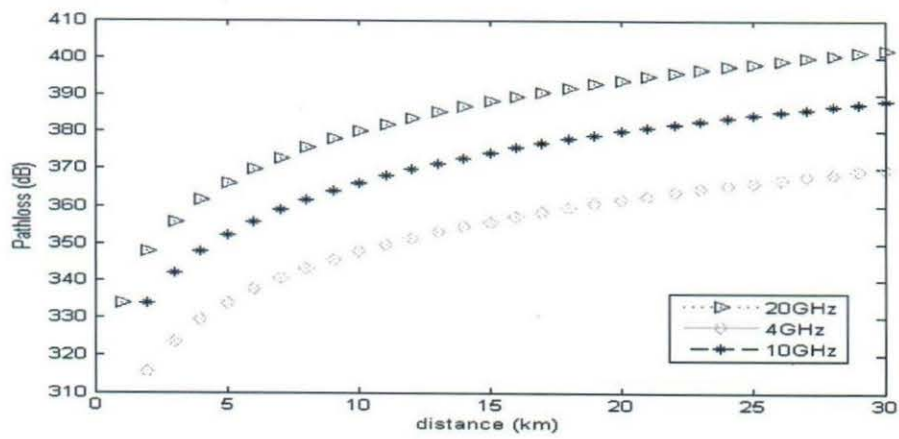


Figure 35. Path loss against separation between two antennas in Makurdi

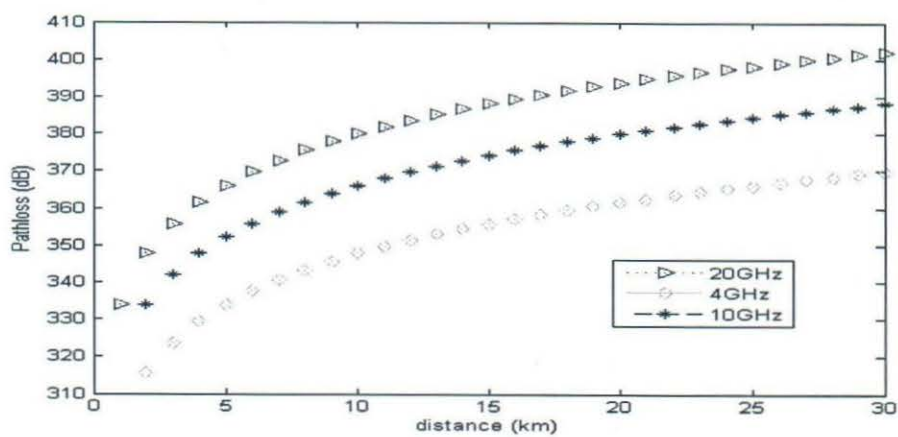


Figure 36. Path loss against separation between two antennas in Mina

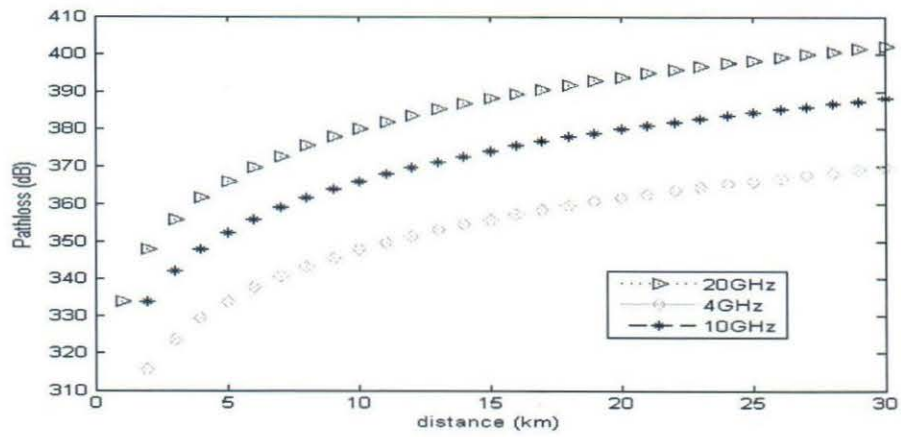


Figure 37. Path loss against separation between two antennas in Jos

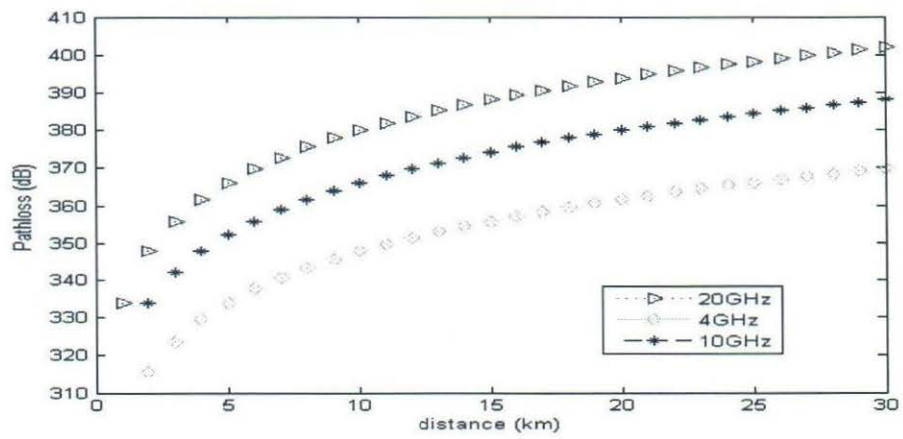


Figure 39. Path loss against separation between two antennas in Gasau

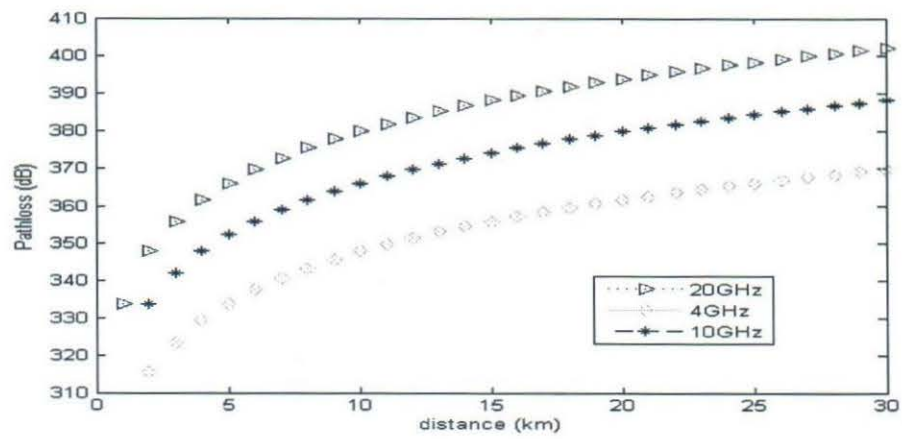


Figure 42. Path loss against separation between two antennas in Katsina

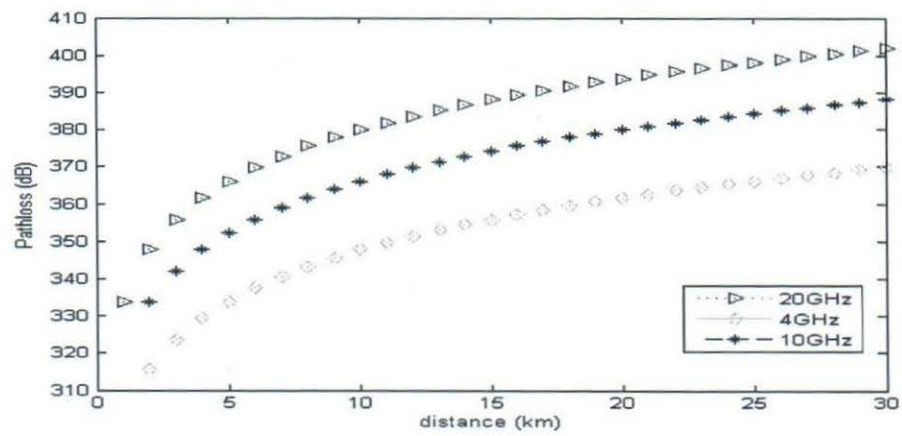


Figure 44. Path loss against separation between two antennas in Yola

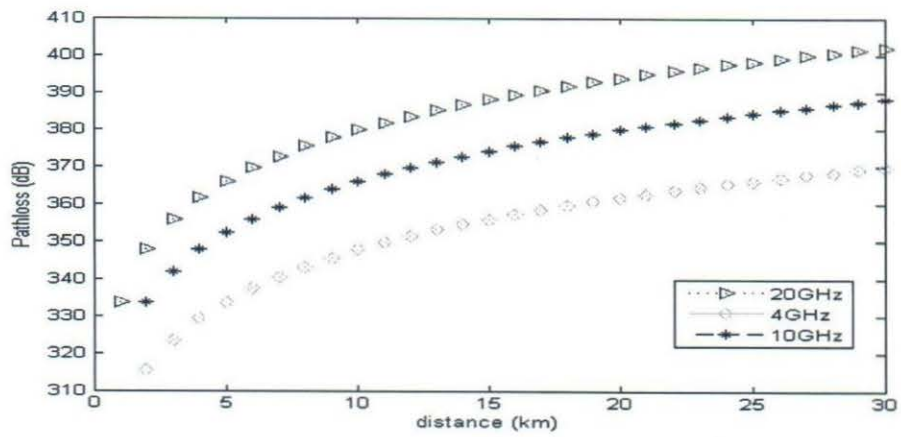


Figure 45. Path loss against separation between two antennas in Bauchi

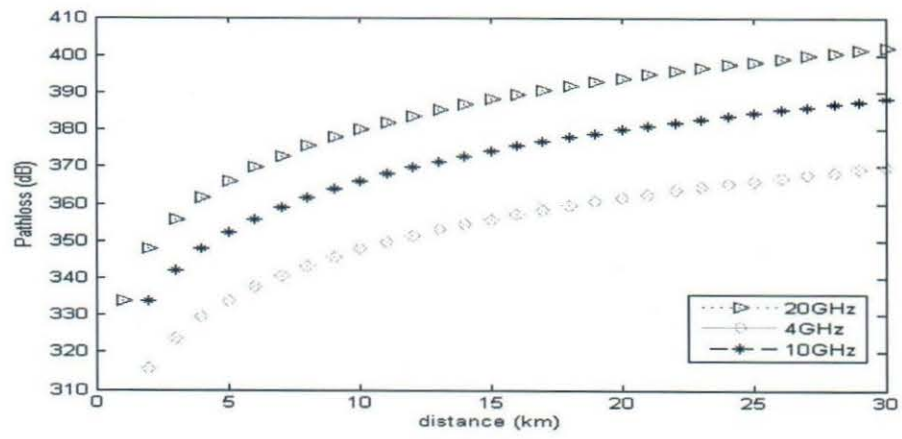


Figure 46. Path loss against separation between two antennas in Damaturu

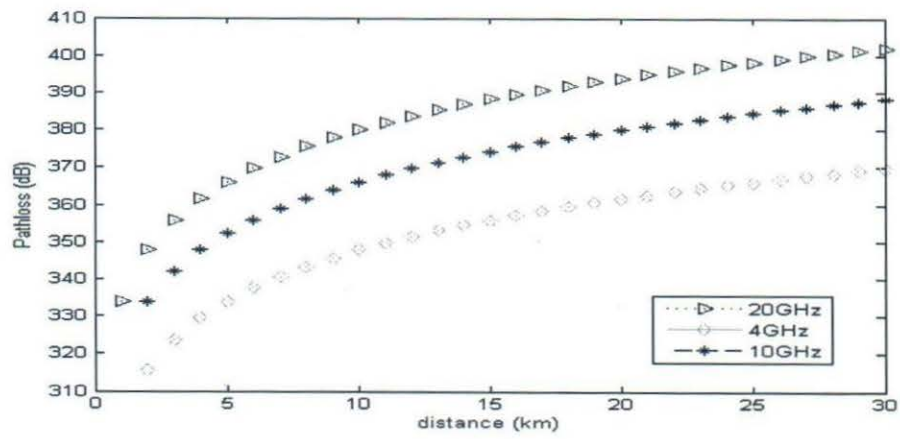


Figure 47. Path loss against separation between two antennas in Dutse

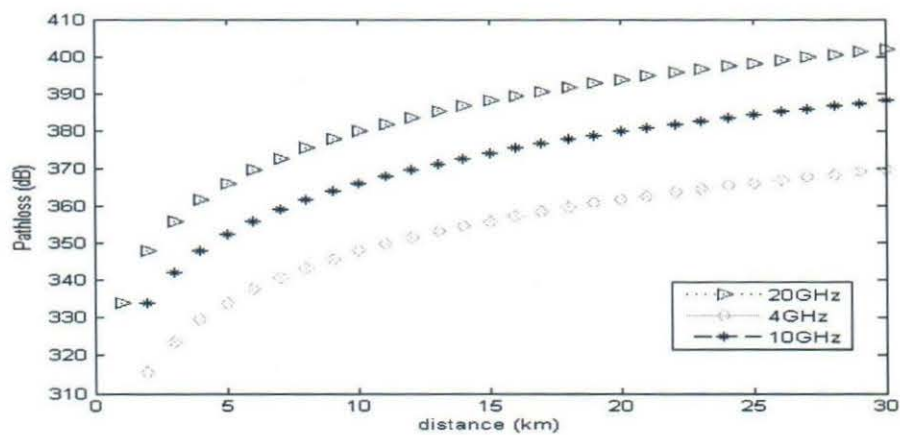


Figure 48. Path loss against separation between two antennas in Gombe

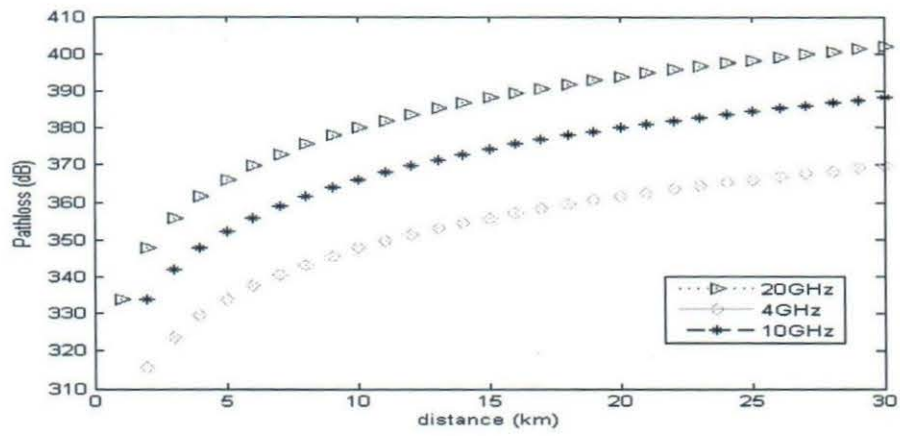


Figure 50. Path loss against separation between two antennas in Maiduguri

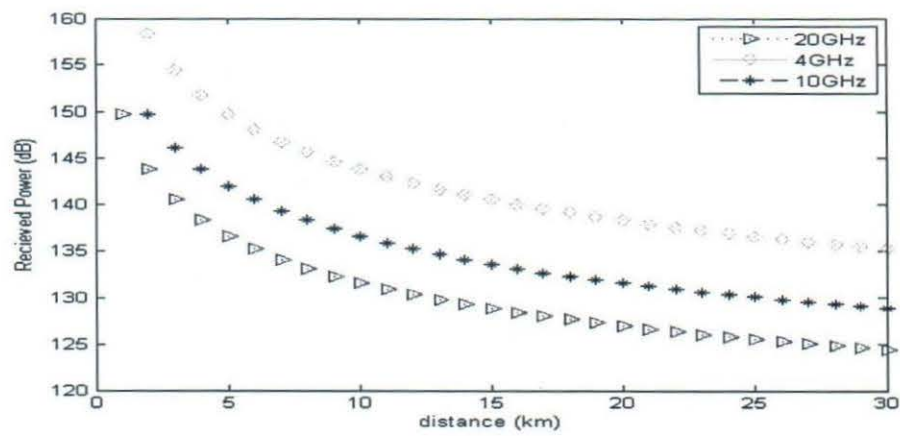


Figure 51. Received power against the separation between two antennas in Abeokuta

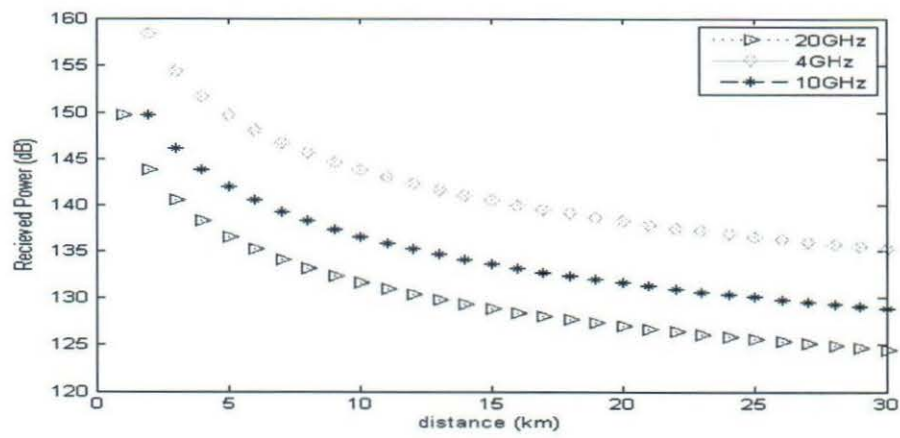


Figure 52. Received power against the separation between two antennas in Ado Ekiti

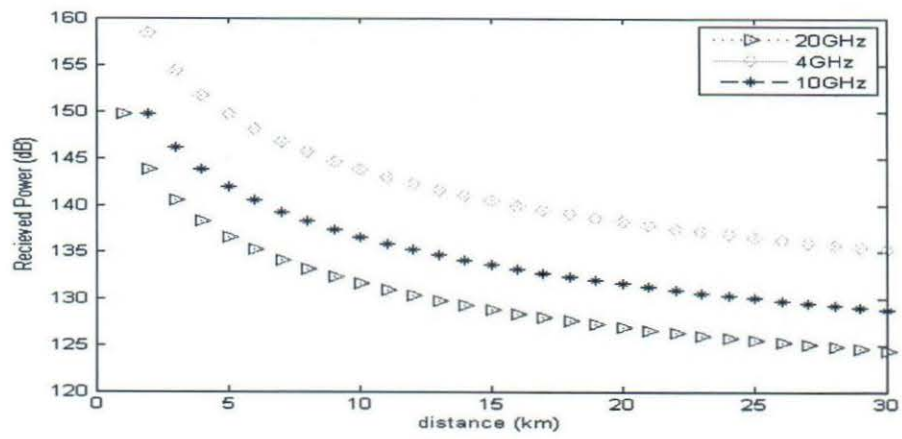


Figure 54. Received power against the separation between two antennas in Ibadan

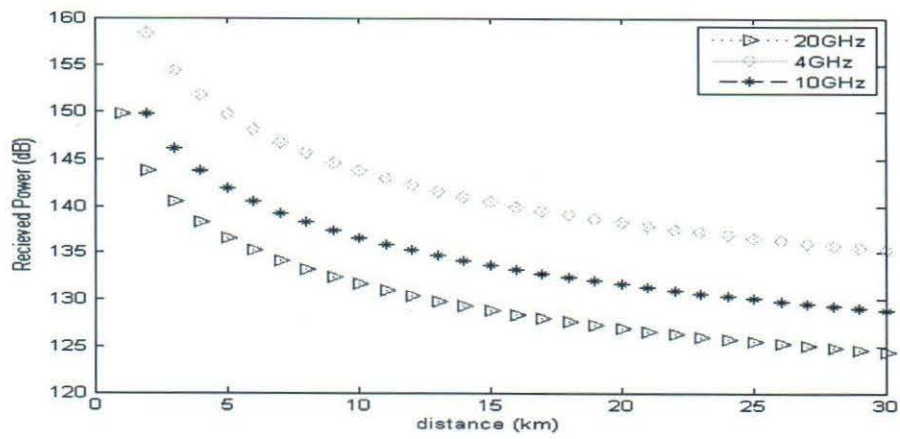


Figure 55. Received power against the separation between two antennas in Ikeja

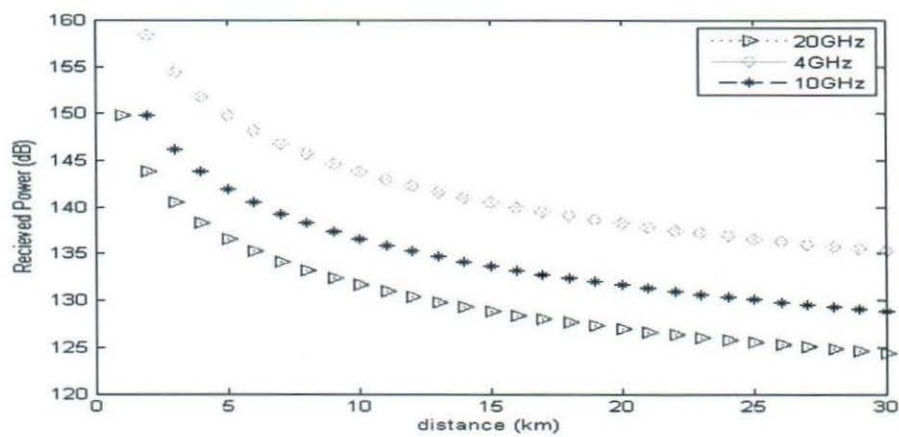


Figure 56. Received power against the separation between two antennas in Osogbo

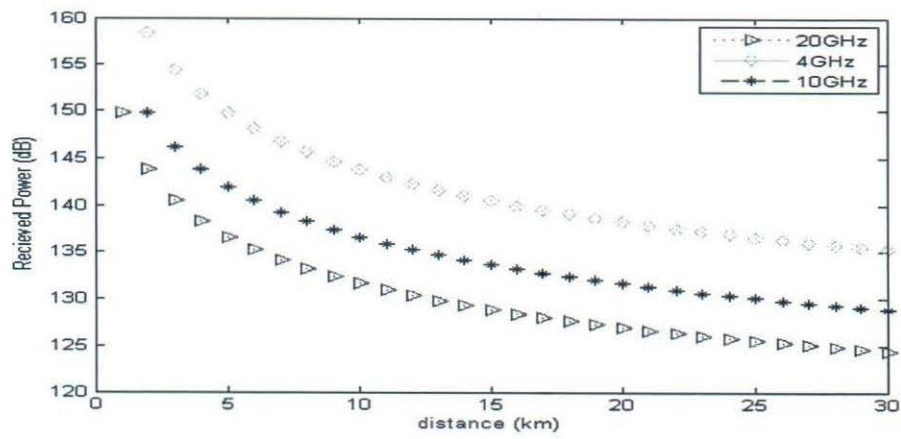


Figure 57. Received power against the separation between two antennas in Abakaliki

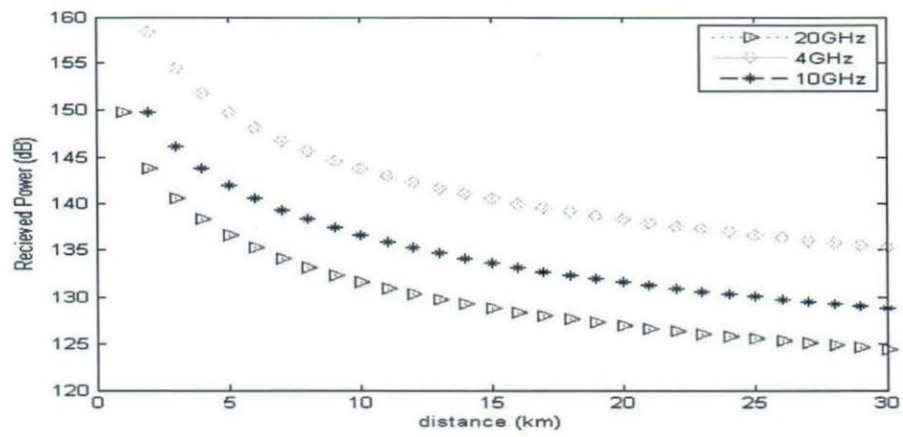


Figure 58. Received power against the separation between two antennas in Awka

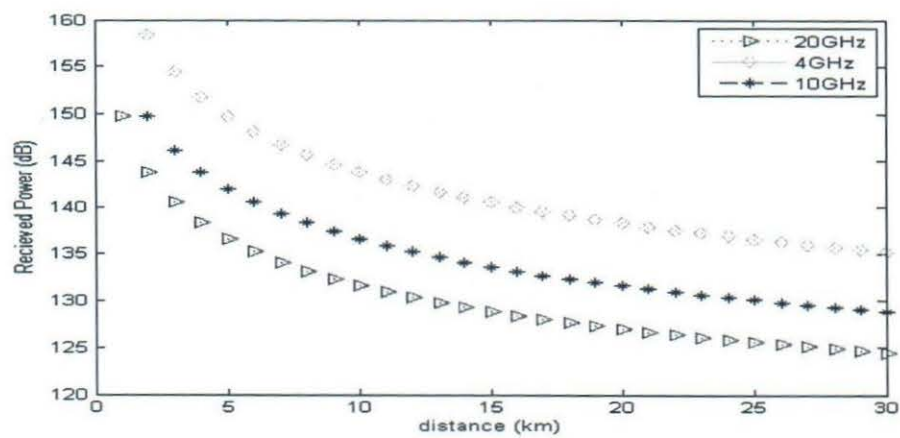


Figure 59. Received power against the separation between two antennas in Enugu

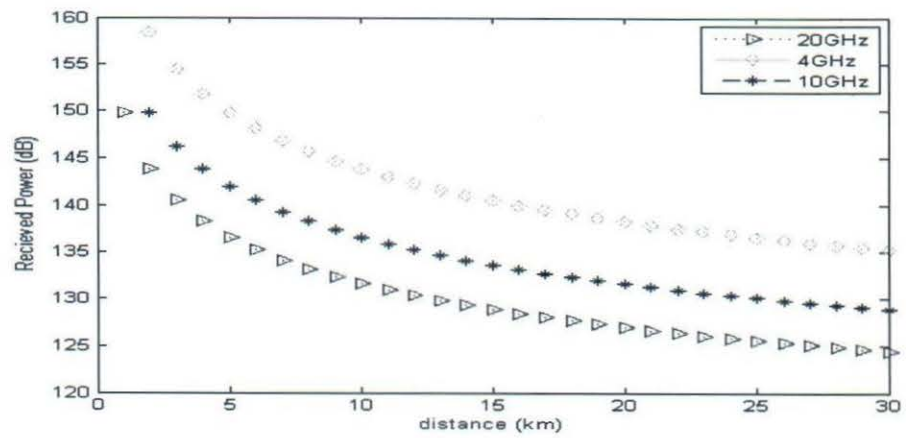


Figure 60. Received power against the separation between two antennas in Owerri

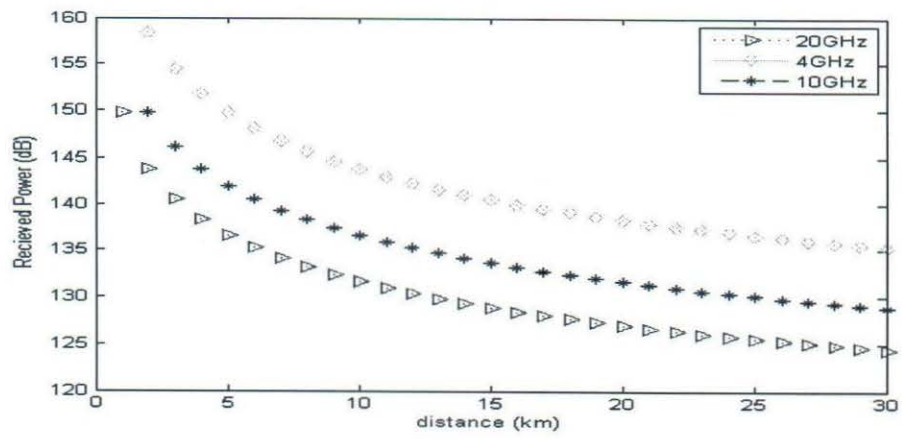


Figure 62. Received power against the separation between two antennas in Asaba

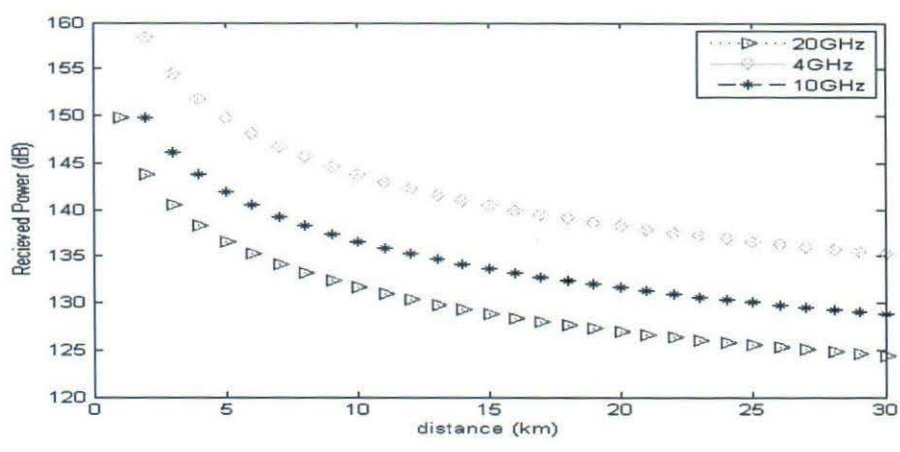


Figure 63. Received power against the separation between two antennas in Benin

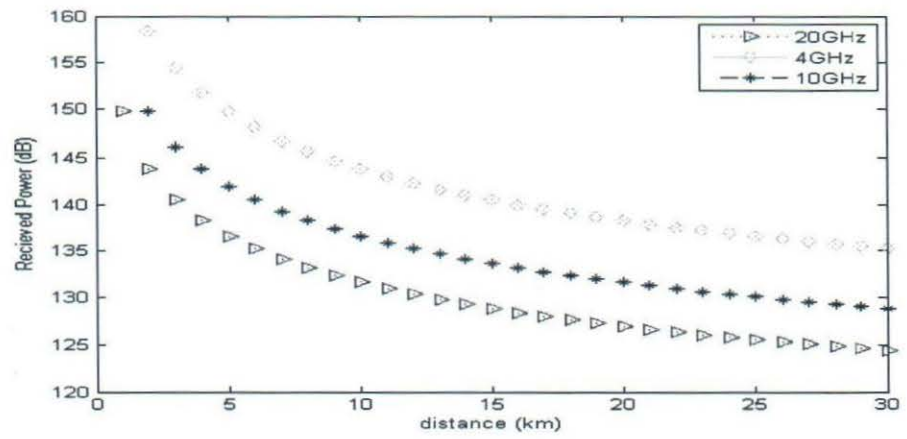


Figure 65. Received power against the separation between two antennas in Port Harcourt

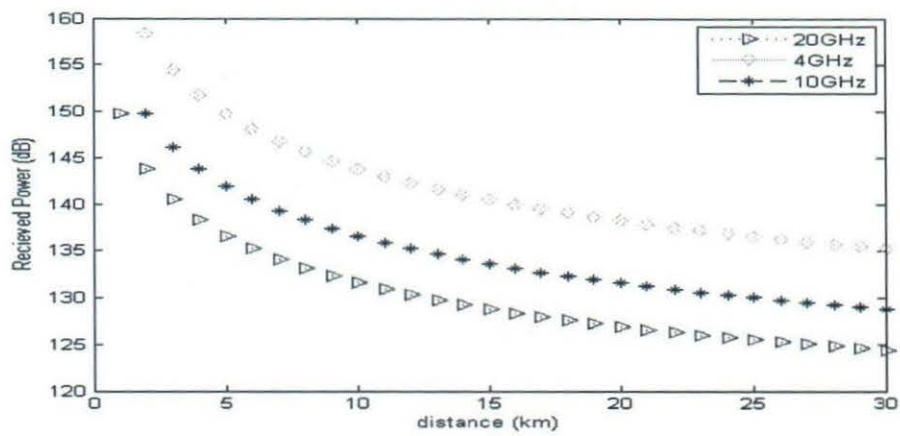


Figure 67. Received power against the separation between two antennas in Yenogoa

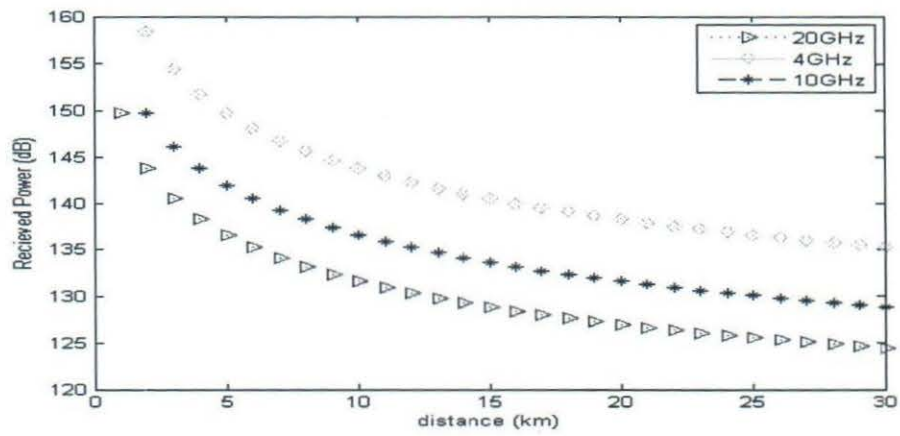


Figure 68. Received power against the separation between two antennas in Abuja

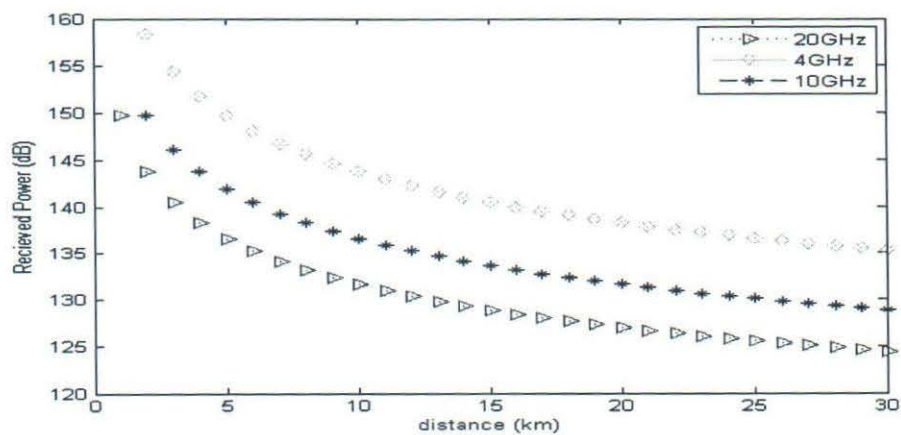


Figure 69. Received power against the separation between two antennas in Illorin

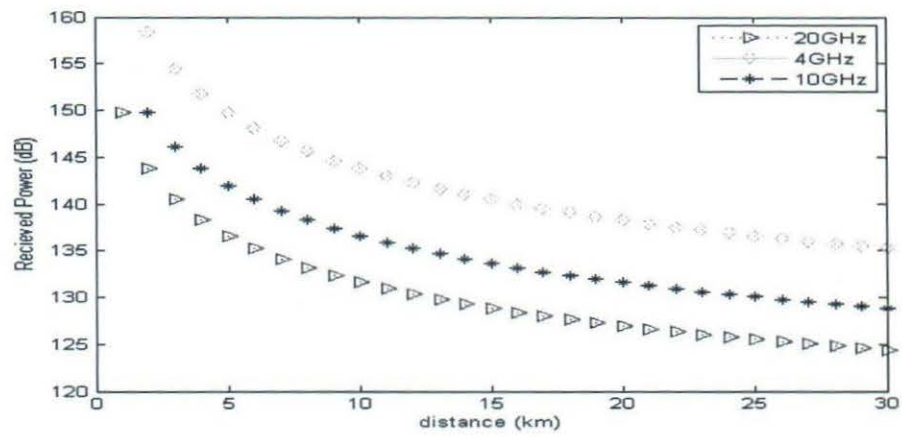


Figure 71. Received power against the separation between two antennas in Lokoja

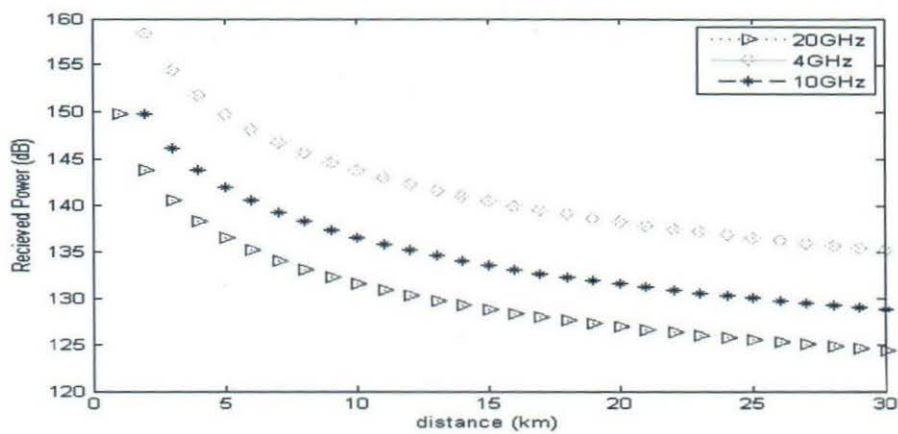


Figure 73. Received power against the separation between two antennas in Mina

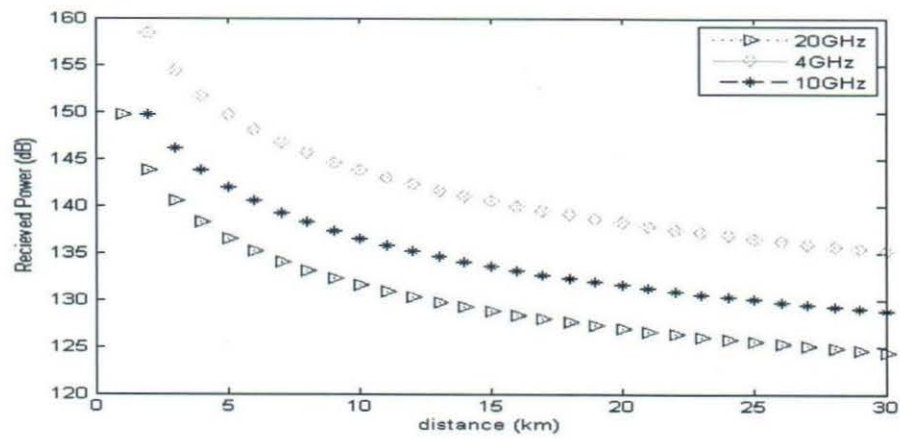


Figure 74. Received power against the separation between two antennas in Jos

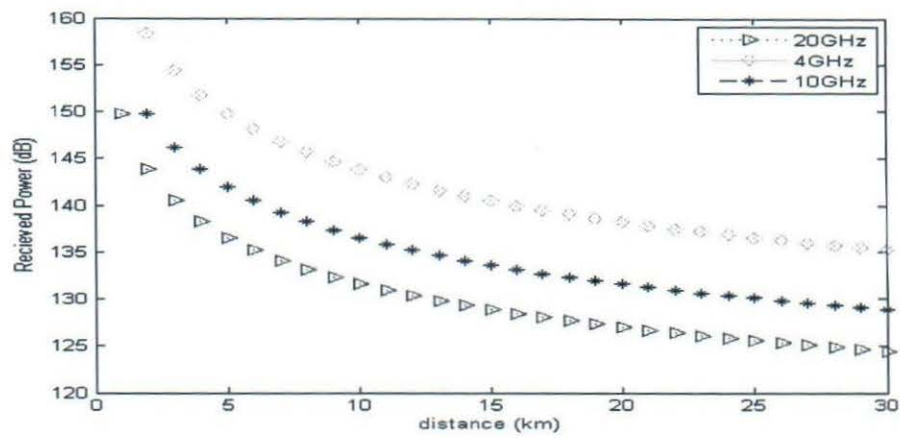


Figure 75. Received power against the separation between two antennas in Birini Kebbi

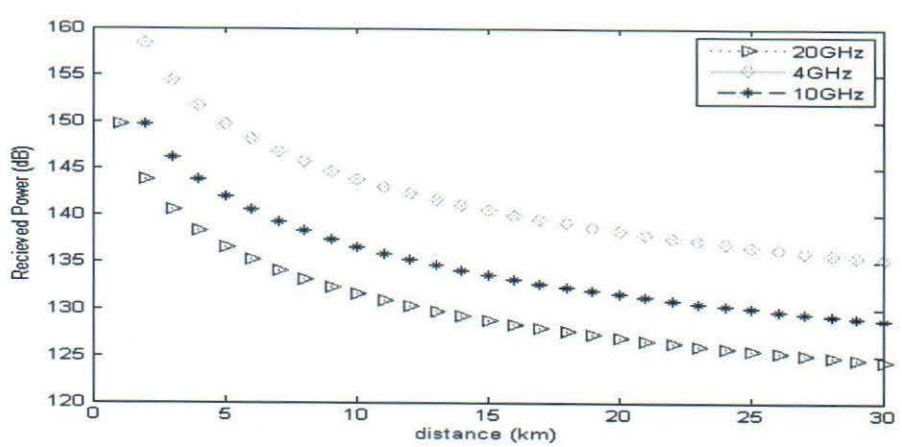


Figure 76. Received power against the separation between two antennas in Gasau

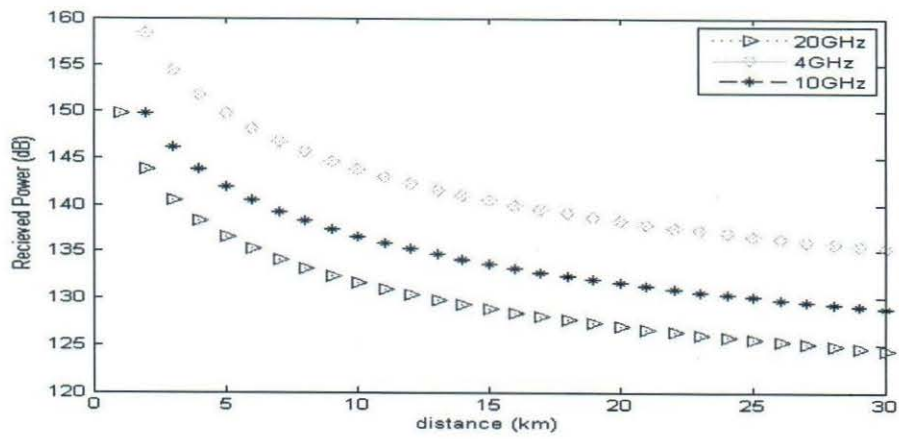


Figure 77. Received power against the separation between two antennas in Kaduna

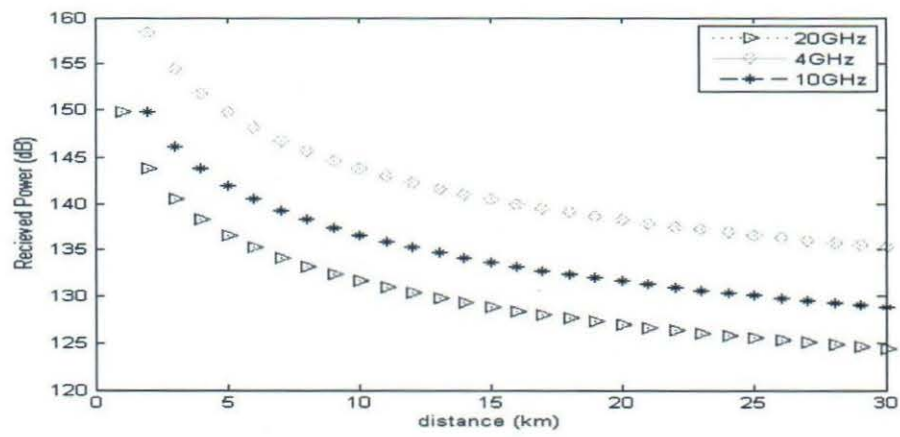


Figure 78. Received power against the separation between two antennas in Kano

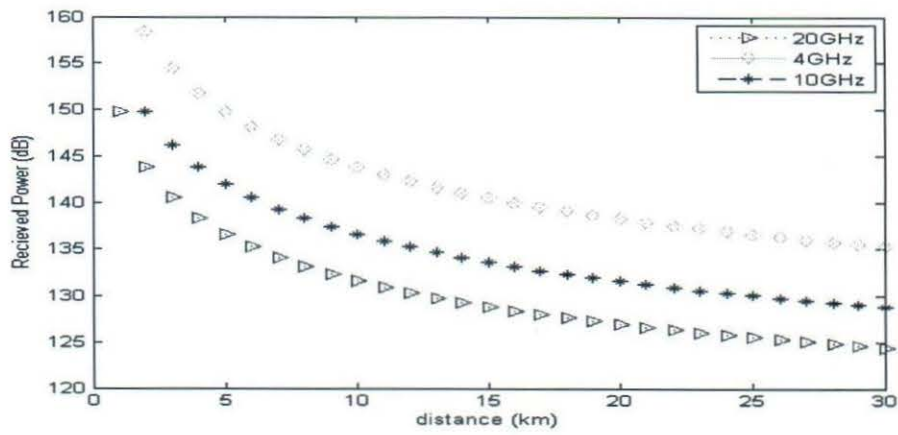


Figure 79. Received power against the separation between two antennas in Katsina

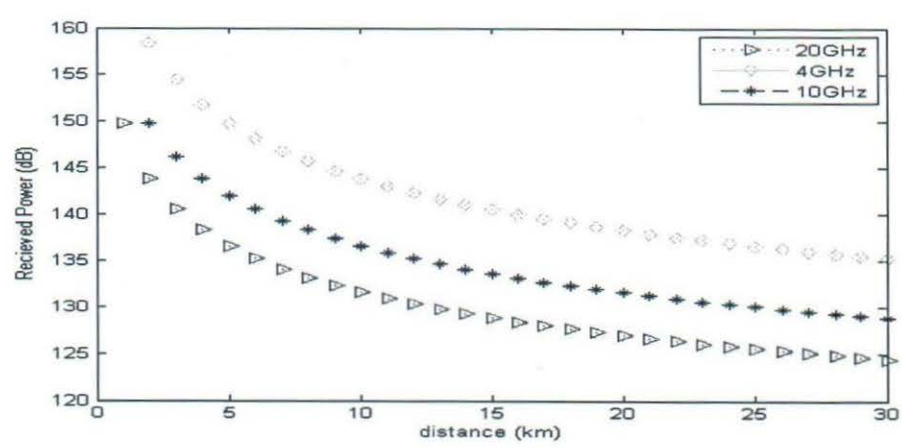


Figure 80. Received power against the separation between two antennas in Sokoto

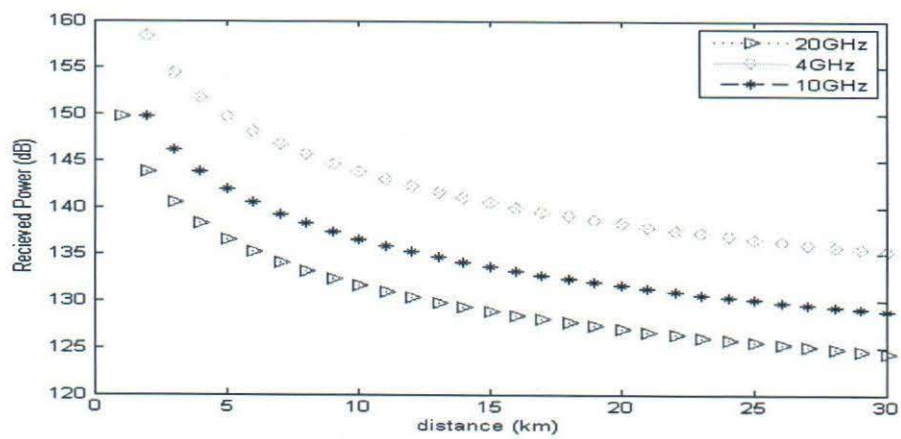


Figure 81. Received power against the separation between two antennas in Bauchi

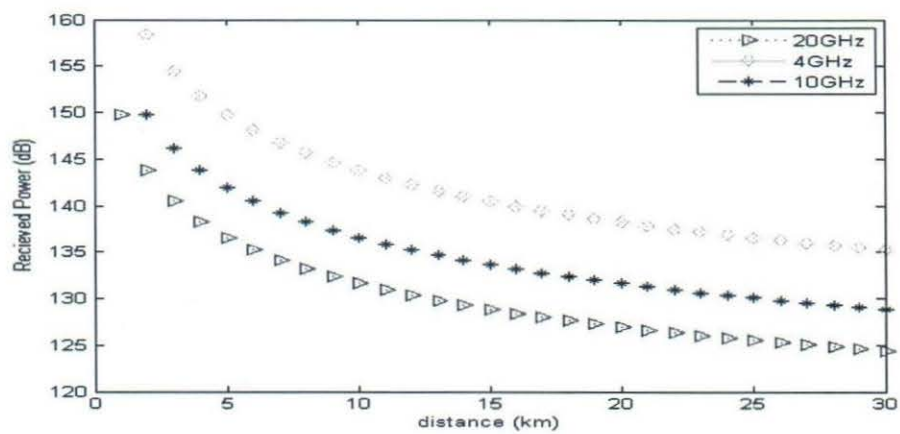


Figure 82. Received power against the separation between two antennas in Damaturu

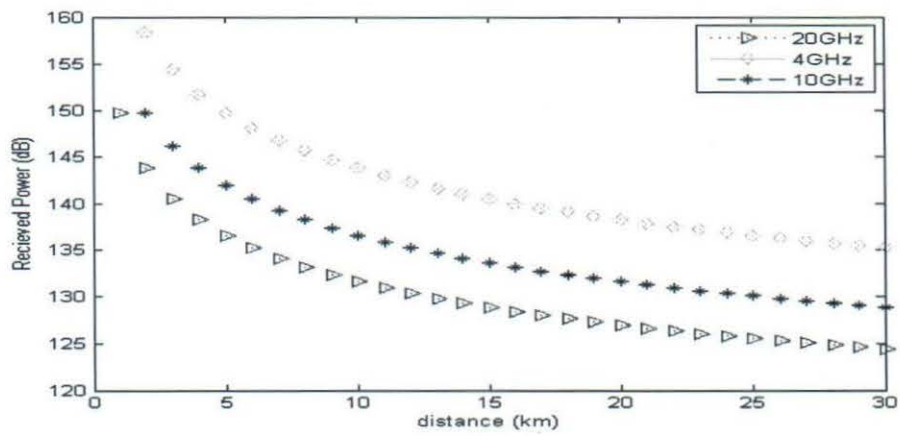


Figure 83. Received power against the separation between two antennas in Dutse

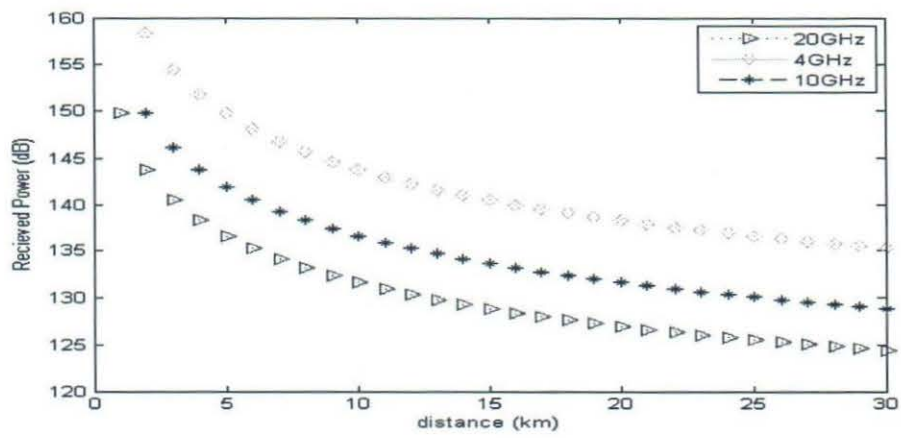


Figure 84. Received power against the separation between two antennas in Gombe

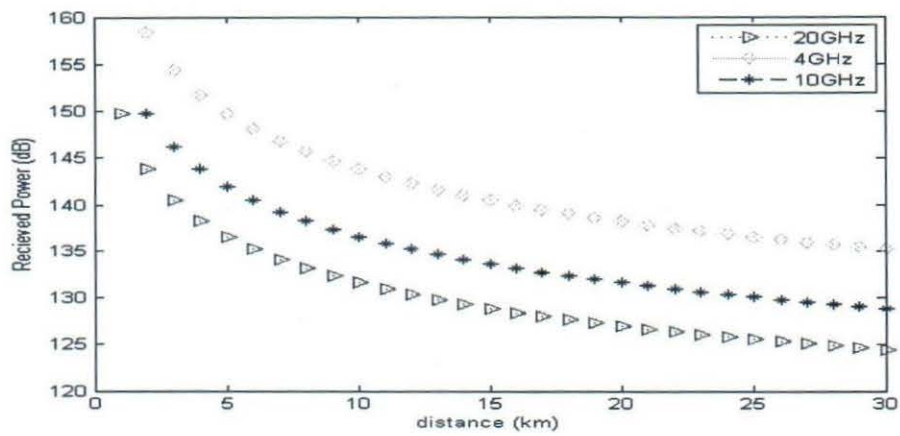


Figure 85. Received power against the separation between two antennas in Jalingo

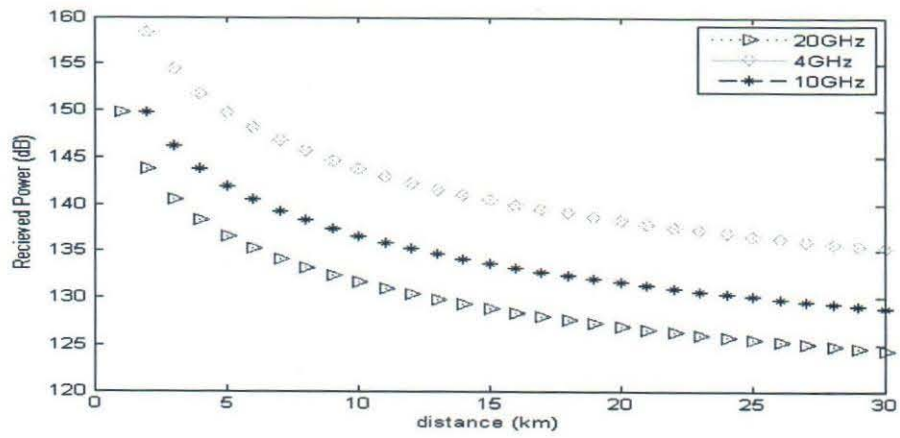


Figure 86. Received power against the separation between two antennas in Maiduguri

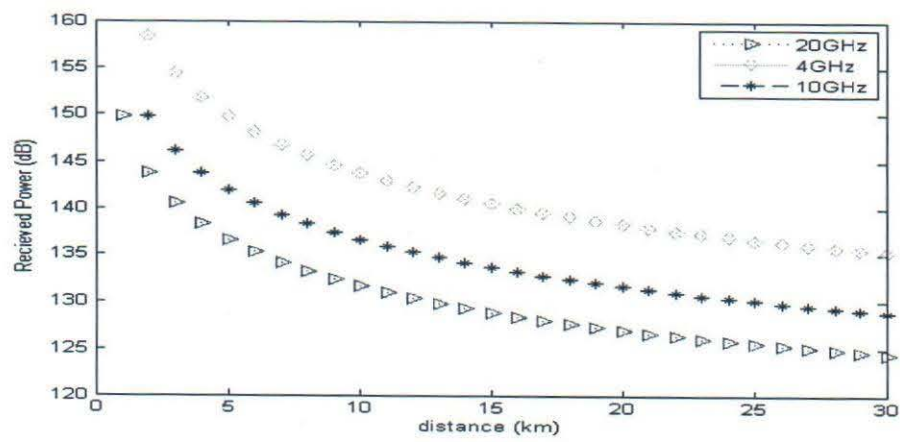


Figure 87. Received power against the separation between two antennas in Yola

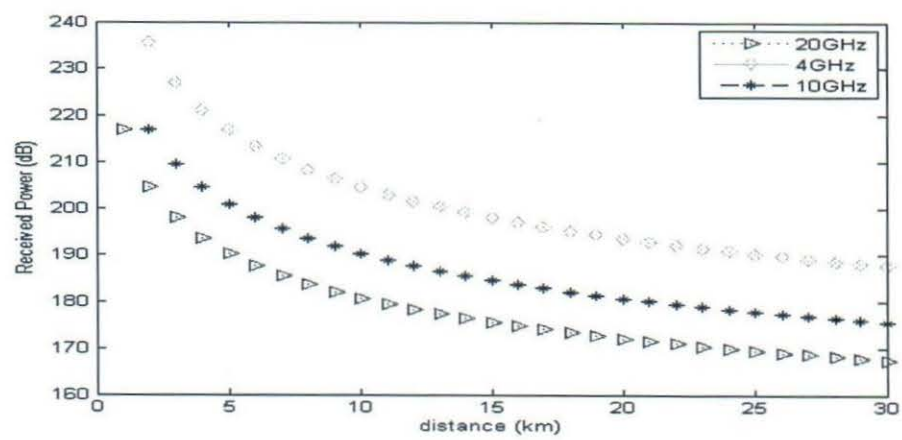


Figure 88. Received power against the separation between two antennas in Free Space

Path loss as a function of distance for rain attenuation and free space at signal of 4GHz

As seen from the figure 13 and figures 14 – 50, mentioned earlier, the output result of rain attenuation model (RAM) is higher compared to the output result of free space propagation model (FSPM); this accounts for the fact that degradation of radio signal occur as they traverse through rain. As illustrated, the two curves rise exponentially as the separation between the transmitter and the receiver increases. Though the two curves rise exponentially in the same manner, there is a relatively higher path loss in the rain attenuation model than the free space model. Also, free space model depend on the permittivity and permeability of the medium in free space. The permittivity and permeability of a medium depends on the intrinsic impedance of the medium. It had been noted that attenuation of the radio signal increases with increase in the intrinsic impedance and also decrease as impedance decreases. This is so because the intrinsic impedance depends solely on permittivity and permeability of the material medium; thus as the value of the permittivity and permeability increases, the value of intrinsic impedance also increases. This has direct effect on the attenuation of radio signals as they traverse through rain. Secondly, as the path loss increases, there is a gradual degradation in the strength of the signals as the separation between antennas increases. The graphs of the two models take an exponential form; is as a result of the fact that attenuation produced increases exponentially as the signal decays gradually. We shall compare the results of the attenuation obtained by taking the least, the middle and the highest values of distances between the two antennas from the tabulated result in tables 2 and 3 in Appendix B. Thus, at a distance of 1km, the path loss of the FSPM at frequencies 4GHz, 10GHz and 20GHz respectively are 198.33, 216.66 and 230.52 dB; while the path loss for the RAM for Abeokuta at these frequencies for the distance of 1km are respectively 302.03, 320.36 and 334.22 dB. At a distance of 15km, the path loss for the FSPM at these frequencies respectively are 252.49, 270.82 and 284.68 dB; while that of the RAM at those frequencies respectively

are 356.19, 374.52 and 388.38 dB. Finally, at a distance of 30km, the path loss for free space model at various frequencies respectively are 266.35, 284.68 and 298.54; while that of the rain attenuation model at various frequencies are 370.06, 388.38 and 402.25 respectively.

Path loss as a function of distance for the rain attenuation model (RAM) and free space propagation model (FSPM) at 10GHZ

The analysis at 10GHz also obtained from figures 13 and 14 – 50 in and tables 2 and 3-49 in Appendix B for free space propagation model and rain attenuation model respectively. It can be shown that, the level at which the signals get impaired (attenuated) at 10GHz is higher compared to the level of impairment at 4GHz. This implies that, attenuation of signals due to rainfall is greatly influenced by the transmission frequency of the signal. The graphs illustrated in figures 13 - 50, show that, as the attenuation increases with increase in frequency. This accounts for the reason why the attenuation produced by the frequency of 10GHz is higher than that of 4GHz. The result also show that the curve for the path loss at 10GHz assume the same shape as the that of the path loss at 4GHz, which takes an exponential form as well. This demonstrates the relationship between attenuation and frequency as discussed earlier.

Path loss as a function for rain attenuation and free space model at 20GHz

The analysis of the behaviour of the graph at 20GHz is similar to 4GHz and 10GHz. As shown in the graphs, the level of attenuation of the radio signal at 20GHz is higher compared to the other operating frequencies. There is considerable increase in attenuation in line with the increase in operating frequencies. This can conclusively be said that an increase in the separation between the two antennas implies higher path loss.

Comparing the path loss, L , at various (37) sites in Nigeria

As illustrated in the graph of the path loss as a function of the separation between the two antennas for the 37 sites presented in figures 14 – 50; there is similarities in the results obtained and hence, the curves for all observation sites. This shows that the result of the RAM for all sites are very close. Consequently, indicating that the attenuation estimate for any region in Nigeria is apparently very similar to almost the entire West African countries because the climatic trends are closely related.

4.7.3 Comparison of the Received Power, P_r , as a function of the separation between the two antennas $d(\text{km})$ for the RAM and FSPM at three different frequencies (4GHz, 10GHz and 20GHz)

The results of analysis confirm that the received power is another parameter that is very significant in communication. The essence of communication is to get the signal to the receiver. In this wise, the parameter was also obtained during simulation. The signal strength at the receive antenna determines the amount of power that is satisfactorily required to obtain coverage in an area. The result of the simulation is illustrated in tables 2 – 39 of Appendix B, for the received power as a function of the separation between the antennas for both the RAM and FSPM. The received power, P_r , was plotted against the corresponding distances between transmit and receive antennas in both the rain attenuation model and the free space propagation model. This is illustrated in figures 51 – 87 for rain attenuation model for 37 sites and figure 88 for free space propagation model.

Received power, P_r , as a function of distance between the receive and transmit antennas for RAM and FSPM for the three different frequencies

The results of analysis confirm that the graphs in figures 51-88, at the three frequencies have similar curve, and slopes down as the distance between the receiver and the transmitter increases and relative to the fact that the path loss increases

with increase in distance between antennas. The graph of the output result for the RAM slopes below that due to free space because of the effect of rain. The result further asserted that due to scattering and absorption of the radio signal by drops of rain, most of the signals intended to reach the receive antenna get impaired as the distance between the receive antenna and transmit antenna increases. In addition, the result also indicate that the amount of power received when propagating in free space condition is greater since the radio waves are not interacting with any particles that will distort the free flow of signals. The analysis reveal that the signals traversing in free space on the other hand traverse under a clear line of site (LoS) condition while the signal traversing in rain have part of the signals being absorbed and part of the signals being scattered in diverse directions. The result of analysis confirm that the receive power in the FSPM is greater compared to the received power due to the RAM. The result of analysis for the three different frequencies has the same pattern. Finally, the output results of the signal at 4GHz has the same shape and slope as the output result of the signals at 10GHz and 20GHz.

4.7.4 Chances of satisfactory performance of wireless communication system in a region dominated by rain.

Microwave line-of-sight propagation is based on the principles of electrodynamics. In practice, fading caused by actual terrain, atmospheric and climatic conditions forces the microwave engineer to take a statistical approach to predicting the power loss and distortion of a received signal over time. Path loss is therefore an important parameter which must be taken into consideration when planning for a radio communication system; this will help a radio engineer determine the distance at which one antenna will be cited from the other. This parameter is also important in determining the hand off speed and cell sizes.

Chapter 5

SUMMARY, CONCLUSION AND RECOMMENDATIONS

5.1 Summary

Precipitation due to rain is the most challenging source of impairment to signal propagation in the microwave and millimeter wave bands. This remains a major problem in the deployment of terrestrial and satellite communication systems, particularly for operations above 3 GHz. Interestingly, the prediction of the attenuation induced over a link is mainly dependent on the precipitation data, preferably those locally measured over such a location. However, the dearth of appropriate precipitation data for estimating rain induced attenuation on satellite and terrestrial links in the tropical climates such as Nigeria has been a major challenge over the years and this affects the accuracy of predicted fade margins as required for the planning of satellite and terrestrial communication links over Nigeria. The attainment of designed availability objectives on microwave and millimeter wave links strongly depends on the local rainfall data for a particular location. Rain attenuation effects have been studied worldwide over the past years and various models for solving the problem have been offered. Nevertheless, at present time, the continuing research is required in the field of designing the reliable microwave communication links, as the higher bandwidth capability links are in demand. In forecasting rain attenuation in Nigeria, the rain drop size measurements obtained from the study and the 14-year variations of one-minute rainfall rates for 37 sites comprising of 36 state capitals and Abuja sourced at Tropical Rainfall Measurement Mission satellite database validated with rainfall prediction estimates from Nigerian Meteorological Agency was treated with the Rain Attenuation Model derived in chapter three. The research reveal that this will help in the planning of satellite and terrestrial communication links over Nigeria. The signals traversing at very high and ultra-high frequencies get impaired when they come in contact with rain. The model obtained describes extensively the extent to which radio signals are affected by rain as was simulated at frequencies of

4GHz, 10GHz and 20GHz for various separations of receive and transmit antennas. The analysis of the study reveals that the model is useful for the calculation of specific microwave attenuation due to rain drops at the frequency range of 3Hz to 100GHz. The analysis also attested that the model provides a simple method for quickly calculating specific microwave attenuation as a function of frequency, separation between two antennas and mean radii of raindrops.

5.2 Conclusion

In the quest to reduce the problem of rainfall attenuation and to update global precipitation database for radio-climatic and other applications, authentic precipitation estimates are needed for modelling the behaviour of wireless communication link. This research reveals that a derived reliable model can also provide a platform for predicting attenuation by rain. The RAM provides a simple and inexpensive method for calculating attenuation of microwave relative to raindrops as they are traversed. The incorporation of the parameters relative to the RAM, a new numerical formula for calculation of specific rain attenuation is therefore established. The validity of the RAM is checked by comparing the results obtained for the specific rain attenuation with those obtained by the free space model. The calculation of microwave attenuation will be carried out for a wide range of operating frequencies and rain rates. This model makes it practical for direct use by wireless communication system designers. Finally, it is important to take into cognizance the effects of drop size and operating frequencies on transmitting microwave during rain.

5.3 Recommendation

After extensive investigation on the effect of rainfall on radio signals, it was noted that an alternative to sourced rainfall data is carrying out the field work and obtaining raw measured data for use with the RAM. However, such quest requires years of observation. It is recommended that such research centre be set up to support future similar predictions. In the process of this study, it was observed that there are some climatic and environmental factors such as fog, mist, trees and buildings. This research covered the effect of rain on radio signals; thus subsequent

research work should be the effect of trees, atmospheric gases, flying objects, mist and fog on microwave attenuation. All these associated factors also contribute to the fading of signals as they traverse from one point to the other. The result of the study gives the radio engineer a better understanding on how to plan radio frequency systems for the purpose of its coverage analysis. Coverage analysis uses the propagation model and rainfall data to predict the radio frequency coverage area of a transmitter and the received signal strength at the end of a wireless link. The path loss from the transmitter to a distance receive and the minimum antenna height to establish LoS communication are obtained. Finally, channel impairment as delay spread due to multi-path fading is established.

- Brussaard, G. (1974). Rain-induced crosspolarisation and raindrop canting. *Electronics Letters*, 10(20):411–412.
- Bryant, G. H., Adimula, I., and Riva, C. (2001). Rain attenuation statistics from rain cell diameters and heights. *International Journal of Satellite Communications*, 19:263–283.
- Calla, O. P. N. and Purohit, I. S. (1971). Study of effect of rain and dust on propagation of radio waves ant millimeter wavelewave. Technical report, International Centre for Radio Science, OM NIW AS A-23 Shastri Nagar Jodhpur.
- Capsoni, C., Fedi, F., Magistroni, C., Paraboni, A., and Pawlina, A. (1987). Data and theory for a new model of the horizontal structure of rain cells for propagation applications. *Radio Sci.*, 22(3):395–404.
- Capsoni, C., Luni, L., Paraboni, A., and Riva, C. (2006). Stratiform and convective rain discrimi- nation deduced from local $p(r)$. *IEEE Transactions on Antennas and Propagation*, 54(11):3566–3569.
- Castanet, L. (2001). *Fade mitigation techniques for new SatCom systems At Ka and V Bands*. Phd thesis,, Department of Electromagnetism and Radar, University of Toulouse.
- Castanet, L., Deloues, T., and Lemorton, J. (2003). Channel modelling based on n-state markov chains for satcom systems simulation. In *Proc. International Conference on Antennas and Propagation*,, pages 119–122.
- Chuang, C. C. and Beard, K. V. (1990). A numerical model for the equilibrium shape of electrified raindrops. *Journal of the Atmospheric Sciences*, 47(11):1374–1389.
- Committee, U. S. (1996). *Handbook on Radio propagation Related to Satellite Communications in Tropical and and Subtropical Countries*,. URSI Standing Committee on Developing Countries, 1996.
- Crane, R. K. (1990). Space-time structure of rain rate fields. *Journal of Geophysical Research*, 95:2011–2020.
- Crook, N. A. (1996). Sensitivity of moist convection forced by boundary layer processes to low-level thermodynamic fields. *Monthly Weather Review*, 124:1767–1785.
- Dossi, L. (1990). Real-time prediction of attenuation for applications to fade countermeasures in satellite communications. *Electronics Letters*, 26(4):250–251.
- Doswell-III, C. A. and Rasmussen, E. N. (1994). The effect of neglecting the virtual temperature correction on cape calculations. *American Meteorological Society*, 9:625–629.
- Drufuca, G. (1974). Rain attenuation statistics for frequencies above 10 ghz from rain gauge observations. *J. Rech. Atmos*, 1(2):399–411.

- Feingold, G. and Levin, Z. (1986). The lognormal fit to raindrop spectra from frontal convective clouds in israel. *Journal of Climate and Applied Meteorology*, 25:1346–1363.
- F'eral, L., Mesnard, F., Sauvageot, H., Castanet, L., and Lemorton, J. (2000). Rain cells shape and orientation distribution in south-west of france. *Phys. Chem. Earth B*, 25(1012):1073–1078.
- F'eral, L., Sauvageot, H., and Castanet, L. (2003). Hycell - a new hybrid model of the rain horizontal distribution for propagation studies: 2. statistical modeling of the rain rate field. *Radio Science*, 38(3):1057.
- Gilbert, E. N. (1985). Energy reception for mobile radio". *BSTJ*, 44:1779.
- Giuli, D., Toccafondi, A., Biffi Gentili, G., and Freni, A. (1991). Tomographic reconstruction of rainfall field through microwave attenuation measurements. *Journal of Applied Meteorology*, 30:1323–1340.
- Gloaguen, C. and Lawergnat, J. (1996). Attenuation due to hydrometeors at 94 -ghz - experimetal results and comparison with theory. *IEEE Microwaves, Antennas and Propagation, Proceedings*, 143(1):79–86.
- Goldhirsh, J. (2000). Two-dimension visualization of rain cell structures. *Radio Science*, 35(3):713–729.
- Gremont, B., Filip, M., Gallois, P., and Bate, S. (1999). Comparative analysis and performance of two predictive fade detection schemes for ka-band fade countermeasures. *IEEE Journal On Selected Areas in Communications*, 17(2180192).
- Gunn, R. and Kinzer, G. D. (1949). The terminal velocity of fall for water. *Journal of Meteorology*, 6:243–248.
- Head, H. T. (1999). The influence of rain on television field strength at u-h frequencies". In *Proc. IRE*, volume 48, pages 1016–1020.
- Henry, T., van der Zanden, Robert, J. W., and Matti, H. A. J. H. (2007). Rain induced bistatic scattering at 60ghz. *Journal on Wireless Communications and Networking*, 6. Article ID 53202 Doi: 10, 1155/2007/53203.
- Hodges, D. D. (2006). *Propagation forecasting for EHF and SHF systems*. Phd thesis,, Department of Electronic and Electrical Engineering, University of Bath.
- Holton, J. R., Curry, J. A., and Pyle, J. A. (2003). *Encyclopedia of Atmospheric Sciences*, volume 3. Elsevier.
- Houze, R. (1993). *Cloud Dynamics*. Academic, San Diego, California.
- Illingworth, A. J. (2004). *Improved precipitation rates and data quality by using polarimetric measurements*. In *Weather Radar: Principles and Advanced Applications*. Springer-Verlag, Berlin.
- ITU (2006). Specific attenuation model for rain for use in prediction methods. In *ITU-R Recommendations and Reports, ITU-R P.838-3*, Geneva, Switzerland, September, 2006.

- Mass, J. (1987). A simulation study of rain attenuation and diversity effects on satellite links. *COMSAT Technival Review*, 17(1):159–187.
- Matricciani, E. (1996). Physical-mathematical model of the dynamics of rain attenuation based on rain rate time series and a two layer vertical structure of precipitation. *Radio Science*, 31(2):281–295.
- Moupfouma, F. and Martin, L. (1995). Modeling of rain rate cumulative distribution for the design of satellite and terrestrial communication systems”,. *Int. Journal of Satellite Communication*, 13(2):105–115.
- Murat, U. (2001). *Cooperative Communication for Improved Wireless Network Transmission; Framework of Virtual Antennas*. University of Waterloo, Canada.
- Oguchi, T. (1991). Effects of incoherent scattering on microwave and millimetre wave. *Electronics Letters*, 27(9):759–761.
- Ojo, J. S., Adewole, M. O., and Sarkar, S. K. (2008). Rain rate and rain attenuation prediction for satellite communication in ku and ka bands over nigeria”. Technical report, Radio and Atmos. Sci. Division, Nat. physical Lab. New Delhi 110012, India.
- Panagopoulos, A. D., Arapoglou, P. D. M., and Cottis, P. G. (2004). Satellite communications at ku, ka, and v bands: Propagation impairments and mitigation techniques. *IEEE Communications Surveys and Tutorials*, 6(3):2–14.
- Papazian, B. P., Hufford, G. A., Achatz, R. J., and Hoffman, J. (1997). Study of the local multipoint distribution service radio channel”,. *IEEE Trans. Broadcasting*, 43(2):175–184.
- Pruppacher, H. R. and Beard, K. V. (1970). A wind tunnel investigation of the internal circulation and shape of water drops falling at terminal velocity in air. *Quart. J. R. Met. Soc.*, 96:247–256.
- Pruppacher, H. R. and Pitter, R. L. (1971). A semi-empirical determination of the shape of cloud and rain drops. *Journal of Atmospheric Sciences*, 28:86–94.
- Saikia, M., Devi, M., Barbara, A. K., and Sarmar, H. K. (2009). Raindrop size distribution profiling by laser disdrometer and rain attenuation of centimeter radio waves, . *Indian Journal of Radio and Space physics*.
- Savic, P. (1953). Circulation and distortion of liquid drops falling through a viscous medium. Report – mt-22., National Research Council of Canad Ottawa.
- Spilhaus, A. F. (1947). Raindrop size, shape, and falling speed. *Journal of Meteorology*, 5:108–110.
- Tat-soon, Y. (1998). An efficient formula for rainfall microwave attenuation”,. *IEEE Transactions on antennas and propagation*, 46(8).
- Testud, J., Oury, S., Black, R. A., Amayenc, P., and Dou, X. (2001). The concept of “normalized” distribution to describe raindrop spectra: A tool for cloud physics and cloud remote sensing. *Journal of Applied Meteorology*, 40:1118–1140.

pplica meteorology, 40:2083–2097.

Townsend, A. J. and Watson, R. J. (2011). The linear relationship between attenuation and average rainfall rate for terrestrial links. *IEEE Transaction on Antennas and Propagation*, 59(3):994–1213.

Townsend, A. J., Watson, R. J., and Hodges, D. D. (2009). Analysis of the variability in the raindrop size distribution and its effect on attenuation. *IEEE Antennas and Propagation Letters*, 6:100–103.

- Theodore, S. and Rappaport (2000). A note on the gamma distribution. *Monthly Weather Review*, 86(4):117–122.
- Tokay, A., Kruger, A., and Krajewski, W. F. (2001). Comparison of drop size distribution measurements by impact and optical disdrometers. *Journal of Applied Meteorology*, 40:2083–2097.
- Townsend, A. J. and Watson, R. J. (2011). The linear relationship between attenuation and average rainfall rate for terrestrial links. *IEEE Transaction on Antennas and Propagation*, 59(3):994–1213.
- Townsend, A. J., Watson, R. J., and Hodges, D. D. (2009). Analysis of the variability in the raindrop size distribution and its effect on attenuation at 20-40 ghz. *IEEE Antennas and Wireless Propagation Letters*, 8:1210–1213.
- Tzler, C. M. (1994). Microwave (1-100ghz) dielectric model of raindrops. *IEEE Transaction on Geoscience and Remote Sensing*, 32(5):947–949.
- Ulaby, F. and El-Rayes, M. (1987). Microwaves dielectric spectrum of vegetation, part ii: Dual-dispersion model. *IEEE Trans. Geosci. and Remote Sensing*, 25(5):550–556.
- Van de Kamp, M. M. J. (1999). *Climatic radiowave propagation models for the design of satellite communication systems*. Phd thesis, University of Eindhoven.
- Wallace, J. M. and Hobbs, P. V. (2006). *Atmospheric Science: An Introductory Survey*. Academic Press, Burlington.
- Walsch, J. and Bertoni, H. L. (1998). A theoretical model of uhf propagation in urban environments. *IEEE Trans. on Antennas and Propagation*, 36:1788–1789.
- Watson, R. J., Mar'ecal, A. R. H., V., and Testud, J. (1999). A rainrate-attenuation-reflectivity relation for use in the spaceborne and airborne sensing of rain. *IEEE Transactions Geoscience And Remote Sensing*, 37(3):1447–1450.
- Yau, M. K. and Rogers, R. R. (1984). An inversion problem on inferring the size distribution of precipitation areas from raingage measurements. *Journal of Atmospheric Sciences*, 41(3):439–447.
- Zinevich, A., Alpert, P., and Messer, H. (2008). Estimation of rainfall field using commercial microwave communication networks of variable density. *Advances in Water Resources*, 31:1470–1480.

APPENDIX A

Time-average Poynting Vector

The Poynting vector represents the particular case of an energy flux vector for electromagnetic energy. For time-harmonic electromagnetic fields, the average power flux over time can be found as follows:

$$\begin{aligned}
 W &= ExH \\
 &= Re(Ee^{j\omega t}) \times Re(He^{j\omega t}) \\
 &= \frac{1}{2}(Ee^{j\omega t} + Ee^{-j\omega t}) \times \frac{1}{2}(He^{j\omega t} + He^{-j\omega t}) \\
 &= \frac{1}{4}(ExH^* + (E^*xH) + (ExHe^{2j\omega t}) + (E^*xH^*e^{-2j\omega t})) \\
 &= \frac{1}{4}[(ExH^*) + (E^*xH) + (ExHe^{2j\omega t}) + (ExH^{2j\omega t})^*] \\
 &= \frac{1}{2}Re(ExH^*) + \frac{1}{2}Re(ExHe^{2j\omega t})
 \end{aligned} \tag{109}$$

If the average over time is given by \bar{W} , then the equation above can be expressed as

$$\begin{aligned}
 \bar{W} &= \frac{1}{T} \int_0^T W(t) dt \\
 \bar{W} &= \frac{1}{T} \int_0^T \left(\frac{1}{2}Re(ExH^*) + \frac{1}{2}Re(ExHe^{2j\omega t}) \right) dt
 \end{aligned} \tag{110}$$

The second term is a sinusoidal curve $Re(e^{2j\omega t}) = \cos 2\omega t$, whose average will be zero; thus this gives

$$\bar{W} = \frac{1}{2}Re(ExH^*) \tag{111}$$

APPENDIX B

One minute rainfall rate measured in mm/h exceeded for 0.01 percent average for 37 sites from January 1998 to December 2012 sourced from Tropical Rainfall Measurement Mission (TRMM) Satellite and validated with Nigerian Meteorological Agency (NIMET) rainfall prediction. Tabulated simulation result showing the path loss and power received in free space and various observation sites.

Table 1. One minute rainfall rate measured in mm/h exceeded for 0.01 percent average for 37 sites from January 1998 to December 2012 sourced from TRMM Satellite and validated with NIMET rainfall prediction.

State Capitals	1998	1999	2000	2001	2002	2003	2004	2005	2006	2007	2008	2009	2010	2011	2012	Mean
Abeokuta	84	96	89	79	92	88	92	77	87	88	92	77	87	88	90	87
Adoekiti	98	102	92	87	95	87	86	87	93	87	86	87	93	90	88	91
Akure	96	107	90	88	92	85	90	91	110	85	90	91	110	103	95	95
Ibadan	92	110	89	85	93	94	92	85	94	94	92	85	94	93	94	92
Ikeja	81	89	69	79	91	83	77	81	76	83	77	81	76	85	91	81
Osogbo	92	110	88	91	95	93	96	87	96	93	96	87	96	91	96	94
Abakiliki	114	131	128	121	133	120	129	123	128	120	129	123	128	130	129	126
Awka	102	117	111	120	119	113	102	101	114	113	102	101	114	112	111	110
Enugu	102	117	111	120	119	113	102	101	114	113	102	101	114	112	111	110
Owerri	116	134	121	129	129	121	115	122	134	121	115	122	134	132	123	125
Umuahia	116	134	121	129	129	121	115	122	134	121	115	122	134	132	123	125
Asaba	101	120	115	115	115	101	111	111	123	101	111	111	123	112	107	112
Benin	102	115	109	110	112	86	99	104	110	86	99	104	110	110	102	104
Calabar	101	106	110	106	107	100	99	106	136	100	99	84	136	122	123	109
Port Harcourt	121	124	118	118	120	107	120	101	117	107	120	101	117	120	119	115
Uyo	125	130	116	130	123	117	120	123	129	117	120	123	129	121	120	123
Yenagoa	113	134	121	118	124	117	135	128	129	117	135	128	129	121	126	125
Abuja	102	94	89	94	101	102	87	84	96	87	84	89	96	91	93	93
Ilorin	83	98	93	90	86	88	93	84	84	93	84	93	84	91	85	89
Lafia	87	93	84	87	101	91	85	79	96	85	79	84	96	93	86	88
Lokoja	95	101	86	86	97	92	94	82	102	94	82	86	102	97	101	93
Makurdi	91	102	95	81	104	97	87	98	96	87	98	95	96	91	93	94
Minna	84	96	79	86	86	84	76	77	87	76	97	79	87	86	88	85
Jos	103	85	85	91	96	92	85	88	98	85	88	85	98	95	89	91
Birni Kebbi	69	72	55	59	74	72	69	70	66	72	69	70	66	66	67	68
Gusau	68	69	74	69	67	78	61	64	71	78	61	64	71	64	77	69
Kaduna	98	89	72	88	81	89	83	80	93	89	83	80	93	89	91	87
Kano	76	69	68	66	67	76	73	67	71	76	73	67	71	71	69	71
Katsina	70	69	63	61	57	69	64	68	65	69	64	68	65	61	64	65
Sokoto	71	64	63	44	67	52	57	60	60	52	57	64	60	59	60	59
Bauchi	92	83	72	84	78	79	66	65	82	79	66	65	82	64	81	76
Damaturu	71	60	63	59	62	86	60	71	65	86	60	71	65	74	80	69
Dutse	73	72	67	66	69	80	68	62	70	80	68	62	70	69	72	70
Gombe	71	70	67	62	71	81	75	68	77	81	75	68	77	72	72	72
Jalingo	91	92	99	91	86	88	111	89	107	88	111	89	107	93	101	96
Maiduguri	67	82	63	67	69	68	72	62	63	68	72	62	63	67	69	68
Yola	81	82	76	77	83	90	91	74	87	90	91	74	87	90	81	84

Table 2. Simulated results showing path and power received for FREE SPACE.

Site	Distance	4GHz		10GHz		20GHz	
		Pathloss	Received Power	Pathloss	Received Power	Pathloss	Received Power
	1	198.33	252.1	216.66	230.78	230.52	216.9
	2	212.19	235.63	230.52	216.9	244.38	204.6
	3	220.3	226.96	238.63	209.53	252.49	198.03
	4	226.06	221.18	244.38	204.6	258.25	193.61
	5	230.52	216.9	248.85	200.93	262.71	190.33
	6	234.17	213.52	252.49	198.03	266.35	187.72
	7	237.25	210.75	255.58	195.64	269.44	185.57
	8	239.92	208.4	258.25	193.61	272.11	183.75
	9	242.28	206.38	260.6	191.86	274.46	182.17
	10	244.38	204.6	262.71	190.33	276.57	180.79
	11	246.29	203.01	264.61	188.95	278.48	179.55
	12	248.03	201.59	266.35	187.72	280.22	178.43
	13	249.63	200.3	267.96	186.6	281.82	177.42
	14	251.11	199.11	269.44	185.57	283.3	176.49
	15	252.49	198.03	270.82	184.63	284.68	175.64
	16	253.78	197.02	272.11	183.75	285.97	174.84
	17	255	196.08	273.32	182.94	287.18	174.1
	18	256.14	195.21	274.46	182.17	288.33	173.41
	19	257.22	194.39	275.55	181.46	289.41	172.77
	20	258.25	193.61	276.57	180.79	290.43	172.16
	21	259.22	192.89	277.55	180.15	291.41	171.58
	22	260.15	192.2	278.48	179.55	292.34	171.03
	23	261.04	191.54	279.37	178.98	293.23	170.51
	24	261.89	190.92	280.22	178.43	294.08	170.02
	25	262.71	190.33	281.03	177.91	294.9	169.55
	26	263.49	189.76	281.82	177.42	295.68	169.1
	27	264.25	189.22	282.57	176.95	296.44	168.67
	28	264.98	188.7	283.3	176.49	297.16	168.26
	29	265.68	188.2	284	176.05	297.87	167.86
	30	266.35	187.72	284.68	175.64	298.54	167.48

FREE SPACE

Table 3. Simulated results showing path and power received for ABEOKUTA.

Site	Distance	4GHz		10GHz		20GHz	
		Pathloss	Received Power	Pathloss	Received Power	Pathloss	Received Power
ABEOKUTA	1	302.03	165.54	320.36	156.07	334.22	149.6
	2	315.9	158.28	334.22	149.6	348.09	143.64
	3	324.01	154.32	342.33	146.06	356.19	140.37
	4	329.76	151.63	348.09	143.64	361.95	138.14
	5	334.22	149.6	352.55	141.82	366.41	136.46
	6	337.87	147.99	356.19	140.37	370.06	135.11
	7	340.95	146.65	359.28	139.17	373.14	134
	8	343.62	145.51	361.95	138.14	375.81	133.05
	9	345.98	144.52	364.3	137.25	378.17	132.22
	10	348.09	143.64	366.41	136.46	380.27	131.48
	11	349.99	142.86	368.32	135.75	382.18	130.83
	12	351.73	142.15	370.06	135.11	383.92	130.24
	13	353.33	141.51	371.66	134.53	385.52	129.69
	14	354.81	140.92	373.14	134	387	129.2
	15	356.19	140.37	374.52	133.5	388.38	128.74
	16	357.49	139.87	375.81	133.05	389.67	128.31
	17	358.7	139.39	377.02	132.62	390.89	127.91
	18	359.84	138.95	378.17	132.22	392.03	127.54
	19	360.92	138.53	379.25	131.84	393.11	127.19
	20	361.95	138.14	380.27	131.48	394.14	126.86
	21	362.92	137.77	381.25	131.15	395.11	126.55
	22	363.85	137.42	382.18	130.83	396.04	126.25
	23	364.74	137.08	383.07	130.52	396.93	125.97
	24	365.59	136.76	383.92	130.24	397.78	125.7
	25	366.41	136.46	384.74	129.96	398.6	125.44
	26	367.2	136.17	385.52	129.69	399.38	125.19
	27	367.95	135.89	386.28	129.44	400.14	124.96
	28	368.68	135.62	387	129.2	400.87	124.73
	29	369.38	135.36	387.71	128.96	401.57	124.51
	30	370.06	135.11	388.38	128.74	402.25	124.3

Table 4. Simulated results showing path and power received for ADOEKITI.

Site	Distance	4GHz		10GHz		20GHz	
		Pathloss	Received Power	Pathloss	Received Power	Pathloss	Received Power
ADOEKITI	1	302.03	165.54	320.36	156.07	334.22	149.6
	2	315.9	158.28	334.22	149.6	348.09	143.64
	3	324.01	154.32	342.33	146.06	356.2	140.37
	4	329.76	151.63	348.09	143.64	361.95	138.14
	5	334.22	149.6	352.55	141.82	366.41	136.46
	6	337.87	147.99	356.2	140.37	370.06	135.11
	7	340.95	146.65	359.28	139.17	373.14	134
	8	343.62	145.51	361.95	138.14	375.81	133.05
	9	345.98	144.52	364.31	137.25	378.17	132.22
	10	348.09	143.64	366.41	136.46	380.28	131.48
	11	349.99	142.86	368.32	135.75	382.18	130.83
	12	351.73	142.15	370.06	135.11	383.92	130.23
	13	353.33	141.51	371.66	134.53	385.52	129.69
	14	354.82	140.92	373.14	134	387	129.2
	15	356.2	140.37	374.52	133.5	388.38	128.74
	16	357.49	139.87	375.81	133.05	389.68	128.31
	17	358.7	139.39	377.02	132.62	390.89	127.91
	18	359.84	138.95	378.17	132.22	392.03	127.54
	19	360.92	138.53	379.25	131.84	393.11	127.19
	20	361.95	138.14	380.28	131.48	394.14	126.86
	21	362.93	137.77	381.25	131.15	395.11	126.55
	22	363.86	137.42	382.18	130.83	396.04	126.25
	23	364.74	137.08	383.07	130.52	396.93	125.97
	24	365.6	136.76	383.92	130.23	397.78	125.7
	25	366.41	136.46	384.74	129.96	398.6	125.44
	26	367.2	136.17	385.52	129.69	399.39	125.19
	27	367.95	135.89	386.28	129.44	400.14	124.96
	28	368.68	135.62	387	129.2	400.87	124.73
	29	369.38	135.36	387.71	128.96	401.57	124.51
	30	370.06	135.11	388.38	128.74	402.25	124.3

Table 5. Simulated results showing path and power received for AKURE.

Site	Distance	4GHz		10GHz		20GHz	
		Pathloss	Received Power	Pathloss	Received Power	Pathloss	Received Power
AKURE	1	302.04	165.54	320.36	156.07	334.23	149.6
	2	315.9	158.28	334.23	149.6	348.09	143.64
	3	324.01	154.32	342.33	146.06	356.2	140.37
	4	329.76	151.62	348.09	143.64	361.95	138.14
	5	334.23	149.6	352.55	141.82	366.41	136.46
	6	337.87	147.99	356.2	140.37	370.06	135.11
	7	340.95	146.65	359.28	139.17	373.14	134
	8	343.63	145.51	361.95	138.14	375.81	133.04
	9	345.98	144.52	364.31	137.25	378.17	132.22
	10	348.09	143.64	366.41	136.46	380.28	131.48
	11	349.99	142.86	368.32	135.75	382.18	130.83
	12	351.73	142.15	370.06	135.11	383.92	130.23
	13	353.34	141.51	371.66	134.53	385.52	129.69
	14	354.82	140.92	373.14	134	387.01	129.2
	15	356.2	140.37	374.52	133.5	388.39	128.74
	16	357.49	139.86	375.81	133.04	389.68	128.31
	17	358.7	139.39	377.03	132.62	390.89	127.91
	18	359.84	138.95	378.17	132.22	392.03	127.54
	19	360.93	138.53	379.25	131.84	393.11	127.19
	20	361.95	138.14	380.28	131.48	394.14	126.86
	21	362.93	137.77	381.25	131.15	395.12	126.55
	22	363.86	137.42	382.18	130.83	396.05	126.25
	23	364.75	137.08	383.07	130.52	396.94	125.97
	24	365.6	136.76	383.92	130.23	397.79	125.7
	25	366.41	136.46	384.74	129.96	398.6	125.44
	26	367.2	136.17	385.52	129.69	399.39	125.19
	27	367.95	135.89	386.28	129.44	400.14	124.96
	28	368.68	135.62	387.01	129.2	400.87	124.73
	29	369.38	135.36	387.71	128.96	401.57	124.51
	30	370.06	135.11	388.39	128.74	402.25	124.3

Table 6. Simulated results showing path and power received for IBADAN.

Site	Distance	4GHz		10GHz		20GHz	
		Pathloss	Received Power	Pathloss	Received Power	Pathloss	Received Power
IBADAN	1	302.04	165.54	320.36	156.07	334.22	149.6
	2	315.9	158.28	334.22	149.6	348.09	143.64
	3	324.01	154.32	342.33	146.06	356.2	140.37
	4	329.76	151.62	348.09	143.64	361.95	138.14
	5	334.22	149.6	352.55	141.82	366.41	136.46
	6	337.87	147.99	356.2	140.37	370.06	135.11
	7	340.95	146.65	359.28	139.17	373.14	134
	8	343.62	145.51	361.95	138.14	375.81	133.04
	9	345.98	144.52	364.31	137.25	378.17	132.22
	10	348.09	143.64	366.41	136.46	380.28	131.48
	11	349.99	142.86	368.32	135.75	382.18	130.83
	12	351.73	142.15	370.06	135.11	383.92	130.23
	13	353.33	141.51	371.66	134.53	385.52	129.69
	14	354.82	140.92	373.14	134	387.01	129.2
	15	356.2	140.37	374.52	133.5	388.39	128.74
	16	357.49	139.87	375.81	133.04	389.68	128.31
	17	358.7	139.39	377.03	132.62	390.89	127.91
	18	359.84	138.95	378.17	132.22	392.03	127.54
	19	360.92	138.53	379.25	131.84	393.11	127.19
	20	361.95	138.14	380.28	131.48	394.14	126.86
	21	362.93	137.77	381.25	131.15	395.11	126.55
	22	363.86	137.42	382.18	130.83	396.05	126.25
	23	364.75	137.08	383.07	130.52	396.93	125.97
	24	365.6	136.76	383.92	130.23	397.79	125.7
	25	366.41	136.46	384.74	129.96	398.6	125.44
	26	367.2	136.17	385.52	129.69	399.39	125.19
	27	367.95	135.89	386.28	129.44	400.14	124.96
	28	368.68	135.62	387.01	129.2	400.87	124.73
	29	369.38	135.36	387.71	128.96	401.57	124.51
	30	370.06	135.11	388.39	128.74	402.25	124.3

Table 7. Simulated results showing path and power received for IKEJA.

Site	Distance	4GHz		10GHz		20GHz	
		Pathloss	Received Power	Pathloss	Received Power	Pathloss	Received Power
IKEJA	1	302.03	165.55	320.36	156.08	334.22	149.6
	2	315.89	158.28	334.22	149.6	348.08	143.64
	3	324	154.32	342.33	146.06	356.19	140.37
	4	329.76	151.63	348.08	143.64	361.95	138.14
	5	334.22	149.6	352.55	141.83	366.41	136.46
	6	337.87	147.99	356.19	140.37	370.05	135.12
	7	340.95	146.65	359.27	139.17	373.14	134
	8	343.62	145.51	361.95	138.14	375.81	133.05
	9	345.98	144.52	364.3	137.25	378.16	132.22
	10	348.08	143.64	366.41	136.46	380.27	131.49
	11	349.99	142.86	368.31	135.75	382.18	130.83
	12	351.73	142.15	370.05	135.12	383.92	130.24
	13	353.33	141.51	371.66	134.53	385.52	129.7
	14	354.81	140.92	373.14	134	387	129.2
	15	356.19	140.37	374.52	133.51	388.38	128.74
	16	357.48	139.87	375.81	133.05	389.67	128.31
	17	358.7	139.39	377.02	132.62	390.88	127.92
	18	359.84	138.95	378.16	132.22	392.03	127.54
	19	360.92	138.53	379.25	131.84	393.11	127.19
	20	361.95	138.14	380.27	131.49	394.13	126.86
	21	362.92	137.77	381.25	131.15	395.11	126.55
	22	363.85	137.42	382.18	130.83	396.04	126.25
	23	364.74	137.08	383.07	130.53	396.93	125.97
	24	365.59	136.76	383.92	130.24	397.78	125.7
	25	366.41	136.46	384.73	129.96	398.6	125.44
	26	367.19	136.17	385.52	129.7	399.38	125.19
	27	367.95	135.89	386.27	129.44	400.14	124.96
	28	368.68	135.62	387	129.2	400.86	124.73
	29	369.38	135.36	387.7	128.96	401.57	124.51
	30	370.05	135.12	388.38	128.74	402.24	124.3

Table 8. Simulated results showing path and power received for OSOGBO

Site	Distance	4GHz		10GHz		20GHz	
		Pathloss	Received Power	Pathloss	Received Power	Pathloss	Received Power
OSOGBO	1	302.04	165.54	320.36	156.07	334.22	149.6
	2	315.9	158.28	334.22	149.6	348.09	143.64
	3	324.01	154.32	342.33	146.06	356.2	140.37
	4	329.76	151.62	348.09	143.64	361.95	138.14
	5	334.22	149.6	352.55	141.82	366.41	136.46
	6	337.87	147.99	356.2	140.37	370.06	135.11
	7	340.95	146.65	359.28	139.17	373.14	134
	8	343.62	145.51	361.95	138.14	375.81	133.04
	9	345.98	144.52	364.31	137.25	378.17	132.22
	10	348.09	143.64	366.41	136.46	380.28	131.48
	11	349.99	142.86	368.32	135.75	382.18	130.83
	12	351.73	142.15	370.06	135.11	383.92	130.23
	13	353.34	141.51	371.66	134.53	385.52	129.69
	14	354.82	140.92	373.14	134	387.01	129.2
	15	356.2	140.37	374.52	133.5	388.39	128.74
	16	357.49	139.86	375.81	133.04	389.68	128.31
	17	358.7	139.39	377.03	132.62	390.89	127.91
	18	359.84	138.95	378.17	132.22	392.03	127.54
	19	360.92	138.53	379.25	131.84	393.11	127.19
	20	361.95	138.14	380.28	131.48	394.14	126.86
	21	362.93	137.77	381.25	131.15	395.12	126.55
	22	363.86	137.42	382.18	130.83	396.05	126.25
	23	364.75	137.08	383.07	130.52	396.93	125.97
	24	365.6	136.76	383.92	130.23	397.79	125.7
	25	366.41	136.46	384.74	129.96	398.6	125.44
	26	367.2	136.17	385.52	129.69	399.39	125.19
	27	367.95	135.89	386.28	129.44	400.14	124.96
	28	368.68	135.62	387.01	129.2	400.87	124.73
	29	369.38	135.36	387.71	128.96	401.57	124.51
	30	370.06	135.11	388.39	128.74	402.25	124.3

Table 9. Simulated results showing path and power received for ABAKALI KI

Site	Distance	4GHz		10GHz		20GHz	
		Pathloss	Received Power	Pathloss	Received Power	Pathloss	Received Power
ABAKALI KI	1	302.05	165.54	320.37	156.07	334.24	149.6
	2	315.91	158.27	334.24	149.6	348.1	143.64
	3	324.02	154.31	342.34	146.05	356.21	140.37
	4	329.77	151.62	348.1	143.64	361.96	138.14
	5	334.24	149.6	352.56	141.82	366.42	136.45
	6	337.88	147.98	356.21	140.37	370.07	135.11
	7	340.96	146.64	359.29	139.16	373.15	133.99
	8	343.64	145.5	361.96	138.14	375.82	133.04
	9	345.99	144.51	364.32	137.24	378.18	132.21
	10	348.1	143.64	366.42	136.45	380.29	131.48
	11	350	142.86	368.33	135.75	382.19	130.82
	12	351.74	142.15	370.07	135.11	383.93	130.23
	13	353.35	141.5	371.67	134.53	385.53	129.69
	14	354.83	140.91	373.15	133.99	387.02	129.19
	15	356.21	140.37	374.53	133.5	388.4	128.73
	16	357.5	139.86	375.82	133.04	389.69	128.31
	17	358.71	139.39	377.04	132.61	390.9	127.91
	18	359.85	138.95	378.18	132.21	392.04	127.54
	19	360.94	138.53	379.26	131.84	393.12	127.19
	20	361.96	138.14	380.29	131.48	394.15	126.86
	21	362.94	137.76	381.26	131.14	395.13	126.54
	22	363.87	137.41	382.19	130.82	396.06	126.24
	23	364.76	137.08	383.08	130.52	396.95	125.96
	24	365.61	136.76	383.93	130.23	397.8	125.69
	25	366.42	136.45	384.75	129.95	398.61	125.44
	26	367.21	136.16	385.53	129.69	399.4	125.19
	27	367.96	135.88	386.29	129.44	400.15	124.95
	28	368.69	135.62	387.02	129.19	400.88	124.73
	29	369.39	135.36	387.72	128.96	401.58	124.51
	30	370.07	135.11	388.4	128.73	402.26	124.3

Table 10. Simulated results showing path and power received for AWKA.

Site	Distance	4GHz		10GHz		20GHz	
		Pathloss	Received Power	Pathloss	Received Power	Pathloss	Received Power
AWKA	1	302.04	165.54	320.37	156.07	334.23	149.6
	2	315.9	158.28	334.23	149.6	348.09	143.64
	3	324.01	154.31	342.34	146.05	356.2	140.37
	4	329.77	151.62	348.09	143.64	361.96	138.14
	5	334.23	149.6	352.56	141.82	366.42	136.46
	6	337.88	147.98	356.2	140.37	370.07	135.11
	7	340.96	146.64	359.29	139.16	373.15	133.99
	8	343.63	145.51	361.96	138.14	375.82	133.04
	9	345.99	144.51	364.31	137.24	378.18	132.21
	10	348.09	143.64	366.42	136.46	380.28	131.48
	11	350	142.86	368.33	135.75	382.19	130.83
	12	351.74	142.15	370.07	135.11	383.93	130.23
	13	353.34	141.51	371.67	134.53	385.53	129.69
	14	354.82	140.92	373.15	133.99	387.01	129.2
	15	356.2	140.37	374.53	133.5	388.39	128.74
	16	357.49	139.86	375.82	133.04	389.68	128.31
	17	358.71	139.39	377.03	132.61	390.89	127.91
	18	359.85	138.95	378.18	132.21	392.04	127.54
	19	360.93	138.53	379.26	131.84	393.12	127.19
	20	361.96	138.14	380.28	131.48	394.15	126.86
	21	362.93	137.77	381.26	131.14	395.12	126.54
	22	363.86	137.41	382.19	130.83	396.05	126.25
	23	364.75	137.08	383.08	130.52	396.94	125.96
	24	365.6	136.76	383.93	130.23	397.79	125.69
	25	366.42	136.46	384.75	129.96	398.61	125.44
	26	367.2	136.16	385.53	129.69	399.39	125.19
	27	367.96	135.88	386.28	129.44	400.15	124.95
	28	368.69	135.62	387.01	129.2	400.87	124.73
	29	369.39	135.36	387.71	128.96	401.58	124.51
	30	370.07	135.11	388.39	128.74	402.25	124.3

Table 11. Simulated result showing path loss and power received for ENUGU.

Site	Distance	4GHz		10GHz		20GHz	
		Pathloss	Received Power	Pathloss	Received Power	Pathloss	Received Power
ENUGU	1	302.04	165.54	320.37	156.07	334.23	149.6
	2	315.9	158.28	334.23	149.6	348.09	143.64
	3	324.01	154.31	342.34	146.05	356.2	140.37
	4	329.77	151.62	348.09	143.64	361.96	138.14
	5	334.23	149.6	352.56	141.82	366.42	136.46
	6	337.88	147.98	356.2	140.37	370.07	135.11
	7	340.96	146.64	359.29	139.16	373.15	133.99
	8	343.63	145.51	361.96	138.14	375.82	133.04
	9	345.99	144.51	364.31	137.24	378.18	132.21
	10	348.09	143.64	366.42	136.46	380.28	131.48
	11	350	142.86	368.33	135.75	382.19	130.83
	12	351.74	142.15	370.07	135.11	383.93	130.23
	13	353.34	141.51	371.67	134.53	385.53	129.69
	14	354.82	140.92	373.15	133.99	387.01	129.2
	15	356.2	140.37	374.53	133.5	388.39	128.74
	16	357.49	139.86	375.82	133.04	389.68	128.31
	17	358.71	139.39	377.03	132.61	390.89	127.91
	18	359.85	138.95	378.18	132.21	392.04	127.54
	19	360.93	138.53	379.26	131.84	393.12	127.19
	20	361.96	138.14	380.28	131.48	394.15	126.86
	21	362.93	137.77	381.26	131.14	395.12	126.54
	22	363.86	137.41	382.19	130.83	396.05	126.25
	23	364.75	137.08	383.08	130.52	396.94	125.96
	24	365.6	136.76	383.93	130.23	397.79	125.69
	25	366.42	136.46	384.75	129.96	398.61	125.44
	26	367.2	136.16	385.53	129.69	399.39	125.19
	27	367.96	135.88	386.28	129.44	400.15	124.95
	28	368.69	135.62	387.01	129.2	400.87	124.73
	29	369.39	135.36	387.71	128.96	401.58	124.51
	30	370.07	135.11	388.39	128.74	402.25	124.3

Table 12. Simulated result showing path loss and power received for OW-ERRI

Site	Distance	4GHz		10GHz		20GHz	
		Pathloss	Received Power	Pathloss	Received Power	Pathloss	Received Power
OWERRI	1	302.05	165.54	320.37	156.07	334.23	149.6
	2	315.91	158.27	334.23	149.6	348.1	143.64
	3	324.02	154.31	342.34	146.05	356.21	140.37
	4	329.77	151.62	348.1	143.64	361.96	138.14
	5	334.23	149.6	352.56	141.82	366.42	136.45
	6	337.88	147.98	356.21	140.37	370.07	135.11
	7	340.96	146.64	359.29	139.16	373.15	133.99
	8	343.64	145.5	361.96	138.14	375.82	133.04
	9	345.99	144.51	364.32	137.24	378.18	132.21
	10	348.1	143.64	366.42	136.45	380.29	131.48
	11	350	142.86	368.33	135.75	382.19	130.82
	12	351.74	142.15	370.07	135.11	383.93	130.23
	13	353.35	141.5	371.67	134.53	385.53	129.69
	14	354.83	140.91	373.15	133.99	387.02	129.19
	15	356.21	140.37	374.53	133.5	388.4	128.73
	16	357.5	139.86	375.82	133.04	389.69	128.31
	17	358.71	139.39	377.04	132.61	390.9	127.91
	18	359.85	138.95	378.18	132.21	392.04	127.54
	19	360.93	138.53	379.26	131.84	393.12	127.19
	20	361.96	138.14	380.29	131.48	394.15	126.86
	21	362.94	137.77	381.26	131.14	395.13	126.54
	22	363.87	137.41	382.19	130.82	396.06	126.24
	23	364.76	137.08	383.08	130.52	396.94	125.96
	24	365.61	136.76	383.93	130.23	397.8	125.69
	25	366.42	136.45	384.75	129.95	398.61	125.44
	26	367.21	136.16	385.53	129.69	399.4	125.19
	27	367.96	135.88	386.29	129.44	400.15	124.95
	28	368.69	135.62	387.02	129.19	400.88	124.73
	29	369.39	135.36	387.72	128.96	401.58	124.51
	30	370.07	135.11	388.4	128.73	402.26	124.3

Table 13. Simulated result showing path loss and power received for UMUAHIA

Site	Distance	4GHz		10GHz		20GHz	
		Pathloss	Received Power	Pathloss	Received Power	Pathloss	Received Power
UMUAHIA	1	302.05	165.54	320.37	156.07	334.23	149.6
	2	315.91	158.27	334.23	149.6	348.1	143.64
	3	324.02	154.31	342.34	146.05	356.21	140.37
	4	329.77	151.62	348.1	143.64	361.96	138.14
	5	334.23	149.6	352.56	141.82	366.42	136.45
	6	337.88	147.98	356.21	140.37	370.07	135.11
	7	340.96	146.64	359.29	139.16	373.15	133.99
	8	343.64	145.5	361.96	138.14	375.82	133.04
	9	345.99	144.51	364.32	137.24	378.18	132.21
	10	348.1	143.64	366.42	136.45	380.29	131.48
	11	350	142.86	368.33	135.75	382.19	130.82
	12	351.74	142.15	370.07	135.11	383.93	130.23
	13	353.35	141.5	371.67	134.53	385.53	129.69
	14	354.83	140.91	373.15	133.99	387.02	129.19
	15	356.21	140.37	374.53	133.5	388.4	128.73
	16	357.5	139.86	375.82	133.04	389.69	128.31
	17	358.71	139.39	377.04	132.61	390.9	127.91
	18	359.85	138.95	378.18	132.21	392.04	127.54
	19	360.93	138.53	379.26	131.84	393.12	127.19
	20	361.96	138.14	380.29	131.48	394.15	126.86
	21	362.94	137.77	381.26	131.14	395.13	126.54
	22	363.87	137.41	382.19	130.82	396.06	126.24
	23	364.76	137.08	383.08	130.52	396.94	125.96
	24	365.61	136.76	383.93	130.23	397.8	125.69
	25	366.42	136.45	384.75	129.95	398.61	125.44
	26	367.21	136.16	385.53	129.69	399.4	125.19
	27	367.96	135.88	386.29	129.44	400.15	124.95
	28	368.69	135.62	387.02	129.19	400.88	124.73
	29	369.39	135.36	387.72	128.96	401.58	124.51
	30	370.07	135.11	388.4	128.73	402.26	124.3

Table 14. Simulated result showing path loss and power received for ASABA

Site	Distance	4GHz		10GHz		20GHz	
		Pathloss	Received Power	Pathloss	Received Power	Pathloss	Received Power
1		302.04	165.54	320.37	156.07	334.23	149.6
2		315.91	158.28	334.23	149.6	348.09	143.64
3		324.01	154.31	342.34	146.05	356.2	140.37
4		329.77	151.62	348.09	143.64	361.96	138.14
5		334.23	149.6	352.56	141.82	366.42	136.46
6		337.88	147.98	356.2	140.37	370.07	135.11
7		340.96	146.64	359.29	139.16	373.15	133.99
8		343.63	145.5	361.96	138.14	375.82	133.04
9		345.99	144.51	364.31	137.24	378.18	132.21
10		348.09	143.64	366.42	136.46	380.28	131.48
11	350	350	142.86	368.33	135.75	382.19	130.83
12		351.74	142.15	370.07	135.11	383.93	130.23
13		353.34	141.51	371.67	134.53	385.53	129.69
14		354.82	140.92	373.15	133.99	387.01	129.19
15		356.2	140.37	374.53	133.5	388.39	128.74
16		357.49	139.86	375.82	133.04	389.68	128.31
17		358.71	139.39	377.03	132.61	390.9	127.91
18		359.85	138.95	378.18	132.21	392.04	127.54
19		360.93	138.53	379.26	131.84	393.12	127.19
20		361.96	138.14	380.28	131.48	394.15	126.86
21		362.93	137.77	381.26	131.14	395.12	126.54
22		363.86	137.41	382.19	130.83	396.05	126.25
23		364.75	137.08	383.08	130.52	396.94	125.96
24		365.6	136.76	383.93	130.23	397.79	125.69
25		366.42	136.46	384.75	129.96	398.61	125.44
26		367.2	136.16	385.53	129.69	399.39	125.19
27		367.96	135.88	386.28	129.44	400.15	124.95
28		368.69	135.62	387.01	129.19	400.88	124.73
29		369.39	135.36	387.71	128.96	401.58	124.51
30		370.07	135.11	388.39	128.74	402.26	124.3

Table 15. Simulated result showing path loss and power received for BENIN

Site	Distance	4GHz		10GHz		20GHz	
		Pathloss	Received Power	Pathloss	Received Power	Pathloss	Received Power
BENIN	1	302.04	165.54	320.37	156.07	334.23	149.6
	2	315.9	158.28	334.23	149.6	348.09	143.64
	3	324.01	154.32	342.34	146.05	356.2	140.37
	4	329.77	151.62	348.09	143.64	361.95	138.14
	5	334.23	149.6	352.55	141.82	366.42	136.46
	6	337.87	147.98	356.2	140.37	370.06	135.11
	7	340.96	146.65	359.28	139.17	373.15	134
	8	343.63	145.51	361.95	138.14	375.82	133.04
	9	345.98	144.52	364.31	137.25	378.17	132.21
	10	348.09	143.64	366.42	136.46	380.28	131.48
	11	350	142.86	368.32	135.75	382.19	130.83
	12	351.74	142.15	370.06	135.11	383.93	130.23
	13	353.34	141.51	371.66	134.53	385.53	129.69
	14	354.82	140.92	373.15	134	387.01	129.2
	15	356.2	140.37	374.53	133.5	388.39	128.74
	16	357.49	139.86	375.82	133.04	389.68	128.31
	17	358.7	139.39	377.03	132.62	390.89	127.91
	18	359.85	138.95	378.17	132.21	392.04	127.54
	19	360.93	138.53	379.25	131.84	393.12	127.19
	20	361.95	138.14	380.28	131.48	394.14	126.86
	21	362.93	137.77	381.26	131.15	395.12	126.54
	22	363.86	137.42	382.19	130.83	396.05	126.25
	23	364.75	137.08	383.08	130.52	396.94	125.96
	24	365.6	136.76	383.93	130.23	397.79	125.69
	25	366.42	136.46	384.74	129.96	398.61	125.44
	26	367.2	136.16	385.53	129.69	399.39	125.19
	27	367.96	135.89	386.28	129.44	400.15	124.95
	28	368.68	135.62	387.01	129.2	400.87	124.73
	29	369.39	135.36	387.71	128.96	401.57	124.51
	30	370.06	135.11	388.39	128.74	402.25	124.3

Table 16. Simulated result showing path loss and power received for CAL-ABAR

Site	Distance	4GHz		10GHz		20GHz	
		Pathloss	Received Power	Pathloss	Received Power	Pathloss	Received Power
CALABAR	1	302.04	165.54	320.37	156.07	334.23	149.6
	2	315.9	158.28	334.23	149.6	348.09	143.64
	3	324.01	154.31	342.34	146.05	356.2	140.37
	4	329.77	151.62	348.09	143.64	361.96	138.14
	5	334.23	149.6	352.56	141.82	366.42	136.46
	6	337.88	147.98	356.2	140.37	370.07	135.11
	7	340.96	146.64	359.29	139.17	373.15	133.99
	8	343.63	145.51	361.96	138.14	375.82	133.04
	9	345.99	144.51	364.31	137.25	378.17	132.21
	10	348.09	143.64	366.42	136.46	380.28	131.48
	11	350	142.86	368.33	135.75	382.19	130.83
	12	351.74	142.15	370.07	135.11	383.93	130.23
	13	353.34	141.51	371.67	134.53	385.53	129.69
	14	354.82	140.92	373.15	133.99	387.01	129.2
	15	356.2	140.37	374.53	133.5	388.39	128.74
	16	357.49	139.86	375.82	133.04	389.68	128.31
	17	358.71	139.39	377.03	132.61	390.89	127.91
	18	359.85	138.95	378.17	132.21	392.04	127.54
	19	360.93	138.53	379.26	131.84	393.12	127.19
	20	361.96	138.14	380.28	131.48	394.14	126.86
	21	362.93	137.77	381.26	131.14	395.12	126.54
	22	363.86	137.41	382.19	130.83	396.05	126.25
	23	364.75	137.08	383.08	130.52	396.94	125.96
	24	365.6	136.76	383.93	130.23	397.79	125.69
	25	366.42	136.46	384.74	129.96	398.61	125.44
	26	367.2	136.16	385.53	129.69	399.39	125.19
	27	367.96	135.88	386.28	129.44	400.15	124.95
	28	368.69	135.62	387.01	129.2	400.87	124.73
	29	369.39	135.36	387.71	128.96	401.58	124.51
	30	370.07	135.11	388.39	128.74	402.25	124.3

Table 17. Simulated result showing path loss and power received for PORT HARCOURT

Site	Distance	4GHz		10GHz		20GHz	
		Pathloss	Received Power	Pathloss	Received Power	Pathloss	Received Power
PORT HARCOURT	1	302.04	165.54	320.37	156.07	334.23	149.6
	2	315.91	158.27	334.23	149.6	348.1	143.64
	3	324.02	154.31	342.34	146.05	356.2	140.37
	4	329.77	151.62	348.1	143.64	361.96	138.14
	5	334.23	149.6	352.56	141.82	366.42	136.46
	6	337.88	147.98	356.2	140.37	370.07	135.11
	7	340.96	146.64	359.29	139.16	373.15	133.99
	8	343.63	145.5	361.96	138.14	375.82	133.04
	9	345.99	144.51	364.31	137.24	378.18	132.21
	10	348.1	143.64	366.42	136.46	380.28	131.48
	11	350	142.86	368.33	135.75	382.19	130.82
	12	351.74	142.15	370.07	135.11	383.93	130.23
	13	353.34	141.51	371.67	134.53	385.53	129.69
	14	354.82	140.91	373.15	133.99	387.01	129.19
	15	356.2	140.37	374.53	133.5	388.39	128.74
	16	357.5	139.86	375.82	133.04	389.68	128.31
	17	358.71	139.39	377.03	132.61	390.9	127.91
	18	359.85	138.95	378.18	132.21	392.04	127.54
	19	360.93	138.53	379.26	131.84	393.12	127.19
	20	361.96	138.14	380.28	131.48	394.15	126.86
	21	362.93	137.77	381.26	131.14	395.12	126.54
	22	363.86	137.41	382.19	130.82	396.05	126.25
	23	364.75	137.08	383.08	130.52	396.94	125.96
	24	365.6	136.76	383.93	130.23	397.79	125.69
	25	366.42	136.46	384.75	129.96	398.61	125.44
	26	367.21	136.16	385.53	129.69	399.39	125.19
	27	367.96	135.88	386.29	129.44	400.15	124.95
	28	368.69	135.62	387.01	129.19	400.88	124.73
	29	369.39	135.36	387.72	128.96	401.58	124.51
	30	370.07	135.11	388.39	128.74	402.26	124.3

Table 18. Simulated result showing path loss and power received for UYO

Site	Distance	4GHz		10GHz		20GHz	
		Pathloss	Received Power	Pathloss	Received Power	Pathloss	Received Power
UYO	1	302.05	165.54	320.37	156.07	334.23	149.6
	2	315.91	158.27	334.23	149.6	348.1	143.64
	3	324.02	154.31	342.34	146.05	356.21	140.37
	4	329.77	151.62	348.1	143.64	361.96	138.14
	5	334.23	149.6	352.56	141.82	366.42	136.45
	6	337.88	147.98	356.21	140.37	370.07	135.11
	7	340.96	146.64	359.29	139.16	373.15	133.99
	8	343.63	145.5	361.96	138.14	375.82	133.04
	9	345.99	144.51	364.32	137.24	378.18	132.21
	10	348.1	143.64	366.42	136.45	380.29	131.48
	11	350	142.86	368.33	135.75	382.19	130.82
	12	351.74	142.15	370.07	135.11	383.93	130.23
	13	353.34	141.5	371.67	134.53	385.53	129.69
	14	354.83	140.91	373.15	133.99	387.02	129.19
	15	356.21	140.37	374.53	133.5	388.4	128.73
	16	357.5	139.86	375.82	133.04	389.69	128.31
	17	358.71	139.39	377.04	132.61	390.9	127.91
	18	359.85	138.95	378.18	132.21	392.04	127.54
	19	360.93	138.53	379.26	131.84	393.12	127.19
	20	361.96	138.14	380.29	131.48	394.15	126.86
	21	362.94	137.77	381.26	131.14	395.12	126.54
	22	363.87	137.41	382.19	130.82	396.06	126.24
	23	364.76	137.08	383.08	130.52	396.94	125.96
	24	365.61	136.76	383.93	130.23	397.8	125.69
	25	366.42	136.45	384.75	129.95	398.61	125.44
	26	367.21	136.16	385.53	129.69	399.4	125.19
	27	367.96	135.88	386.29	129.44	400.15	124.95
	28	368.69	135.62	387.02	129.19	400.88	124.73
	29	369.39	135.36	387.72	128.96	401.58	124.51
	30	370.07	135.11	388.4	128.73	402.26	124.3

Table 19. Simulated result showing path loss and power received for YENOGOA

Site	Distance	4GHz		10GHz		20GHz	
		Pathloss	Received Power	Pathloss	Received Power	Pathloss	Received Power
YENOGOA	1	302.05	165.54	320.37	156.07	334.24	149.6
	2	315.91	158.27	334.24	149.6	348.1	143.64
	3	324.02	154.31	342.34	146.05	356.21	140.37
	4	329.77	151.62	348.1	143.64	361.96	138.14
	5	334.24	149.6	352.56	141.82	366.42	136.45
	6	337.88	147.98	356.21	140.37	370.07	135.11
	7	340.96	146.64	359.29	139.16	373.15	133.99
	8	343.64	145.5	361.96	138.14	375.82	133.04
	9	345.99	144.51	364.32	137.24	378.18	132.21
	10	348.1	143.64	366.42	136.45	380.29	131.48
	11	350	142.86	368.33	135.75	382.19	130.82
	12	351.74	142.15	370.07	135.11	383.93	130.23
	13	353.35	141.5	371.67	134.53	385.53	129.69
	14	354.83	140.91	373.15	133.99	387.02	129.19
	15	356.21	140.37	374.53	133.5	388.4	128.73
	16	357.5	139.86	375.82	133.04	389.69	128.31
	17	358.71	139.39	377.04	132.61	390.9	127.91
	18	359.85	138.95	378.18	132.21	392.04	127.54
	19	360.94	138.53	379.26	131.84	393.12	127.19
	20	361.96	138.14	380.29	131.48	394.15	126.86
	21	362.94	137.77	381.26	131.14	395.13	126.54
	22	363.87	137.41	382.19	130.82	396.06	126.24
	23	364.76	137.08	383.08	130.52	396.94	125.96
	24	365.61	136.76	383.93	130.23	397.8	125.69
	25	366.42	136.45	384.75	129.95	398.61	125.44
	26	367.21	136.16	385.53	129.69	399.4	125.19
	27	367.96	135.88	386.29	129.44	400.15	124.95
	28	368.69	135.62	387.02	129.19	400.88	124.73
	29	369.39	135.36	387.72	128.96	401.58	124.51
	30	370.07	135.11	388.4	128.73	402.26	124.3

Table 20. Simulated result showing path loss and power received for ABUJA

Site	Distance	4GHz		10GHz		20GHz	
		Pathloss	Received Power	Pathloss	Received Power	Pathloss	Received Power
ABUJA	1	302.04	165.54	320.36	156.07	334.22	149.6
	2	315.9	158.28	334.22	149.6	348.09	143.64
	3	324.01	154.32	342.33	146.06	356.2	140.37
	4	329.76	151.62	348.09	143.64	361.95	138.14
	5	334.22	149.6	352.55	141.82	366.41	136.46
	6	337.87	147.99	356.2	140.37	370.06	135.11
	7	340.95	146.65	359.28	139.17	373.14	134
	8	343.62	145.51	361.95	138.14	375.81	133.04
	9	345.98	144.52	364.31	137.25	378.17	132.22
	10	348.09	143.64	366.41	136.46	380.28	131.48
	11	349.99	142.86	368.32	135.75	382.18	130.83
	12	351.73	142.15	370.06	135.11	383.92	130.23
	13	353.33	141.51	371.66	134.53	385.52	129.69
	14	354.82	140.92	373.14	134	387.01	129.2
	15	356.2	140.37	374.52	133.5	388.39	128.74
	16	357.49	139.87	375.81	133.04	389.68	128.31
	17	358.7	139.39	377.03	132.62	390.89	127.91
	18	359.84	138.95	378.17	132.22	392.03	127.54
	19	360.92	138.53	379.25	131.84	393.11	127.19
	20	361.95	138.14	380.28	131.48	394.14	126.86
	21	362.93	137.77	381.25	131.15	395.11	126.55
	22	363.86	137.42	382.18	130.83	396.05	126.25
	23	364.75	137.08	383.07	130.52	396.93	125.97
	24	365.6	136.76	383.92	130.23	397.79	125.7
	25	366.41	136.46	384.74	129.96	398.6	125.44
	26	367.2	136.17	385.52	129.69	399.39	125.19
	27	367.95	135.89	386.28	129.44	400.14	124.96
	28	368.68	135.62	387.01	129.2	400.87	124.73
	29	369.38	135.36	387.71	128.96	401.57	124.51
	30	370.06	135.11	388.39	128.74	402.25	124.3

Table 21. Simulated result showing path loss and power received for IL-LORIN

Site	Distance	4GHz		10GHz		20GHz	
		Pathloss	Received Power	Pathloss	Received Power	Pathloss	Received Power
IL-LORIN	1	302.03	165.54	320.36	156.07	334.22	149.6
	2	315.9	158.28	334.22	149.6	348.09	143.64
	3	324.01	154.32	342.33	146.06	356.2	140.37
	4	329.76	151.63	348.09	143.64	361.95	138.14
	5	334.22	149.6	352.55	141.82	366.41	136.46
	6	337.87	147.99	356.2	140.37	370.06	135.11
	7	340.95	146.65	359.28	139.17	373.14	134
	8	343.62	145.51	361.95	138.14	375.81	133.05
	9	345.98	144.52	364.3	137.25	378.17	132.22
	10	348.09	143.64	366.41	136.46	380.27	131.48
	11	349.99	142.86	368.32	135.75	382.18	130.83
	12	351.73	142.15	370.06	135.11	383.92	130.24
	13	353.33	141.51	371.66	134.53	385.52	129.69
	14	354.82	140.92	373.14	134	387	129.2
	15	356.2	140.37	374.52	133.5	388.38	128.74
	16	357.49	139.87	375.81	133.05	389.67	128.31
	17	358.7	139.39	377.02	132.62	390.89	127.91
	18	359.84	138.95	378.17	132.22	392.03	127.54
	19	360.92	138.53	379.25	131.84	393.11	127.19
	20	361.95	138.14	380.27	131.48	394.14	126.86
	21	362.92	137.77	381.25	131.15	395.11	126.55
	22	363.85	137.42	382.18	130.83	396.04	126.25
	23	364.74	137.08	383.07	130.52	396.93	125.97
	24	365.6	136.76	383.92	130.24	397.78	125.7
	25	366.41	136.46	384.74	129.96	398.6	125.44
	26	367.2	136.17	385.52	129.69	399.38	125.19
	27	367.95	135.89	386.28	129.44	400.14	124.96
	28	368.68	135.62	387	129.2	400.87	124.73
	29	369.38	135.36	387.71	128.96	401.57	124.51
	30	370.06	135.11	388.38	128.74	402.25	124.3

Table 22. Simulated result showing path loss and power received for LAFIA

Site	Distance	4GHz		10GHz		20GHz	
		Pathloss	Received Power	Pathloss	Received Power	Pathloss	Received Power
LAFIA	1	302.03	165.54	320.36	156.07	334.22	149.6
	2	315.9	158.28	334.22	149.6	348.09	143.64
	3	324.01	154.32	342.33	146.06	356.2	140.37
	4	329.76	151.63	348.09	143.64	361.95	138.14
	5	334.22	149.6	352.55	141.82	366.41	136.46
	6	337.87	147.99	356.2	140.37	370.06	135.11
	7	340.95	146.65	359.28	139.17	373.14	134
	8	343.62	145.51	361.95	138.14	375.81	133.05
	9	345.98	144.52	364.3	137.25	378.17	132.22
	10	348.09	143.64	366.41	136.46	380.27	131.48
	11	349.99	142.86	368.32	135.75	382.18	130.83
	12	351.73	142.15	370.06	135.11	383.92	130.24
	13	353.33	141.51	371.66	134.53	385.52	129.69
	14	354.82	140.92	373.14	134	387	129.2
	15	356.2	140.37	374.52	133.5	388.38	128.74
	16	357.49	139.87	375.81	133.05	389.67	128.31
	17	358.7	139.39	377.02	132.62	390.89	127.91
	18	359.84	138.95	378.17	132.22	392.03	127.54
	19	360.92	138.53	379.25	131.84	393.11	127.19
	20	361.95	138.14	380.27	131.48	394.14	126.86
	21	362.92	137.77	381.25	131.15	395.11	126.55
	22	363.85	137.42	382.18	130.83	396.04	126.25
	23	364.74	137.08	383.07	130.52	396.93	125.97
	24	365.6	136.76	383.92	130.24	397.78	125.7
	25	366.41	136.46	384.74	129.96	398.6	125.44
	26	367.2	136.17	385.52	129.69	399.38	125.19
	27	367.95	135.89	386.28	129.44	400.14	124.96
	28	368.68	135.62	387	129.2	400.87	124.73
	29	369.38	135.36	387.71	128.96	401.57	124.51
	30	370.06	135.11	388.38	128.74	402.25	124.3

Table 24. Simulated result showing path loss and power received for MAKURDI

Site	Distance	4GHz		10GHz		20GHz	
		Pathloss	Received Power	Pathloss	Received Power	Pathloss	Received Power
1		302.04	165.54	320.36	156.07	334.23	149.6
2		315.9	158.28	334.23	149.6	348.09	143.64
3		324.01	154.32	342.33	146.06	356.2	140.37
4		329.76	151.62	348.09	143.64	361.95	138.14
5		334.23	149.6	352.55	141.82	366.41	136.46
6		337.87	147.99	356.2	140.37	370.06	135.11
7		340.95	146.65	359.28	139.17	373.14	134
8		343.63	145.51	361.95	138.14	375.81	133.04
9		345.98	144.52	364.31	137.25	378.17	132.22
10		348.09	143.64	366.41	136.46	380.28	131.48
11		349.99	142.86	368.32	135.75	382.18	130.83
12		351.73	142.15	370.06	135.11	383.92	130.23
13		353.34	141.51	371.66	134.53	385.52	129.69
14		354.82	140.92	373.14	134	387.01	129.2
15		356.2	140.37	374.52	133.5	388.39	128.74
16		357.49	139.86	375.81	133.04	389.68	128.31
17		358.7	139.39	377.03	132.62	390.89	127.91
18		359.84	138.95	378.17	132.22	392.03	127.54
19		360.93	138.53	379.25	131.84	393.11	127.19
20		361.95	138.14	380.28	131.48	394.14	126.86
21		362.93	137.77	381.25	131.15	395.12	126.55
22		363.86	137.42	382.18	130.83	396.05	126.25
23		364.75	137.08	383.07	130.52	396.93	125.97
24		365.6	136.76	383.92	130.23	397.79	125.7
25		366.41	136.46	384.74	129.96	398.6	125.44
26		367.2	136.17	385.52	129.69	399.39	125.19
27		367.95	135.89	386.28	129.44	400.14	124.96
28		368.68	135.62	387.01	129.2	400.87	124.73
29		369.38	135.36	387.71	128.96	401.57	124.51
30		370.06	135.11	388.39	128.74	402.25	124.3

MAKURDI

Table 25. Simulated result showing path loss and power received for MINA

Site	Distance	4GHz		10GHz		20GHz	
		Pathloss	Received Power	Pathloss	Received Power	Pathloss	Received Power
MINA	1	302.03	165.55	320.36	156.08	334.22	149.6
	2	315.9	158.28	334.22	149.6	348.08	143.64
	3	324	154.32	342.33	146.06	356.19	140.37
	4	329.76	151.63	348.08	143.64	361.95	138.14
	5	334.22	149.6	352.55	141.83	366.41	136.46
	6	337.87	147.99	356.19	140.37	370.06	135.11
	7	340.95	146.65	359.28	139.17	373.14	134
	8	343.62	145.51	361.95	138.14	375.81	133.05
	9	345.98	144.52	364.3	137.25	378.17	132.22
	10	348.08	143.64	366.41	136.46	380.27	131.48
	11	349.99	142.86	368.32	135.75	382.18	130.83
	12	351.73	142.15	370.06	135.11	383.92	130.24
	13	353.33	141.51	371.66	134.53	385.52	129.69
	14	354.81	140.92	373.14	134	387	129.2
	15	356.19	140.37	374.52	133.5	388.38	128.74
	16	357.48	139.87	375.81	133.05	389.67	128.31
	17	358.7	139.39	377.02	132.62	390.89	127.91
	18	359.84	138.95	378.17	132.22	392.03	127.54
	19	360.92	138.53	379.25	131.84	393.11	127.19
	20	361.95	138.14	380.27	131.48	394.14	126.86
	21	362.92	137.77	381.25	131.15	395.11	126.55
	22	363.85	137.42	382.18	130.83	396.04	126.25
	23	364.74	137.08	383.07	130.53	396.93	125.97
	24	365.59	136.76	383.92	130.24	397.78	125.7
	25	366.41	136.46	384.74	129.96	398.6	125.44
	26	367.19	136.17	385.52	129.69	399.38	125.19
	27	367.95	135.89	386.27	129.44	400.14	124.96
	28	368.68	135.62	387	129.2	400.87	124.73
	29	369.38	135.36	387.7	128.96	401.57	124.51
	30	370.06	135.11	388.38	128.74	402.25	124.3

Table 26. Simulated result showing path loss and power received for JOS

Site	Distance	4GHz		10GHz		20GHz	
		Pathloss	Received Power	Pathloss	Received Power	Pathloss	Received Power
1		302.04	165.54	320.36	156.07	334.22	149.6
2		315.9	158.28	334.22	149.6	348.09	143.64
3		324.01	154.32	342.33	146.06	356.2	140.37
4		329.76	151.63	348.09	143.64	361.95	138.14
5		334.22	149.6	352.55	141.82	366.41	136.46
6		337.87	147.99	356.2	140.37	370.06	135.11
7		340.95	146.65	359.28	139.17	373.14	134
8		343.62	145.51	361.95	138.14	375.81	133.05
9		345.98	144.52	364.31	137.25	378.17	132.22
10		348.09	143.64	366.41	136.46	380.28	131.48
11		349.99	142.86	368.32	135.75	382.18	130.83
12		351.73	142.15	370.06	135.11	383.92	130.23
13		353.33	141.51	371.66	134.53	385.52	129.69
14		354.82	140.92	373.14	134	387	129.2
15		356.2	140.37	374.52	133.5	388.38	128.74
16		357.49	139.87	375.81	133.05	389.68	128.31
17		358.7	139.39	377.03	132.62	390.89	127.91
18		359.84	138.95	378.17	132.22	392.03	127.54
19		360.92	138.53	379.25	131.84	393.11	127.19
20		361.95	138.14	380.28	131.48	394.14	126.86
21		362.93	137.77	381.25	131.15	395.11	126.55
22		363.86	137.42	382.18	130.83	396.04	126.25
23		364.74	137.08	383.07	130.52	396.93	125.97
24		365.6	136.76	383.92	130.23	397.78	125.7
25		366.41	136.46	384.74	129.96	398.6	125.44
26		367.2	136.17	385.52	129.69	399.39	125.19
27		367.95	135.89	386.28	129.44	400.14	124.96
28		368.68	135.62	387	129.2	400.87	124.73
29		369.38	135.36	387.71	128.96	401.57	124.51
30		370.06	135.11	388.38	128.74	402.25	124.3

Table 27. Simulated result showing path loss and power received for BIRINI KEBBI

Site	Distance	4GHz		10GHz		20GHz	
		Pathloss	Received Power	Pathloss	Received Power	Pathloss	Received Power
BIRINI KEBBI	1	302.02	165.55	320.35	156.08	334.21	149.61
	2	315.89	158.28	334.21	149.61	348.08	143.65
	3	324	154.32	342.32	146.06	356.19	140.38
	4	329.75	151.63	348.08	143.65	361.94	138.14
	5	334.21	149.61	352.54	141.83	366.4	136.46
	6	337.86	147.99	356.19	140.38	370.05	135.12
	7	340.94	146.65	359.27	139.17	373.13	134
	8	343.61	145.51	361.94	138.14	375.8	133.05
	9	345.97	144.52	364.29	137.25	378.16	132.22
	10	348.08	143.65	366.4	136.46	380.26	131.49
	11	349.98	142.86	368.31	135.76	382.17	130.83
	12	351.72	142.16	370.05	135.12	383.91	130.24
	13	353.32	141.51	371.65	134.54	385.51	129.7
	14	354.81	140.92	373.13	134	386.99	129.2
	15	356.19	140.38	374.51	133.51	388.37	128.74
	16	357.48	139.87	375.8	133.05	389.66	128.32
	17	358.69	139.4	377.01	132.62	390.88	127.92
	18	359.83	138.95	378.16	132.22	392.02	127.54
	19	360.91	138.54	379.24	131.84	393.1	127.19
	20	361.94	138.14	380.26	131.49	394.13	126.86
	21	362.91	137.77	381.24	131.15	395.1	126.55
	22	363.85	137.42	382.17	130.83	396.03	126.25
	23	364.73	137.09	383.06	130.53	396.92	125.97
	24	365.59	136.77	383.91	130.24	397.77	125.7
	25	366.4	136.46	384.73	129.96	398.59	125.44
	26	367.19	136.17	385.51	129.7	399.37	125.2
	27	367.94	135.89	386.27	129.44	400.13	124.96
	28	368.67	135.62	386.99	129.2	400.86	124.73
	29	369.37	135.37	387.7	128.97	401.56	124.51
	30	370.05	135.12	388.37	128.74	402.24	124.3

Table 28. Simulated result showing path loss and power received for GASAU

Site	Distance	4GHz		10GHz		20GHz	
		Pathloss	Received Power	Pathloss	Received Power	Pathloss	Received Power
GASAU	1	302.02	165.55	320.35	156.08	334.21	149.6
	2	315.89	158.28	334.21	149.6	348.08	143.65
	3	324	154.32	342.32	146.06	356.19	140.38
	4	329.75	151.63	348.08	143.65	361.94	138.14
	5	334.21	149.6	352.54	141.83	366.4	136.46
	6	337.86	147.99	356.19	140.38	370.05	135.12
	7	340.94	146.65	359.27	139.17	373.13	134
	8	343.61	145.51	361.94	138.14	375.8	133.05
	9	345.97	144.52	364.3	137.25	378.16	132.22
	10	348.08	143.65	366.4	136.46	380.27	131.49
	11	349.98	142.86	368.31	135.76	382.17	130.83
	12	351.72	142.16	370.05	135.12	383.91	130.24
	13	353.32	141.51	371.65	134.54	385.51	129.7
	14	354.81	140.92	373.13	134	386.99	129.2
	15	356.19	140.38	374.51	133.51	388.37	128.74
	16	357.48	139.87	375.8	133.05	389.67	128.32
	17	358.69	139.4	377.02	132.62	390.88	127.92
	18	359.83	138.95	378.16	132.22	392.02	127.54
	19	360.91	138.54	379.24	131.84	393.1	127.19
	20	361.94	138.14	380.27	131.49	394.13	126.86
	21	362.92	137.77	381.24	131.15	395.1	126.55
	22	363.85	137.42	382.17	130.83	396.03	126.25
	23	364.73	137.09	383.06	130.53	396.92	125.97
	24	365.59	136.77	383.91	130.24	397.77	125.7
	25	366.4	136.46	384.73	129.96	398.59	125.44
	26	367.19	136.17	385.51	129.7	399.38	125.2
	27	367.94	135.89	386.27	129.44	400.13	124.96
	28	368.67	135.62	386.99	129.2	400.86	124.73
	29	369.37	135.37	387.7	128.97	401.56	124.51
	30	370.05	135.12	388.37	128.74	402.24	124.3

Table 29. Simulated result showing path loss and power received for KADUNA

Site	Distance	4GHz		10GHz		20GHz	
		Pathloss	Received Power	Pathloss	Received Power	Pathloss	Received Power
KADUNA	1	302.03	165.54	320.36	156.07	334.22	149.6
	2	315.9	158.28	334.22	149.6	348.08	143.64
	3	324.01	154.32	342.33	146.06	356.19	140.37
	4	329.76	151.63	348.08	143.64	361.95	138.14
	5	334.22	149.6	352.55	141.82	366.41	136.46
	6	337.87	147.99	356.19	140.37	370.06	135.11
	7	340.95	146.65	359.28	139.17	373.14	134
	8	343.62	145.51	361.95	138.14	375.81	133.05
	9	345.98	144.52	364.3	137.25	378.17	132.22
	10	348.08	143.64	366.41	136.46	380.27	131.48
	11	349.99	142.86	368.32	135.75	382.18	130.83
	12	351.73	142.15	370.06	135.11	383.92	130.24
	13	353.33	141.51	371.66	134.53	385.52	129.69
	14	354.81	140.92	373.14	134	387	129.2
	15	356.19	140.37	374.52	133.5	388.38	128.74
	16	357.49	139.87	375.81	133.05	389.67	128.31
	17	358.7	139.39	377.02	132.62	390.89	127.91
	18	359.84	138.95	378.17	132.22	392.03	127.54
	19	360.92	138.53	379.25	131.84	393.11	127.19
	20	361.95	138.14	380.27	131.48	394.14	126.86
	21	362.92	137.77	381.25	131.15	395.11	126.55
	22	363.85	137.42	382.18	130.83	396.04	126.25
	23	364.74	137.08	383.07	130.52	396.93	125.97
	24	365.59	136.76	383.92	130.24	397.78	125.7
	25	366.41	136.46	384.74	129.96	398.6	125.44
	26	367.2	136.17	385.52	129.69	399.38	125.19
	27	367.95	135.89	386.28	129.44	400.14	124.96
	28	368.68	135.62	387	129.2	400.87	124.73
	29	369.38	135.36	387.7	128.96	401.57	124.51
	30	370.06	135.11	388.38	128.74	402.25	124.3

Table 30. Simulated results showing path and power received for KANO

Site	Distance	4GHz		10GHz		20GHz	
		Pathloss	Received Power	Pathloss	Received Power	Pathloss	Received Power
KANO	1	302.03	165.55	320.35	156.08	334.21	149.6
	2	315.89	158.28	334.21	149.6	348.08	143.65
	3	324	154.32	342.32	146.06	356.19	140.38
	4	329.75	151.63	348.08	143.65	361.94	138.14
	5	334.21	149.6	352.54	141.83	366.4	136.46
	6	337.86	147.99	356.19	140.38	370.05	135.12
	7	340.94	146.65	359.27	139.17	373.13	134
	8	343.61	145.51	361.94	138.14	375.8	133.05
	9	345.97	144.52	364.3	137.25	378.16	132.22
	10	348.08	143.65	366.4	136.46	380.27	131.49
	11	349.98	142.86	368.31	135.76	382.17	130.83
	12	351.72	142.16	370.05	135.12	383.91	130.24
	13	353.32	141.51	371.65	134.53	385.51	129.7
	14	354.81	140.92	373.13	134	387	129.2
	15	356.19	140.38	374.51	133.51	388.38	128.74
	16	357.48	139.87	375.8	133.05	389.67	128.31
	17	358.69	139.4	377.02	132.62	390.88	127.92
	18	359.83	138.95	378.16	132.22	392.02	127.54
	19	360.91	138.54	379.24	131.84	393.1	127.19
	20	361.94	138.14	380.27	131.49	394.13	126.86
	21	362.92	137.77	381.24	131.15	395.11	126.55
	22	363.85	137.42	382.17	130.83	396.04	126.25
	23	364.74	137.09	383.06	130.53	396.92	125.97
	24	365.59	136.77	383.91	130.24	397.78	125.7
	25	366.4	136.46	384.73	129.96	398.59	125.44
	26	367.19	136.17	385.51	129.7	399.38	125.2
	27	367.94	135.89	386.27	129.44	400.13	124.96
	28	368.67	135.62	387	129.2	400.86	124.73
	29	369.37	135.36	387.7	128.97	401.56	124.51
	30	370.05	135.12	388.38	128.74	402.24	124.3

Table 31. Simulated results showing path and power received for KATSINA

Site	Distance	4GHz		10GHz		20GHz	
		Pathloss	Received Power	Pathloss	Received Power	Pathloss	Received Power
KATSINA	1	302.02	165.55	320.35	156.08	334.21	149.61
	2	315.89	158.29	334.21	149.61	348.07	143.65
	3	324	154.32	342.32	146.06	356.18	140.38
	4	329.75	151.63	348.07	143.65	361.94	138.15
	5	334.21	149.61	352.54	141.83	366.4	136.46
	6	337.86	147.99	356.18	140.38	370.05	135.12
	7	340.94	146.65	359.27	139.17	373.13	134
	8	343.61	145.51	361.94	138.15	375.8	133.05
	9	345.97	144.52	364.29	137.25	378.16	132.22
	10	348.07	143.65	366.4	136.46	380.26	131.49
	11	349.98	142.87	368.31	135.76	382.17	130.83
	12	351.72	142.16	370.05	135.12	383.91	130.24
	13	353.32	141.51	371.65	134.54	385.51	129.7
	14	354.8	140.92	373.13	134	386.99	129.2
	15	356.18	140.38	374.51	133.51	388.37	128.74
	16	357.47	139.87	375.8	133.05	389.66	128.32
	17	358.69	139.4	377.01	132.62	390.88	127.92
	18	359.83	138.95	378.16	132.22	392.02	127.54
	19	360.91	138.54	379.24	131.84	393.1	127.19
	20	361.94	138.15	380.26	131.49	394.13	126.86
	21	362.91	137.77	381.24	131.15	395.1	126.55
	22	363.84	137.42	382.17	130.83	396.03	126.25
	23	364.73	137.09	383.06	130.53	396.92	125.97
	24	365.58	136.77	383.91	130.24	397.77	125.7
	25	366.4	136.46	384.73	129.96	398.59	125.44
	26	367.18	136.17	385.51	129.7	399.37	125.2
	27	367.94	135.89	386.27	129.44	400.13	124.96
	28	368.67	135.62	386.99	129.2	400.86	124.73
	29	369.37	135.37	387.69	128.97	401.56	124.52
	30	370.05	135.12	388.37	128.74	402.24	124.31

Table 32. Simulated results showing path and power received for SOKOTO

Site	Distance	4GHz		10GHz		20GHz	
		Pathloss	Received Power	Pathloss	Received Power	Pathloss	Received Power
SOKOTO	1	302.02	165.55	320.35	156.08	334.21	149.61
	2	315.88	158.29	334.21	149.61	348.07	143.65
	3	323.99	154.33	342.32	146.06	356.18	140.38
	4	329.75	151.63	348.07	143.65	361.93	138.15
	5	334.21	149.61	352.53	141.83	366.4	136.46
	6	337.85	147.99	356.18	140.38	370.04	135.12
	7	340.94	146.65	359.26	139.17	373.13	134
	8	343.61	145.51	361.93	138.15	375.8	133.05
	9	345.96	144.52	364.29	137.25	378.15	132.22
	10	348.07	143.65	366.4	136.46	380.26	131.49
	11	349.98	142.87	368.3	135.76	382.17	130.83
	12	351.72	142.16	370.04	135.12	383.91	130.24
	13	353.32	141.52	371.64	134.54	385.51	129.7
	14	354.8	140.92	373.13	134	386.99	129.2
	15	356.18	140.38	374.51	133.51	388.37	128.74
	16	357.47	139.87	375.8	133.05	389.66	128.32
	17	358.68	139.4	377.01	132.62	390.87	127.92
	18	359.83	138.96	378.15	132.22	392.02	127.55
	19	360.91	138.54	379.23	131.84	393.1	127.2
	20	361.93	138.15	380.26	131.49	394.12	126.86
	21	362.91	137.78	381.24	131.15	395.1	126.55
	22	363.84	137.42	382.17	130.83	396.03	126.25
	23	364.73	137.09	383.06	130.53	396.92	125.97
	24	365.58	136.77	383.91	130.24	397.77	125.7
	25	366.4	136.46	384.72	129.96	398.59	125.44
	26	367.18	136.17	385.51	129.7	399.37	125.2
	27	367.94	135.89	386.26	129.45	400.12	124.96
	28	368.66	135.63	386.99	129.2	400.85	124.73
	29	369.37	135.37	387.69	128.97	401.55	124.52
	30	370.04	135.12	388.37	128.74	402.23	124.31

Table 33. Simulated results showing path and power received for BAUCHI

Site	Distance	4GHz		10GHz		20GHz	
		Pathloss	Received Power	Pathloss	Received Power	Pathloss	Received Power
	1	302.03	165.55	320.35	156.08	334.22	149.6
	2	315.89	158.28	334.22	149.6	348.08	143.65
	3	324	154.32	342.33	146.06	356.19	140.37
	4	329.75	151.63	348.08	143.65	361.94	138.14
	5	334.22	149.6	352.54	141.83	366.41	136.46
	6	337.86	147.99	356.19	140.37	370.05	135.12
	7	340.95	146.65	359.27	139.17	373.14	134
	8	343.62	145.51	361.94	138.14	375.81	133.05
	9	345.97	144.52	364.3	137.25	378.16	132.22
	10	348.08	143.65	366.41	136.46	380.27	131.49
	11	349.99	142.86	368.31	135.75	382.18	130.83
	12	351.73	142.16	370.05	135.12	383.92	130.24
	13	353.33	141.51	371.65	134.53	385.52	129.7
BAUCHI	14	354.81	140.92	373.14	134	387	129.2
	15	356.19	140.37	374.52	133.51	388.38	128.74
	16	357.48	139.87	375.81	133.05	389.67	128.31
	17	358.69	139.4	377.02	132.62	390.88	127.92
	18	359.84	138.95	378.16	132.22	392.02	127.54
	19	360.92	138.54	379.24	131.84	393.11	127.19
	20	361.94	138.14	380.27	131.49	394.13	126.86
	21	362.92	137.77	381.24	131.15	395.11	126.55
	22	363.85	137.42	382.18	130.83	396.04	126.25
	23	364.74	137.08	383.06	130.53	396.93	125.97
	24	365.59	136.77	383.92	130.24	397.78	125.7
	25	366.41	136.46	384.73	129.96	398.59	125.44
	26	367.19	136.17	385.52	129.7	399.38	125.19
	27	367.95	135.89	386.27	129.44	400.13	124.96
	28	368.67	135.62	387	129.2	400.86	124.73
	29	369.37	135.36	387.7	128.97	401.56	124.51
	30	370.05	135.12	388.38	128.74	402.24	124.3

Table 34. Simulated results showing path and power received for DAMATURU

Site	Distance	4GHz		10GHz		20GHz	
		Pathloss	Received Power	Pathloss	Received Power	Pathloss	Received Power
DAMATURU	1	302.02	165.55	320.35	156.08	334.21	149.6
	2	315.89	158.28	334.21	149.6	348.08	143.65
	3	324	154.32	342.32	146.06	356.19	140.38
	4	329.75	151.63	348.08	143.65	361.94	138.14
	5	334.21	149.6	352.54	141.83	366.4	136.46
	6	337.86	147.99	356.19	140.38	370.05	135.12
	7	340.94	146.65	359.27	139.17	373.13	134
	8	343.61	145.51	361.94	138.14	375.8	133.05
	9	345.97	144.52	364.3	137.25	378.16	132.22
	10	348.08	143.65	366.4	136.46	380.27	131.49
	11	349.98	142.86	368.31	135.76	382.17	130.83
	12	351.72	142.16	370.05	135.12	383.91	130.24
	13	353.32	141.51	371.65	134.54	385.51	129.7
	14	354.81	140.92	373.13	134	386.99	129.2
	15	356.19	140.38	374.51	133.51	388.37	128.74
	16	357.48	139.87	375.8	133.05	389.67	128.32
	17	358.69	139.4	377.01	132.62	390.88	127.92
	18	359.83	138.95	378.16	132.22	392.02	127.54
	19	360.91	138.54	379.24	131.84	393.1	127.19
	20	361.94	138.14	380.27	131.49	394.13	126.86
	21	362.92	137.77	381.24	131.15	395.1	126.55
	22	363.85	137.42	382.17	130.83	396.03	126.25
	23	364.73	137.09	383.06	130.53	396.92	125.97
	24	365.59	136.77	383.91	130.24	397.77	125.7
	25	366.4	136.46	384.73	129.96	398.59	125.44
	26	367.19	136.17	385.51	129.7	399.38	125.2
	27	367.94	135.89	386.27	129.44	400.13	124.96
	28	368.67	135.62	386.99	129.2	400.86	124.73
	29	369.37	135.37	387.7	128.97	401.56	124.51
	30	370.05	135.12	388.37	128.74	402.24	124.3

Table 35. Simulated results showing path and power received for DUTSE

Site	Distance	4GHz		10GHz		20GHz	
		Pathloss	Received Power	Pathloss	Received Power	Pathloss	Received Power
DUTSE	1	302.03	165.55	320.35	156.08	334.21	149.6
	2	315.89	158.28	334.21	149.6	348.08	143.65
	3	324	154.32	342.32	146.06	356.19	140.38
	4	329.75	151.63	348.08	143.65	361.94	138.14
	5	334.21	149.6	352.54	141.83	366.4	136.46
	6	337.86	147.99	356.19	140.38	370.05	135.12
	7	340.94	146.65	359.27	139.17	373.13	134
	8	343.61	145.51	361.94	138.14	375.8	133.05
	9	345.97	144.52	364.3	137.25	378.16	132.22
	10	348.08	143.65	366.4	136.46	380.27	131.49
	11	349.98	142.86	368.31	135.76	382.17	130.83
	12	351.72	142.16	370.05	135.12	383.91	130.24
	13	353.32	141.51	371.65	134.54	385.51	129.7
	14	354.81	140.92	373.13	134	387	129.2
	15	356.19	140.38	374.51	133.51	388.38	128.74
	16	357.48	139.87	375.8	133.05	389.67	128.32
	17	358.69	139.4	377.02	132.62	390.88	127.92
	18	359.83	138.95	378.16	132.22	392.02	127.54
	19	360.91	138.54	379.24	131.84	393.1	127.19
	20	361.94	138.14	380.27	131.49	394.13	126.86
	21	362.92	137.77	381.24	131.15	395.1	126.55
	22	363.85	137.42	382.17	130.83	396.04	126.25
	23	364.74	137.09	383.06	130.53	396.92	125.97
	24	365.59	136.77	383.91	130.24	397.78	125.7
	25	366.4	136.46	384.73	129.96	398.59	125.44
	26	367.19	136.17	385.51	129.7	399.38	125.2
	27	367.94	135.89	386.27	129.44	400.13	124.96
	28	368.67	135.62	387	129.2	400.86	124.73
	29	369.37	135.37	387.7	128.97	401.56	124.51
	30	370.05	135.12	388.38	128.74	402.24	124.3

Table 36. Simulated results showing path and power received for GOMBE

Site	Distance	4GHz		10GHz		20GHz	
		Pathloss	Received Power	Pathloss	Received Power	Pathloss	Received Power
GOMBE	1	302.03	165.55	320.35	156.08	334.22	149.6
	2	315.89	158.28	334.22	149.6	348.08	143.65
	3	324	154.32	342.32	146.06	356.19	140.38
	4	329.75	151.63	348.08	143.65	361.94	138.14
	5	334.22	149.6	352.54	141.83	366.4	136.46
	6	337.86	147.99	356.19	140.38	370.05	135.12
	7	340.94	146.65	359.27	139.17	373.13	134
	8	343.62	145.51	361.94	138.14	375.8	133.05
	9	345.97	144.52	364.3	137.25	378.16	132.22
	10	348.08	143.65	366.4	136.46	380.27	131.49
	11	349.98	142.86	368.31	135.76	382.17	130.83
	12	351.72	142.16	370.05	135.12	383.91	130.24
	13	353.33	141.51	371.65	134.53	385.51	129.7
	14	354.81	140.92	373.13	134	387	129.2
	15	356.19	140.38	374.51	133.51	388.38	128.74
	16	357.48	139.87	375.8	133.05	389.67	128.31
	17	358.69	139.4	377.02	132.62	390.88	127.92
	18	359.83	138.95	378.16	132.22	392.02	127.54
	19	360.92	138.54	379.24	131.84	393.1	127.19
	20	361.94	138.14	380.27	131.49	394.13	126.86
	21	362.92	137.77	381.24	131.15	395.11	126.55
	22	363.85	137.42	382.17	130.83	396.04	126.25
	23	364.74	137.09	383.06	130.53	396.93	125.97
	24	365.59	136.77	383.91	130.24	397.78	125.7
	25	366.4	136.46	384.73	129.96	398.59	125.44
	26	367.19	136.17	385.51	129.7	399.38	125.19
	27	367.94	135.89	386.27	129.44	400.13	124.96
	28	368.67	135.62	387	129.2	400.86	124.73
	29	369.37	135.36	387.7	128.97	401.56	124.51
	30	370.05	135.12	388.38	128.74	402.24	124.3

Table 37. Simulated results showing path and power received for JALINGO

Site	Distance	4GHz		10GHz		20GHz	
		Pathloss	Received Power	Pathloss	Received Power	Pathloss	Received Power
JALINGO	1	302.04	165.54	320.36	156.07	334.23	149.6
	2	315.9	158.28	334.23	149.6	348.09	143.64
	3	324.01	154.32	342.34	146.06	356.2	140.37
	4	329.76	151.62	348.09	143.64	361.95	138.14
	5	334.23	149.6	352.55	141.82	366.41	136.46
	6	337.87	147.98	356.2	140.37	370.06	135.11
	7	340.96	146.65	359.28	139.17	373.14	134
	8	343.63	145.51	361.95	138.14	375.81	133.04
	9	345.98	144.52	364.31	137.25	378.17	132.22
	10	348.09	143.64	366.41	136.46	380.28	131.48
	11	349.99	142.86	368.32	135.75	382.18	130.83
	12	351.74	142.15	370.06	135.11	383.92	130.23
	13	353.34	141.51	371.66	134.53	385.52	129.69
	14	354.82	140.92	373.14	134	387.01	129.2
	15	356.2	140.37	374.52	133.5	388.39	128.74
	16	357.49	139.86	375.81	133.04	389.68	128.31
	17	358.7	139.39	377.03	132.62	390.89	127.91
	18	359.84	138.95	378.17	132.22	392.03	127.54
	19	360.93	138.53	379.25	131.84	393.11	127.19
	20	361.95	138.14	380.28	131.48	394.14	126.86
	21	362.93	137.77	381.25	131.15	395.12	126.55
	22	363.86	137.42	382.18	130.83	396.05	126.25
	23	364.75	137.08	383.07	130.52	396.94	125.96
	24	365.6	136.76	383.92	130.23	397.79	125.7
	25	366.41	136.46	384.74	129.96	398.6	125.44
	26	367.2	136.17	385.52	129.69	399.39	125.19
	27	367.95	135.89	386.28	129.44	400.14	124.96
	28	368.68	135.62	387.01	129.2	400.87	124.73
	29	369.38	135.36	387.71	128.96	401.57	124.51
	30	370.06	135.11	388.39	128.74	402.25	124.3

Table 38. Simulated results showing path and power received for MAID-UGURI

Site	Distance	4GHz		10GHz		20GHz	
		Pathloss	Received Power	Pathloss	Received Power	Pathloss	Received Power
MAIDUGURI	1	302.02	165.55	320.35	156.08	334.21	149.61
	2	315.89	158.28	334.21	149.61	348.08	143.65
	3	324	154.32	342.32	146.06	356.19	140.38
	4	329.75	151.63	348.08	143.65	361.94	138.14
	5	334.21	149.61	352.54	141.83	366.4	136.46
	6	337.86	147.99	356.19	140.38	370.05	135.12
	7	340.94	146.65	359.27	139.17	373.13	134
	8	343.61	145.51	361.94	138.14	375.8	133.05
	9	345.97	144.52	364.29	137.25	378.16	132.22
	10	348.08	143.65	366.4	136.46	380.26	131.49
	11	349.98	142.86	368.31	135.76	382.17	130.83
	12	351.72	142.16	370.05	135.12	383.91	130.24
	13	353.32	141.51	371.65	134.54	385.51	129.7
	14	354.81	140.92	373.13	134	386.99	129.2
	15	356.19	140.38	374.51	133.51	388.37	128.74
	16	357.48	139.87	375.8	133.05	389.66	128.32
	17	358.69	139.4	377.01	132.62	390.88	127.92
	18	359.83	138.95	378.16	132.22	392.02	127.54
	19	360.91	138.54	379.24	131.84	393.1	127.19
	20	361.94	138.14	380.26	131.49	394.13	126.86
	21	362.91	137.77	381.24	131.15	395.1	126.55
	22	363.85	137.42	382.17	130.83	396.03	126.25
	23	364.73	137.09	383.06	130.53	396.92	125.97
	24	365.59	136.77	383.91	130.24	397.77	125.7
	25	366.4	136.46	384.73	129.96	398.59	125.44
	26	367.19	136.17	385.51	129.7	399.37	125.2
	27	367.94	135.89	386.27	129.44	400.13	124.96
	28	368.67	135.62	386.99	129.2	400.86	124.73
	29	369.37	135.37	387.7	128.97	401.56	124.51
	30	370.05	135.12	388.37	128.74	402.24	124.3

Table 39. Simulated results showing path and power received for YOLA

Site	Distance	4GHz		10GHz		20GHz	
		Pathloss	Received Power	Pathloss	Received Power	Pathloss	Received Power
YOLA	1	302.03	165.55	320.36	156.08	334.22	149.6
	2	315.89	158.28	334.22	149.6	348.08	143.64
	3	324	154.32	342.33	146.06	356.19	140.37
	4	329.76	151.63	348.08	143.64	361.95	138.14
	5	334.22	149.6	352.55	141.83	366.41	136.46
	6	337.87	147.99	356.19	140.37	370.06	135.11
	7	340.95	146.65	359.28	139.17	373.14	134
	8	343.62	145.51	361.95	138.14	375.81	133.05
	9	345.98	144.52	364.3	137.25	378.17	132.22
	10	348.08	143.64	366.41	136.46	380.27	131.48
	11	349.99	142.86	368.32	135.75	382.18	130.83
	12	351.73	142.15	370.06	135.11	383.92	130.24
	13	353.33	141.51	371.66	134.53	385.52	129.7
	14	354.81	140.92	373.14	134	387	129.2
	15	356.19	140.37	374.52	133.5	388.38	128.74
	16	357.48	139.87	375.81	133.05	389.67	128.31
	17	358.7	139.39	377.02	132.62	390.89	127.91
	18	359.84	138.95	378.17	132.22	392.03	127.54
	19	360.92	138.53	379.25	131.84	393.11	127.19
	20	361.95	138.14	380.27	131.48	394.14	126.86
	21	362.92	137.77	381.25	131.15	395.11	126.55
	22	363.85	137.42	382.18	130.83	396.04	126.25
	23	364.74	137.08	383.07	130.53	396.93	125.97
	24	365.59	136.76	383.92	130.24	397.78	125.7
	25	366.41	136.46	384.74	129.96	398.6	125.44
	26	367.19	136.17	385.52	129.7	399.38	125.19
	27	367.95	135.89	386.27	129.44	400.14	124.96
	28	368.68	135.62	387	129.2	400.86	124.73
	29	369.38	135.36	387.7	128.96	401.57	124.51
	30	370.06	135.11	388.38	128.74	402.24	124.3

APPENDIX C

Simulation Program Listing

```

% Simulation of the Path Loss (L) for 3 frequencies
% #####
% read rainfall data
M=csvread('rainfall.csv');
%year
syear = [1998,1999,2000,2001,2002,2003,2004,2005,2006,2007,2008,2009,
2010,2011,2012]
% State Capitals (Data Locations)
MeanR = zeros(1,37);
SDv = zeros(1,37);
Lr = zeros(30,3); % pathloss in rain
Lp = zeros(30,3); % pathloss in free space
Pr = zeros(30,3); % received power
Prp = zeros(30,3); % power recieved in free space
%location = cell(37);
n=15;
location = {'Abeokuta','Adoekiti','Akure','Ibadan','Ikeja','Osogbo','Abakiliki',
'Awka','Enugu'...
'Owerri','Umuahia','Asaba','Benin','Calabar','Port Harcourt',
'Uyo','Yenagoa','Abuja','Ilorin','Lafia'...
'Lokoja','Makurdi','Minna','Jos','Birini Kebbi','Gusau','Kaduna',
'Kano','Katsina','Sokoto','Bauchi'...
'Damaturu','Dutse','Gombe','Jalingo','Maiduguri','Yola'};

for i= 1:37
    fprintf('\n');
    %fprintf(location(i));
    R=0;
    for j=1:15
        R = R + M(i,j);
        fprintf('%10.2\t',M(i,j))
    end
    MeanR(i) = R/15;
    DEV=0;
    for j=1:15
        DEV = DEV + (M(i,j)-MeanR(i));
    end
    SDv(i) = sqrt((DEV)^2/(n-1));
end

```

```

%print
for j = 1:15;
    %fprintf('\t');
    fprintf('%10.0f\t',syear(j));
end
fprintf('\n');
for i =1:1:37;
    %disp (location(i));
    %sprintf('%s',location(i));
    %fprintf('\t');
    for j = 1:1:15;
        fprintf('%10.0f\t',M(i,j));
    end
    fprintf('%10.0f\t',MeanR(i));
    fprintf('%18.14f\t',SDv(i));
    fprintf('\n');
end

% calculate the value of L
%  $L = (4 \times \text{Pi} \times a^2) / (\text{lambda}^2 \times \text{Dt} \times \text{Dr}) \times e^{-(\text{Nd} \times \text{Qtototal} \times a)}$ 
% caculate power received as a function of transmitted power and distance
% where  $L = \text{Ps}/\text{Pr}$ ,  $\text{Pr} = \text{Ps}/L$ 
% calculate path loss in free space ( $L_p$ )
%  $L_p(\text{dB}) = 32.45 + (20 \times \log(a)) + (20 \times \log(\text{frequencies}(i)))$ 
% relationship of  $\text{Pr}$  and  $a$  in free space
%  $\text{Pr} = \text{Ps}/L_p$ 

disp '#####A program to calculate the value of L#####'
disp 'Where  $L = (4 \times \text{Pi} \times a^2) / (\text{lambda}^2 \times \text{Dt} \times \text{Dr}) \times e^{-(\text{Nd} \times \text{Qtototal} \times a)}$ '

#####Constants#####
DtDr = 1;
No = 0.08;
alpha = 4.1;
beta = 0.21;
Ps = 50000;

##### variables #####
disp 'Input Frequency Values:'
f1 = input('The first frequency = ');
f2 = input('The second frequency = ');
f3 = input('The Third frequency = ');
##### initialize #####
ai = (0.25+0.45)/2;
c = Ps/(4*pi);

Nd = No*exp(-(alpha * R^(-beta))*ai);

```

```

%vectorise the frequency inputs

frequencies = [f1, f2, f3];

disp 'Effect of Rainfall (Antenna Loss (L)) for;'

fprintf('\t');
fprintf('%10.2f\t', f1);
fprintf('%10.2f\t', f2);
fprintf('%10.2f\n', f3);
%Calculate L for each value a=distance between two antennas
for site =1:37;
    for a =1:1:30;
        fprintf('%g\t',a);
        for i = 1:3;
            f = frequencies(i);
            R = MeanR(site);
            Nd = No*exp(-(alpha * R^(-beta))*ai);
            C0 = -0.277+2.22*exp(-0.007*f)*cos(13.446+0.484*f);
            C1 = 1.67-23.683*exp(-0.017*f)*cos(0.685+488*f);
            C2 = 3.66+69.546*exp(-0.018*f)*cos(13.02+0.495*f);
            C3 = -1.929-67.452*exp(-0.02*f)*cos(56.809+0.5*f);
            Qtotal = C0+C1*ai+C2*ai^2+C3*ai^3;
            lambda = c/frequencies(i);
            L = 10* log((4*pi*a^2)/((lambda^2)*DtDr)*(exp(Nd*Qtotal)));
            Lr(a,i) = L;
            Pr(a,i) = Ps/L;
            fprintf('%10.2f\t',Lr(a,i),Pr(a,i));
        end
    end

    fprintf('\n');
end

%generate Pictorial representation: graph

figure(site);
for a = 1:1:30
    for i = 1:3 %frequencies
        if frequencies(i)==f1
            plot(a,Lr(a,i),'gd-')
        elseif frequencies(i)==f2
            plot(a,Lr(a,i),'K*--')
        else
            plot(a,Lr(a,i),'b>:')
        end
    end
end
xlabel('distance (km)');
ylabel('Pathloss (dB)');

```

```

        legend('30MHz','10MHz','20MHz');
        %legend(num2dtr(frequencies(1)), num2str(frequencies(2)),...
        %num2str(frequencies(3)), 'location', 'northeastoutside');
        hold all
        warning('off','all')
    end
end

disp 'Effect of Free space (Antenna Loss (L)) for;'

fprintf('\t');
fprintf('%10.2f\t', f1);
fprintf('%10.2f\t', f2);
fprintf('%10.2f\n', f3);
for a=1:1:30;
    fprintf('%g\t',a);
    for i = 1:3;
        Lp(a,i) = 32.45+(20*log(a))+(20*log(frequencies(i)));
        Prp(a,i) = Ps/Lp(a,i);
        fprintf('%10.2f\t',Lp(a,i),Prp(a,i));
    end
    fprintf('\n');
end

%generate Pictorial representation of received power
figure(site+1);
for a = 1:1:30
    for i = 1:3 %frequencies
        if frequencies(i)==f1
            plot(a,Lp(a,i),'gd-')
        elseif frequencies(i)==f2
            plot(a,Lp(a,i),'K*--')
        else
            plot(a,Lp(a,i),'b>:')
        end
    end
    xlabel('distance (km)');
    ylabel('Pathloss (dB)');
    legend('30MHz','10MHz','20MHz');
    %legend(num2str(frequencies(1)), num2str(frequencies(2)),...
    %num2str(frequencies(3)), 'location', 'northeastoutside');
    hold all
    warning('off','all')
end

%generate Pictorial representation of received power
figure(site+2);
for a = 1:1:30

```

```

        fprintf('%10.2\t',M(i,j))
    end
    MeanR(i) = R/15;
    DEV=0;
    for j=1:15
        DEV = DEV + (M(i,j)-MeanR(i));
    end
    SDv(i) = sqrt((DEV)^2/(n-1));
end

%print
for j = 1:15;
    %fprintf('\t');
    fprintf('%10.0f\t',syear(j));
end
fprintf('\n');
for i =1:1:37;
    %disp (location(i));
    %sprintf('%s',location(i));
    %fprintf('\t');
    for j = 1:1:15;
        fprintf('%10.0f\t',M(i,j));
    end
    fprintf('%10.0f\t',MeanR(i));
    fprintf('%18.14f\t',SDv(i));
    fprintf('\n');
end

% calculate the value of L
%  $L = (4 \times \pi \times a^2) / (\lambda^2 \times D_t \times D_r) \times e^{-(N_d \times Q_{total} \times a)}$ 
% caculate power received as a function of transmitted power and distance
% where  $L = P_s/P_r$ ,  $P_r = P_s/L$ 
% calculate path loss in free space ( $L_p$ )
%  $L_p(\text{dB}) = 32.45 + (20 \times \log(a)) + (20 \times \log(\text{frequencies}(i)))$ 
% relationship of  $P_r$  and  $a$  in free space
%  $P_r = P_s/L_p$ 

disp '#####A program to calculate the value of L#####'
disp 'Where  $L = (4 \times \pi \times a^2) / (\lambda^2 \times D_t \times D_r) \times e^{-(N_d \times Q_{total} \times a)}$ '

#####Constants#####
DtDr = 1;
No = 0.08;
alpha = 4.1;
beta = 0.21;
Ps = 50000;

##### variables #####

```

```

disp 'Input Frequency Values:'
f1 = input('The first frequency = ');
f2 = input('The second frequency = ');
f3 = input('The Third frequency = ');
##### initialize #####
ai = (0.25+0.45)/2;
c = Ps/(4*pi);

Nd = No*exp(-(alpha * R^(-beta))*ai);

%vectorise the frequency inputs

frequencies = [f1, f2, f3];

disp 'Effect of Rainfall (Antenna Loss (L)) for;'

fprintf('\t');
fprintf('%10.2f\t', f1);
fprintf('%10.2f\t', f2);
fprintf('%10.2f\n', f3);
%Calculate L for each value a=distance between two antennas
for site =1:37;
    for a =1:1:30;
        fprintf('%g\t',a);
        for i = 1:3;
            f = frequencies(i);
            R = MeanR(site);
            Nd = No*exp(-(alpha * R^(-beta))*ai);
            C0 = -0.277+2.22*exp(-0.007*f)*cos(13.446+0.484*f);
            C1 = 1.67-23.683*exp(-0.017*f)*cos(0.685+488*f);
            C2 = 3.66+69.546*exp(-0.018*f)*cos(13.02+0.495*f);
            C3 = -1.929-67.452*exp(-0.02*f)*cos(56.809+0.5*f);
            Qtotal = C0+C1*ai+C2*ai^2+C3*ai^3;
            lambda = c/frequencies(i);
            L = 10* log((4*pi*a^2)/((lambda^2)*DtDr)*(exp(Nd*Qtotal)));
            Lr(a,i) = L;
            Pr(a,i) = Ps/L;
            fprintf('%10.2f\t',Lr(a,i),Pr(a,i));
        end
        fprintf('\n');
    end
end

%generate Pictorial representation: graph

figure(site);
for a = 1:1:30
    for i = 1:3 %frequencies
        if frequencies(i)==f1

```



```
        plot(a,Pr(a,i),'gd-')
    elseif frequencies(i)==f2
        plot(a,Pr(a,i),'K*--')
    else
        plot(a,Pr(a,i),'b>:')
    end
end
end
xlabel('distance (km)');
ylabel('Recieved Power (dB)');
legend('30MHz','10MHz','20MHz');
%legend(num2dtr(frequencies(1)), num2str(frequencies(2)),...
%num2str(frequencies(3)),'location', 'norteastoutside');
hold all
warning('off','all')
end
end
```